4-21-2011 12:00 AM

Audible Acoustic Emissions for Monitoring High-Shear Granulation

Erin M. Hansuld, *The University of Western Ontario*

Supervisor: Dr. Lauren Briens, *The University of Western Ontario*

A thesis submitted in partial fulfillment of the requirements for the Doctor of Philosophy degree in Chemical and Biochemical Engineering

AUDIBLE ACOUSTIC EMISSIONS FOR MONITORING HIGH-SHEAR GRANULATION

(Spine title: Audible Acoustics for Monitoring High-Shear Granulation)

(Thesis format: Integrated Article)

by

Erin M. Hansuld

Graduate Program in Engineering Science
Department of Chemical and Biochemical Engineering

A thesis submitted in partial fulfillment
of the requirements for the degree of
Doctor of Philosophy

The School of Graduate and Postdoctoral Studies
The University of Western Ontario
London, Ontario, Canada
April 2011

THE UNIVERSITY OF WESTERN ONTARIO
School of Graduate and Postdoctoral Studies

CERTIFICATE OF EXAMINATION

Supervisor

_____
Dr. Lauren Briens

Supervisory Committee

Dr. Cedric Briens

Dr. Amyn Sayani

Examiners

_____
Dr. Jim Litster

_____
Dr. James Lacefield

_____
Dr. Andrew Hrymak

_____
Dr. Ajay Ray

The thesis by

Erin Mitchell Hansuld

entitled:

Audible Acoustic Emissions for Monitoring High-Shear Granulation

is accepted in partial fulfillment of the
requirements for the degree of
Doctor of Philosophy

_____ _____
Date Chair of the Thesis Examination Board

Abstract

High-shear wet granulation is a size enlargement process commonly used by the pharmaceutical industry to improve powder properties for downstream processes, such as tabletting. Granule growth however, is difficult to predict because the final product is sensitive to raw material properties and processing conditions. Development of process analytical technologies (PATs) is recommended by regulators to improve process understanding and monitor quality online.

This work investigates the robustness of AAEs as PAT for high-shear granulation. Condenser microphones suspended in the air exhaust were used to collect AAEs from granulation. Applying power spectral density (PSD) analysis, trends related to wetting and end-point were identified between 20 and 250 Hz. A consistent decrease in PSD was observed with end-point, independent of formulation, material properties and process parameters. A design of experiment (DOE) showed the decrease results from increases in granule size and density, two critical quality attributes. Multivariate analysis confirmed AAEs could be used to monitor changes in size and density online. AAEs were also sensitive to changes in impeller speed, spray rate and total binder volume, suggesting these parameters could be used to adjust processes in real-time and achieve desired product attributes. The source of granulation AAEs was investigated by rotating spheres and wet granules of known size in stainless steel beakers. The results confirmed a relationship to particle size, and revealed AAEs are generated by particle-particle interactions. Overall, the research supports adoption of AAEs as a PAT for high-shear granulation to increase process knowledge and improve product quality.

Keywords

pharmaceutical, granulation, acoustic emissions, sound, process monitoring, spectral analysis, multivariate analysis, design of experiment

Co-Authorship Statement

Chapters 3, 4, 5 and 6 are research studies that have either been published or are ready for submission to peer-reviewed journals. The individual contributions of the authors of each journal article are stated.

Chapter 3

Audible acoustics in high-shear granulation: Application of frequency filtering

***Authors*:** E.M. Hansuld, L. Briens, J.A.B. McCann, A. Sayani

Status: Published in the *International Journal of Pharmaceutics, 378, 37-44, 2009*.

E. Hansuld conducted all experimental work with assistance from J.A.B. McCann. All data analysis was performed by E. Hansuld. The manuscript was written and revised by E. Hansuld. Drafts of the paper were reviewed by L. Briens, J.A.B. McCann and A. Sayani. Guidance for the work was provided by L. Briens, J.A.B. McCann and A. Sayani.

Chapter 4

An investigation of the relationship between audible acoustic emissions and particle size

***Authors*:** E.M. Hansuld, L. Briens, A. Sayani, J.A.B. McCann

Status: Will be submitted to *Powder Technology*

E. Hansuld conducted all experimental work, analyzed the data, and wrote the manuscript. Drafts of the manuscript were reviewed by L. Briens, J.A.B. McCann and A. Sayani. Guidance for the work was provided by L. Briens and J.A.B. McCann.

Chapter 5

Monitoring quality attributes for high-shear granulation with audible acoustic emissions

***Authors*:** E.M. Hansuld, L. Briens, A. Sayani, J.A.B. McCann

Status: Will be submitted to *Powder Technology*

E. Hansuld conducted all experimental work, analyzed the data, and wrote the manuscript. Drafts of the manuscript were reviewed by L. Briens, J.A.B. McCann and A. Sayani. Guidance for the work was provided by L. Briens and J.A.B. McCann.

Chapter 6

The effect of process parameters on audible acoustic emissions from high-shear granulation

***Authors*:** E.M. Hansuld, L. Briens, A. Sayani, J.A.B. McCann

Status: Will be submitted to the *Journal of Pharmaceutical Sciences*

E. Hansuld conducted all experimental work, analyzed the data, and wrote the manuscript. Drafts of the manuscript were reviewed by L. Briens, J.A.B. McCann and A. Sayani. Guidance for the work was provided by L. Briens and J.A.B. McCann.

Acknowledgments

I would like to thank my supervisor, Dr. Lauren Briens for providing me with the opportunity to collaborate with GlaxoSmithKline, and for the support and flexibility she showed throughout my doctoral degree. Thank you to Dr. Amyn Sayani for enabling me to complete three and half years of research at GlaxoSmithKline in Mississauga. I felt like a true employee and am grateful for the chances I was given to share my research with others. I would also like to extend my sincere gratitude to Dr. Joe McCann for his dedication and the guidance he selflessly provided. Thank you for seeing my potential and helping me to succeed.

Funding provided by the National Science and Engineering Research Council (NSERC), in the form of CGS-M, PGS-D and CGS-D scholarships is greatly appreciated, as well as the financial contributions from GlaxoSmithKline.

Thank you to Zane Arp, Vijay Akunuri, Christopher Blowes, Ian Buxton, Peter Coles, Buffy Hudson-Curtis, Gommatie Khusial, Paul McAllister, Avinash Sharma, Andrei Shklar and Francois Yacoub of GlaxoSmithKline for their technical contributions and support, as well as Phil Hyland, Brent Cook, Bettina Fong, Robert Metcalfe, Pritpal Sodhi and Tony Younan for their assistance in the pilot plant. Harvey Bauhs of Dalimar Instruments, Des O'Grady from Mettler-Toledo, and Tamara Byrne from Umetrics are also acknowledged for their technical assistance.

Lastly, I would like to recognize my family and friends, I feel very blessed and grateful for the love and encouragement you have shown me throughout this journey. Special thanks to my parents, Cam and Jean Hansuld for allowing me to find my own path and supporting me along the way, and to Tony Lafrance for his love, acceptance and sense of humour (souliers d'éléphant). This work is dedicated to my grandfathers, John Hansuld and Harold Mitchell, for inspiring me through their own pursuits of lifelong learning.

Table of Contents

List of Tables

List of Figures

List of Appendices

List of Abbreviations

AAE	Audible acoustic emissions
ANOVA	Analysis of variance
c	Speed of sound wave
C	Loadings matrix for Y
d50	Median particle diameter
DFT	Discrete Fourier transform
DOE	Design of experiment
E	Residuals matrix for X
ESWF	Elemental strength of wave at impeller blade frequency
f	Frequency
F	Residuals matrix for Y
FBRM	Focused beam reflectance measurement
FCD	Fluidized couette device
FDA	U.S. Food and Drug Administration
ICH	International conference of harmonization of technical requirements for registration of pharmaceuticals for human use
ICP	Integrated circuit piezoelectric
LOD	Loss on drying
MCC	Microcrystalline cellulose
NIR	Near-infrared spectroscopy

OPLS	Orthogonal projection to latent structures by means of partial least squares
P	Loadings matrix for X
PAT	Process analytical technology
PCA	Principal component analysis
PLS	Projection to latent structures by means of partial least squares
PLS-DA	Partial least squares discriminant analysis
PSD	Power spectral density
RMS	Root mean square
RSD	Relative standard deviation
SM	Midsized sieve fraction
T	Scores matrix for X
t[1]	Scores for first principal component associated with X
t[2]	Scores for second principal component associated with X
TD	Tap density
TPSD	Total power spectral density
U	Scores matrix for Y
u[1]	Scores for first principal component associated with Y
u[2]	Scores for second principal component associated with Y
VIP	Variable importance to projection
w*c	Combination of projection weights for X (w) and Y (c)
w*c[1]	Projection weights associated with the first principal component

w*c[2]	Projection weights associated with the second principal component
X	Variable matrix
Y	Response matrix
λ	wavelength

Chapter 1

1. Introduction

High-shear wet granulation is the process by which primary powder particles are incorporated into larger agglomerates to facilitate downstream processing and improve product attributes. The process is complex and product quality can be affected by variability in raw material inputs or processing parameters. To improve process flexibility and product consistency, regulatory bodies are recommending the development of technologies for online monitoring. This work explores the use of audible acoustic emissions to monitor high-shear wet granulation and detect end-point, where end-point is defined as the achievement of desired quality attributes. The following section provides an introduction to the high-shear granulation process, process monitoring, audible acoustic emissions, and signal analysis.

1.1. High-shear wet granulation

Wet granulation is a process for size enlargement, where small primary particles are joined together using agitation and a liquid binder. The purpose is to improve the properties of very fine cohesive powders used in products such as, pharmaceuticals, ceramics, detergents and fertilizers [1]. Granulation is commonly used in the pharmaceutical industry to prepare powders for tablet manufacturing. Fine powders are granulated to improve flow during tabletting and reduce the potential for dusting.

The formation of granules also helps to reduce segregation and improve the content uniformity of the final product [2].

1.1.1. Granulation equipment

There are three main types of granulators used in pharmaceutical manufacturing: tumbling granulators, mixer granulators and fluidized-bed granulators. In tumbling granulators, such as drum and disc granulators, particles are agglomerated by a tumbling motion resulting from the combination of gravity and centrifugal forces. Tumbling granulators are able to accommodate large batch-sizes but cannot be used to manufacture granules smaller than 1 mm. In mixer granulators, agglomerates are formed by mixing a bed of powder with an agitator while adding a liquid binder. The intensity of the motion produces granules that are smaller and denser than granules from tumbling or fluidized-bed granulators but less spherical. The added intensity reduces the amount of liquid required, leading to shorter drying times. Examples include low-speed mixers, planetary mixers and high-speed mixers. In fluidized-bed granulators, air is used to agitate the particles while spraying binder through a nozzle located above, inside, or below the powder bed. The agitation is less aggressive than mechanical mixing and the granules are typically more porous [3].

The focus for this thesis is granulation in high-speed mixer granulators, also known as high-shear granulators. High-shear granulators are used extensively in the pharmaceutical industry because they are capable of producing granules that are small

(typically less than 1 mm) and dense, making them ideal for blending and tabletting. In addition, a wide range of materials can be accommodated, including cohesive or sticky powders, and viscous binder solutions. High-shear granulators are available for both continuous and batch operation with either vertical or horizontal mixing shafts. Figure 1.1 shows a schematic representation of a typical high-shear granulator. Characteristic features of the equipment design include a stainless steel granulator bowl and a central impeller blade, used to agitate the powder and promote densification. The speed of rotation is typically between 60 and 800 rpm, depending on the equipment scale and corresponds to tip speeds of approximately 10 m/s [1]. A chopper blade may also be located off center to help break apart large agglomerates or promote growth of smaller particles. The speed of rotation for the chopper is typically between 500 and 3500 rpm [1, 4].

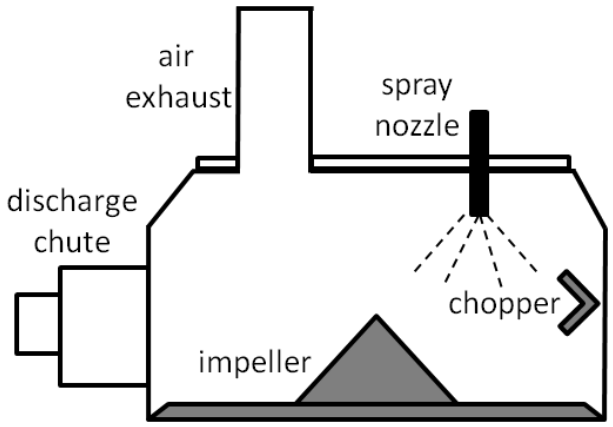

Figure 1.1 Schematic for high-shear granulator.

1.1.2. Powder flow in high-shear granulators

In high-shear granulators, powder flow is initiated by the transfer of momentum from the impeller to the powder and propagated by a series of particle-particle and particle-equipment collisions [5]. The flow of fine, unfluidized powder is poorly understood and as a result there are no generally accepted models for predicting flow patterns during granulation [1]. A study by Litster et al. [6] using a high-speed camera and imaging software, defined two flow regimes for dry powder in vertical shaft mixers, bumping and roping (Figure 1.2). Bumping occurs at low impeller speeds and is characterized by movement of the powder bed up and down as the impeller blades pass underneath. The bed of powder rotates slowly but little vertical turnover is observed. Roping occurs at higher impeller speeds and is characterized by a toroidal motion, where material is forced up the vessel wall and then collapses back down towards the centre.

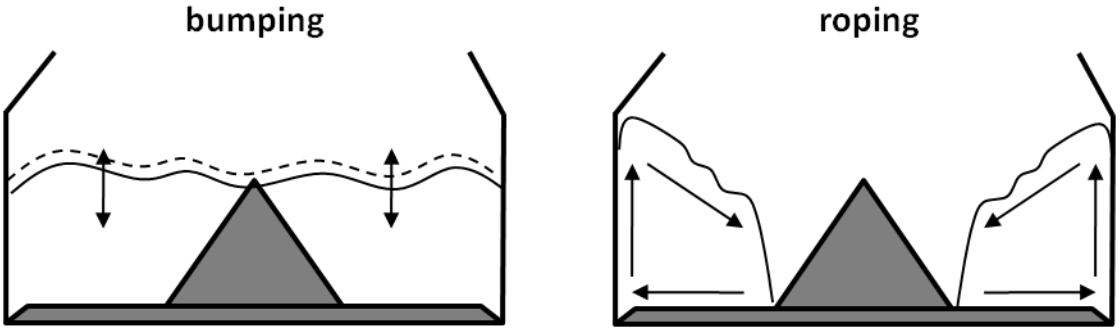

Figure 1.2 Flow regimes for fine, cohesive powder in a vertical-shaft mixer. Adapted from [6].

Studies of flow behaviour during granulation show particle velocities and the forces acting on particles vary with axial, radial and tangential location, as well as binder volume [5, 7-9]. Saito et al. [7] used positron emission tracking to show particle velocity

is proportional to the speed of rotation near the impeller and significantly less near the surface. They also showed there are different regions of size-dependent flow within the granulator. Plank et al. [8] studied the velocity of particles at the surface using a high-speed camera and found the velocity increases when the particles first become cohesive and again at the transition to dense agglomerates. Darelius et al. [9] used a high-speed camera to show friction is inversely related to cohesion. When water is added the liquid acts as a lubricant and friction between the powder and the wall is reduced. As a result, the introduction of binder is thought to add additional complexity to granule flow behaviour.

1.1.3. Granulation mechanisms

Granulation takes place according to three different rate processes: wetting and nucleation, consolidation and growth, attrition and breakage (Figure 1.3). Wetting refers to the initial introduction of liquid and the attempt to evenly distribute it throughout the blend. Nucleation occurs when the liquid joins together nearby primary particles in weak structures known as nuclei. The nuclei form the basis for granule growth, which occurs when particles and/or nuclei collide and stick together. Whether a collision results in coalescence depends on a number of factors, including the mechanical properties of the granules and the availability of liquid at the granule surface [3, 10]. Studies show granule growth increases exponentially when the pore saturation reaches between 80 and 100 percent [1]. As granules grow, they also consolidate due to the agitation forces present with mixing. Consolidation increases the granule

strength and forces excess liquid to the surface. Agitation can also cause breakage in granules that are weak or poorly formed. In addition, dried granules may undergo attrition or breakage during downstream processing or handling [3, 10].

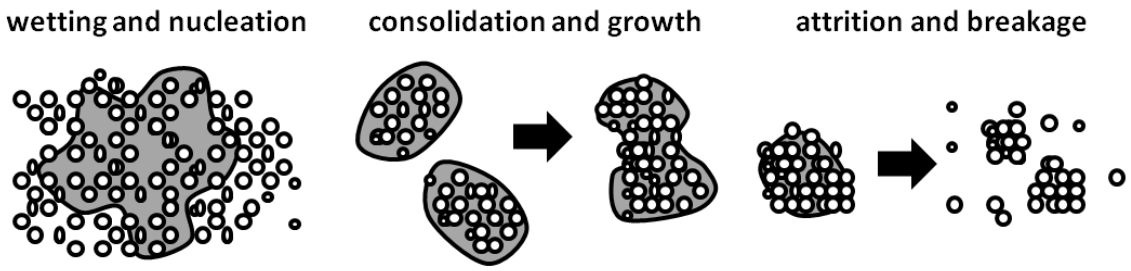

Figure 1.3 Schematic of granulation rate processes. Adapted from [10].

1.1.4. Granule growth stages

Given the above mentioned rate processes, granulation proceeds according to a series of stages. The system starts out as a mixture of dry powder and nucleation begins once the liquid binder is introduced. Nucleation is followed by granule growth, which typically proceeds according to either a steady growth or induction mechanism (Figure 1.4). Steady growth is characterized by a linear increase in granule size and has been observed in systems where the granules are weak and deformable. The elastic nature of the granules results in large contact areas during collisions, promoting coalescence. If saturation exceeds a critical level, steady growth will transition to rapid growth. Induction growth is characterized by a delay period, where there is relatively little change in granule size. The granules are not as deformable and must consolidate until a sufficient amount of liquid is present on the granule surface, at which point rapid growth occurs. From rapid growth, both steady and induction systems can become over

wet masses or slurries if saturation is continued [10, 11]. The transition from steady or induction growth to rapid growth and over wetting is often rapid and can be affected by minor changes in material inputs or process parameters. As a result, maintaining consistent product attributes is often a challenge [1, 3]. Factors shown to affect granule growth include the initial particle size distribution, binder content, binder surface tension and impeller speed [10]. Development of an online system to monitor granule growth would help accommodate minor process variability and improve control.

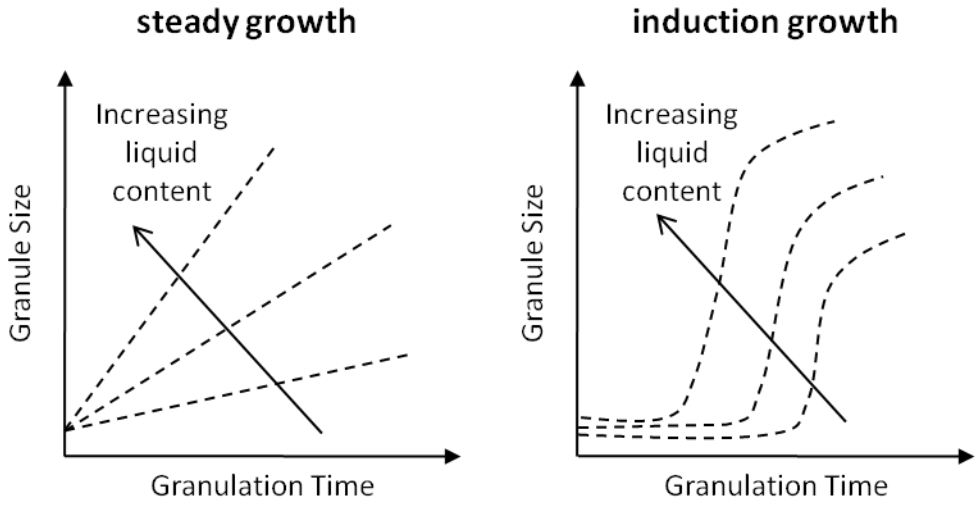

Figure 1.4 Comparison of steady and induction growth with increasing liquid content. Adapted from [11].

1.2. Process analytical technologies

The complexity of the high-shear granulation process makes it difficult to measure product quality during processing. As a result, current pharmaceutical development and manufacturing practices rely on a series of offline tests to determine whether a final product meets quality requirements. The FDA and other regulatory organizations,

however, are encouraging the development of process analytical technologies (PATs) to acquire process data online and build quality assurance into the manufacturing process. The objective is to promote increased understanding of pharmaceutical processes and sources of variability. By increasing understanding it would be possible to design more robust manufacturing practices, where instead of placing tight controls on process inputs, operating parameters could be adjusted to accommodate variability and achieve consistent product quality [12].

Development of PATs requires an understanding of the physical and chemical properties affecting product quality, as well as how these properties are influenced by changes in process parameters, such as impeller speed or binder volume. A design space approach is recommended to understand the interaction of various input variables and process parameters in relation to product quality [12]. The design space is a subset of the knowledge space, where the knowledge space represents what is known about the process, including failure regions, and the design space refers to the set of operating situations where the final product is acceptable. The process may be further optimized to define a target range for normal operation, known as the control space, but operation anywhere within the design space is considered acceptable from a regulatory standpoint (Figure 1.5) [12]. The design space is useful for understanding how a product performs under a variety of operating conditions, and developing a robust process where variability in materials, process parameters and equipment can be accommodated.

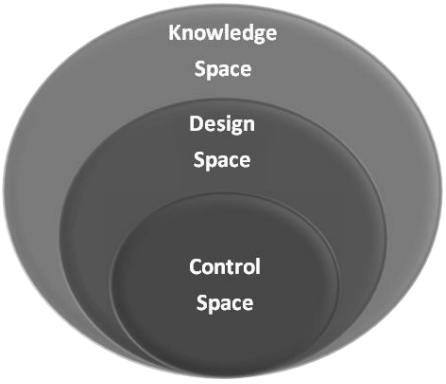

Figure 1.5 Schematic representation of the design space approach.

A statistical approach known as Design of Experiment (DOE) is often used in conjunction with a design space to understand complex interactions between variables [13]. DOE uses statistical principles to develop objective investigations, where a number of factors are varied simultaneously in a controlled manner [14]. The investigations are designed to approximate real processes, where a number of variables are involved and individual effects may not be linear or additive. The incorporation of statistics enables distinctions to be made between significant effects and experimental error, as well as correlative and causal relationships. As a result, it is possible to identify the root cause of variability and how it affects the process as a whole [13].

A number of technologies are being developed as PAT tools for granulation, including power consumption, near-infrared spectroscopy (NIR), imaging, focused beam reflectance measurement (FBRM), stress, vibration, and acoustics. Chapter 2 will provide a more detailed discussion of the application and development of these tools.

1.3. Acoustic emissions

The focus for this thesis is the development of audible acoustic emissions (AAEs) as a technology for monitoring high-shear wet granulation. The term acoustics refers to the generation, transmission and reception of energy in the form of vibrational waves in matter [15]. Particle vibration can be parallel or perpendicular to the wave direction, classifying the wave as longitudinal or transverse, respectively. Longitudinal waves can exist in any phase, but transverse waves can only propagate through solids. Both types of waves can be described by the following relationship:

$$c = \lambda f \qquad (1)$$

Where c is the speed, f is the frequency and λ is the wavelength. The speed depends on the elasticity and density of the matter the wave propagates through and the frequency is the reciprocal of the time required for one cycle of a sinusoidal tone. Frequencies in the audible range, between 20 and 20,000 Hz, are known as sound waves and can be detected by the human ear. Frequencies below 20 Hz are infrasonic waves and frequencies above 20,000 Hz are ultrasonic waves [16]. Frequencies in the audible range were examined in this work, based on reports from operators that they could hear a change in sound when granulation batches were complete.

Acoustic emissions for granulation processes are believed to result from particle-particle and particle-equipment collisions, as well as the friction generated by contact and flow

[17-20]. Leach and Rubin [17, 18] studied ultrasonic acoustic emissions generated by the rotation of glass and metallic spheres between 50 µm and 3 cm in size. The frequency of the ultrasonic waves was found to vary inversely with particle size and could be used to characterize the shape and width of the size distribution. The relationship was later extended to include particles of irregular shape using gravel [19]. Hidaka and Shimosaka [20] studied the acoustic emissions from particle flow for a group of steel spheres moving down an incline to show a positive correlation between the acoustic pressure and the macroscopic velocity of flowing particles. The results suggest particle size is a primary factor in the acoustic emissions generated from granulation but further research is required for a complete understanding of the relationship.

1.3.1. Acoustic sensors

In this work, acoustic emissions from the granulation process were collected using ICP® (integrated circuit piezoelectric) condenser microphones. Condenser microphones operate on the principles of transduction to transform sound pressure fluctuations into capacitance variations, which are then converted to electrical voltages. Inside the sensor, a thin diaphragm is located a short distance away from a backplate, where a voltage is applied. The sound waves cause the diaphragm to oscillate, changing the distance between the diaphragm and the backplate and generating an oscillating voltage that is proportional to the original pressure fluctuations. In ICP microphones, the backplate is pre-polarized by an electret layer of charged particles [21].

The positioning of the microphone depends on the frequency of the waves being collected. Ultrasonic waves attenuate significantly in air and therefore the microphone must be placed in contact with the equipment [22]. As a result, the detected signals are thought to correspond to particle-equipment collisions in the vicinity of the sensor. AAEs, however, propagate through air with minimal attenuation and have been detected using a microphone suspended in the granulator air exhaust [23]. The air exhaust location is advantageous because it does not require equipment contact and the detected signals are thought to be more representative of the overall process.

1.3.2. Sampling

The voltage signal acquired during granulation is a continuous analog signal. For computer processing, the signal must be converted to a digital format by sampling at discrete time intervals. According to the Nyquist theorem, the minimum sampling frequency must be at least twice the maximum frequency of the signal being acquired. For example, a sampling rate of at least 40,000 Hz must be used to represent data in the audible range, where the maximum frequency is 20,000 Hz. The maximum frequency is sometimes referred to as the Nyquist frequency. The purpose of using the Nyquist frequency is to prevent aliasing, or signal distortion that can occur when a continuous signal is reconstructed in a digit format. Figure 1.6 shows an example of an aliased signal and an adequately sampled signal. It can be seen that the frequency of the original signal will be misrepresented if there are any fewer than two samples per cycle [24].

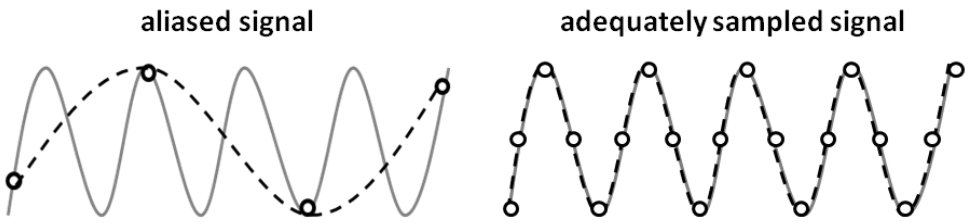

Figure 1.6 Aliasing when a signal is under sampled compared to adequate sampling. Adapted from [24].

1.4. Signal analysis

Figure 1.7 shows a sample of a raw acoustic signal collected during high-shear granulation. The magnitude of the signal is observed to change over time but further analysis is required to identify distinct features related to process behaviours. In this research, a variety of signal analysis techniques were examined; however, the best results were achieved using a combination of the discrete Fourier transform (DFT) analysis and multivariate data analysis.

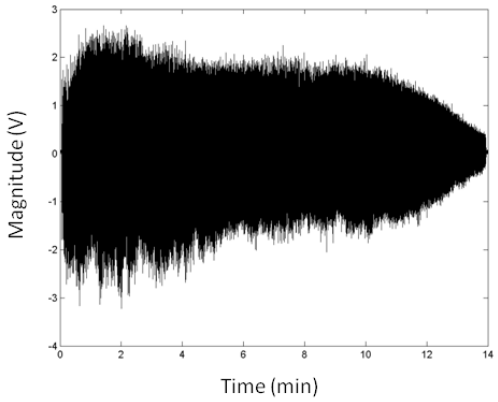

Figure 1.7 Sample of a raw acoustic signal from a high-shear granulation process.

1.4.1. DFT

Any signal can be represented in either the time-domain or the frequency-domain. The time-domain representation provides information on the amplitude of the signal over time. For information on the frequency content, the signal must be transformed to the frequency-domain using the discrete Fourier transform (DFT). The DFT is based on Fourier's theorem, which states that any waveform in the time domain can be reconstructed as a weighted sum of sine waves, each with a particular amplitude and phase. From the DFT, it is possible to identify the individual frequency components in the original signal and the relative contribution of each [24]. The DFT is a complex number comprised of a real part, the magnitude and a complex part, the phase. Squaring the magnitude of each frequency component provides a measure of power, also known as the power spectral density (PSD). To investigate how the PSD changes with time, the time-domain signal is divided into intervals of fixed length and the PSD is computed for each interval. This procedure, known as windowing is useful for process monitoring applications because it provides information on how the acoustic signal changes throughout the process [25].

1.4.2. Multivariate data analysis

Multivariate data analysis is used to extract meaningful information from large, noisy datasets comprised of variables that are highly correlated. There are two common types of multivariate analysis, principal component analysis (PCA) and projection to latent structures by means of partial least squares (PLS). Both PCA and PLS apply the

principles of projection to represent multidimensional data more simply. In PCA, the first step is plotting the data in a multidimensional space, such that each row in the initial dataset is represented by a single point (Figure 1.8, A). The data are usually preprocessed by mean centering and scaling, to create a symmetrical distribution with similar variance. Figure 1.8 shows an example using three variables, but the same approach is applicable for a higher number of variables. When all the data has been plotted, the points form a cluster (Figure 1.8, B) and a straight line, known as a principal component can be used to approximate the data according to least squares. The original data are projected onto the line and the new coordinates are known as the scores (Figure 1.8, C). The weights applied to the original observations to form the scores are known as loadings. The final equation for the transformation is as follows:

$$X = 1x' + TP' + E \qquad (2)$$

Where $1x'$ represents the variable averages after preprocessing, T represents the scores, P represents the loadings, and E represents the residuals. Additional principal components may be added to represent any remaining variability in the data, in which case the data will be projected onto a plane or hyper-plane formed by the principal components (Figure 1.8, D) [26].

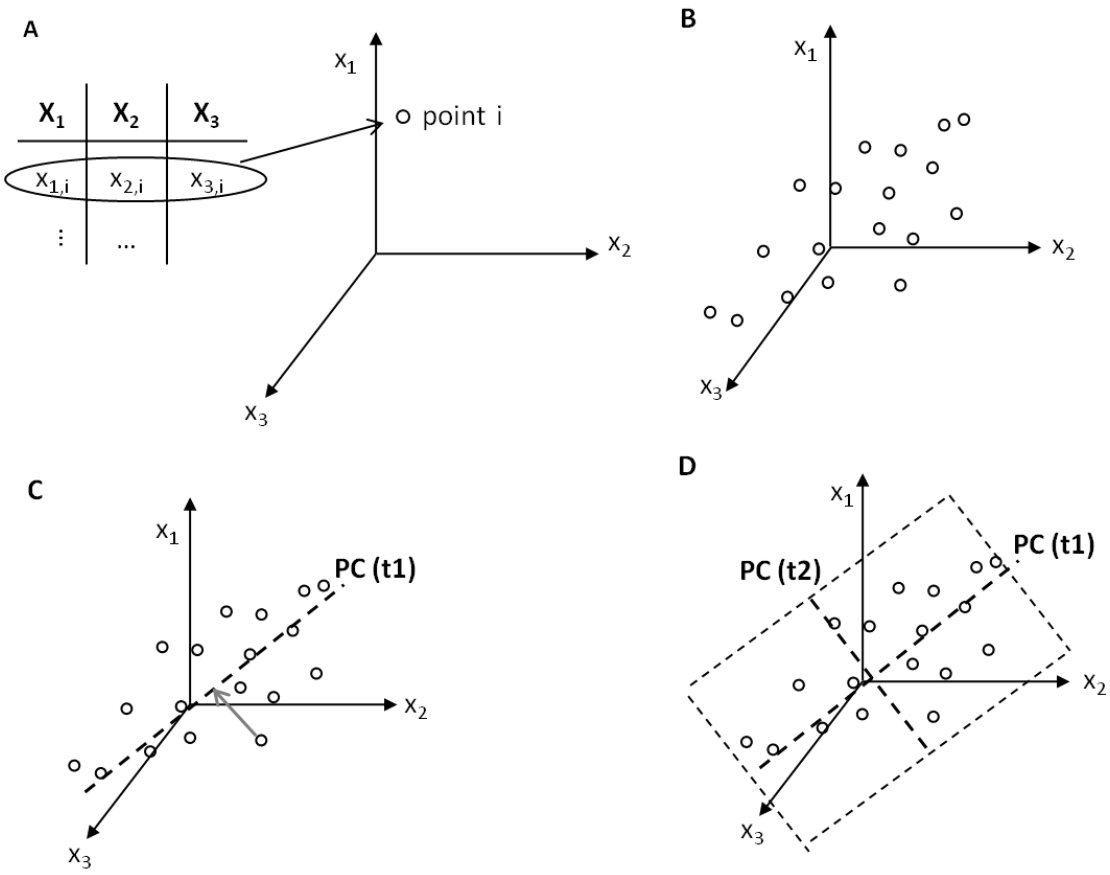

Figure 1.8 Representation of multivariate projection principles. Adapted from [26].

PLS is similar to PCA, except there are two datasets, *X* and *Y.* Each dataset is plotted in a separate space and principal components are simultaneously fit to each. The objective when fitting the principal components is to represent the data in *X* and *Y*, while also describing the relationship between *X* and *Y.* As a result, there are two sets of equations, one for *X* and one for *Y*:

$$X = 1x' + TP' + E \qquad (3)$$

$$Y = 1y' + UC' + F \qquad (4)$$

Where, *1x'* and *1y'*represent the variable averages after pre-processing, *T* and *U* represent the scores matrices, *P'* and *C'* represent the transposed loadings matrices, and *E* and *F* represent the residuals, for *X* and *Y* respectively. PLS differs from PCA because it is possible to investigate the ability to predict changes in *Y* using the variables in *X.* This is useful for PAT development because an online measurement, such as acoustic emissions can be related to process outputs, such as particle size distribution or tablet hardness [26].

1.5. Thesis objectives

The objective of this thesis was to develop AAEs as a technology for monitoring high-shear granulation, in accordance with the regulatory guidance objectives for PATs. The objective was to not only demonstrate a relationship between changes in AAEs and the granulation process but also to investigate the origin of such relationships and build process knowledge. In addition, it was desired to understand the robustness of the technology in terms of detecting changes in critical quality attributes and process parameters. These objectives are addressed over the subsequent chapters, as follows:

Chapter 2: Provides a summary of PAT technology development for granulation.

Chapter 3: Uses AAEs to develop process signatures for granulations with three formulations, using physical property measurements to confirm granulation end-point. A multivariate method is also developed to identify the frequency groups most relevant

to the granulation processes. From the AAE profiles a consistent decrease in intensity is observed to coincide with granulation end-point, independent of formulation.

Chapter 4: Investigates the relationship between the intensity of the AAEs and particle size suggested in Chapter 3, by isolating emissions from particle-particle and particle-equipment interactions. This is accomplished by rotating spheres and granules of known size in stainless steel beakers, removing the potential influence of the impeller and water addition.

Chapter 5: Applies a DOE methodology to investigate the effect of changes in size and density on the decrease in AAEs identified in Chapter 3. In addition, multivariate techniques are used to assess the ability to monitor changes in size and density online via the AAEs.

Chapter 6: Expands on the development of AAEs for online use by investigating the sensitivity of AAEs to changes in three process conditions: impeller speed, water addition rate, and total binder volume.

Chapter 7: Summarizes the progress made in the development of AAEs as a PAT technology and discusses potential applications as well as opportunities for future work.

1.6. References

[1] Litster, J., Ennis, B. & Liu, L. (2004). *The science and engineering of granulation processes*. The Netherlands: Kluwer Academic Publishers.

[2] Sherrington, P.J. & Oliver, R. (2006). Granulation. In A.S. Goldberg (Ed.), *Monographs in powder science and technology*. London: Heyden.

[3] Snow, R.H., Allen, T., Ennis, B.J. & Litster, J.D. (2008). Solid-solid operations and processing. In D.W. Green & R.H. Perry (Eds.), *Perry's chemical Engineers' handbook* [AccessEngineering]. Retrieved from www.accessengineering.com.

[4] Reynolds, G.K., Phung, K.L. & Nilpawar, A.M. (2007). High shear granulation. In A.D. Salman, M.J. Hounslow & J.P.K. Seville (Eds.), *Handbook of powder technology, granulation*, 1st edition. The Netherlands: Elsevier.

[5] Sato, Y., Nakamura, H. & Watano, S. (2008). Numerical analysis of agitator torque and particle motion in a high shear mixer. *Powder technology, 186,* 130-136.

[6] Litster, J.D., Hapgood, K.P., Michaels, J.N., Sims, A., Roberts, M. & Kameneni, S.K. (2002). Scale-up of mixer granulators for effective liquid distribution. *Powder technology*, *124*, 272-280.

[7] Saito, Y., Fan, X., Ingram, A. & Seville, J.P.K. (2011). A new approach to high-shear mixer granulation using positron emission particle tracking. *Chemical engineering science, 66*, 563-569.

[8] Plank, R., Diehl, B., Grinstead, H. & Zega, J. (2003). Quantifying liquid coverage and powder flux in high-shear granulators. *Powder technology, 134*, 223-234.

[9] Darelius, A., Lennartsson, E., Rasmuson, A., Björn, I.N. & Folestad, S. (2007). Measurement of the velocity field and frictional properties of wet masses in a high shear mixer. *Chemical engineering science, 62,* 2366-2374.

[10] Iveson, S.M., Litster, J.D., Hapgood, K. & Ennis, B.J. (2001). Nucleation, growth and breakage phenomena in agitated wet granulation processes: a review. *Powder technology, 117,* 3-39.

[11] Iveson, S.M., Wauters, P.A.L., Forrest, S., Litster, J.D., Meesters, G.M.H. & Scarlett, B. (2001). Growth regime map for liquid-bound granules: further development and experimental validation. *Powder technology, 117,* 83-97.

[12] U.S. Department of Health and Human Services, Food and Drug Administration, Center for Drug Evaluation and Research (CDER) & Center for Biologics Evaluation and Research (CBER). (2008). *Guidance for industry Q8 pharmaceutical development, second revision*. Retrieved from http://www.fda.gov/downloads/Drugs/GuidanceComplianceRegulatoryInformation/Guidances/ucm073507.pdf.

[13] Box, G.E.P., Hunter, W.G. & Hunter, J.S. (1978). *Statistics for experimenters: an introduction to design, data analysis and model building*. New York: John Wiley & Sons Inc.

[14] Soravia, S. & Orth, A. (2009). Design of experiments. *Ulmann's encyclopedia of industrial chemistry.* Retrieved from onlinelibrary.wiley.com.

[15] Kinsler, L.E., Frey, A.R., Coppens, A.B. & Sanders, J.V. (2000). *Fundamentals of acoustics.* United States of America: John Wiley & Sons Inc.

[16] Boyd, J. & Varley, J. (2001). The uses of passive measurement of acoustic emissions from chemical engineering processes. *Chemical engineering science*, *56*, 1749-1767.

[17] Leach, M.F. & Rubin, G.A. (1977). Particle size determination from acoustic emissions. *Powder technology, 16,* 153-158.

[18] Leach, M.F. & Rubin, G.A. (1978). Analysis of Gaussian size distribution of rigid particles from their acoustic emissions, *Powder technology*, *19*, 189-195.

[19] Leach, M.F. & Rubin, G.A. (1978). Size analysis of particles of irregular shape from their acoustic emissions, *Powder technology*, *21*, 263-267.

[20] Hidaka, J. & Shimosaka, A. (1993). Parameters of radiated sound and state variables in flowing particles, *International journal of modern physics B, 7*, 1965-1974.

[21] Valentino, M. (2005). Microphone handbook test and measurement microphones, *PCB piezotronics vibration division*. Retrieved from www.pcb.com/Linked_DocumentsA/Vibration/Microphone_Handbook.pdf.

[22] Bass, H.E., Campanella, A.J., Chambers, J.P. & Lindsay, R.B. (2008). Sound absorption. *AccessScience, McGraw-Hill Companies*. Retrieved from www.accessscience.com.

[23] Briens, L., Daniher, D. & Tallevi, A. (2007). Monitoring high-shear granulation using sound and vibration measurements. *The international journal of pharmaceutics, 331,* 54-60.

[24] National Instruments. (1998). Introduction to analysis in LabVIEW. *LabVIEW user manual*. Texas: National Instruments Corporation.

[25] National Instruments. (2004). Frequency analysis. *LabVIEW analysis concepts.* Retrieved from www.ni.com/pdf/manuals/370192c.pdf.

[26] Eriksson, L., Johansson, E., Kettaneh-Wold, N., Trygg, J., Wikström, C. & Wold, S. (2006). *Multi- and megavariate data analysis Part I basic principles and applications, 2nd edition*. Sweden: Umetrics.

Chapter 2

2. PAT development for granulation processes

A number of technologies have been investigated for monitoring granulation online. The technologies range from those that monitor granule growth directly by measuring changes in particle size, to indirect techniques such as vibration or acoustic emission monitoring. A variety of intrusive and non-intrusive sensors have been developed and various degrees of signal processing have been employed. The following chapter summarizes the primary technologies developed for granulation monitoring: power consumption, near-infrared spectroscopy, imaging and focused beam reflectance measurements, stress and vibration, as well as acoustic emissions.

2.1. Power consumption

Power consumption was one of the earliest PAT tools developed for monitoring high-shear granulation. Early research shows the power exerted by the impeller changes as the granules grow and consolidate, and the overall trend can be related to the stages of granulation [1-2]. Power consumption can be determined by measuring the electrical power consumed with a wattmeter, or by measuring the torque of the agitator. Measuring the electrical power is the preferred method because it is more straightforward and can be applied to mixers of any size or scale [1]. Comparisons of the two methods show there is no significant difference between the techniques [1, 3].

A representative power consumption profile is shown in Figure 2.1 along with the associated granulation stages, as defined by Leuenberger et al. [2]. The profile was divided by drawing tangents to the curves and identifying the points where they intersect. Stage I corresponds to the start of wetting, where there is little growth and as a result the power consumption remains relatively constant; stage II corresponds to the start of agglomeration and an increase in power consumption; stage III represents the achievement of useful granules and a plateau in power consumption; stage IV corresponds to over wetting and fluctuations in power consumption; and stage V represents the transition to a suspension and a decrease in power consumption. The primary feature of interest is the plateau in stage III, which was shown to correspond to granulation end-point and the achievement of ideal granule properties, as defined by measurements of size distribution, bulk and tap density, flow properties and friability. In addition, the resulting tablets were shown to have optimal hardness, disintegration, friability and weight characteristics [1]. Bier et al. [1] demonstrated the scalability of the technique by acquiring measurements for five different types of granulators. Some differences were noted in the power consumption profiles but the ratio of granulating liquid to batch size was constant at the transitions points for stages II, III and IV [1].

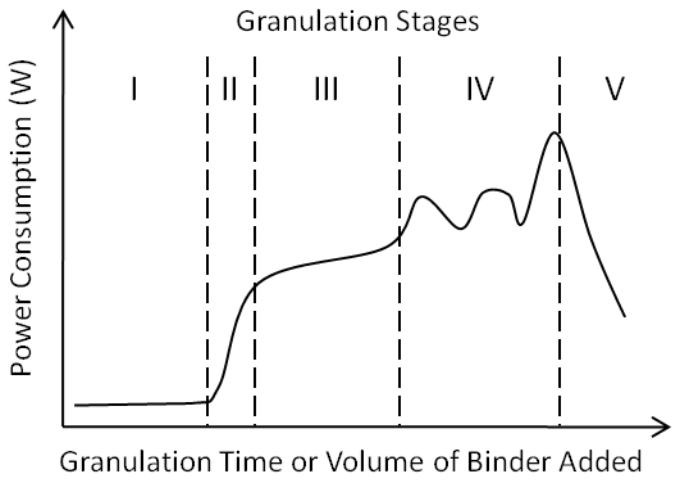

Figure 2.1 Sample power consumption profile. Adapted from [2].

As research expanded, it was found that a plateau did not correspond to end-point for all formulations [4] and signal analysis techniques were applied to extract more information from the power consumption measurements. Terashita et al. [5] showed the minimum standard deviation between 420 and 540 s and the minimum intensity at 5.4 Hz corresponded to granulation end-point. Similarly, Watano et al. [6] showed the minimum coefficient of variation corresponded to granulation end-point and was consistent with a narrower size distribution. In work by Laicher et al. [7] and Holm et al. [8] the derivative was computed, generating a peak in the region where the plateau is usually observed. The peak was found to be more precise for identifying end-point and corresponded to more homogenous particle size distributions. However, when applying the peak detection method to formulations with varying ratios of lactose and corn starch, Holm et al. [8] found it was only possible to identify the beginning of the peak for formulations with low starch content. As a result, it was preferable to use a predetermined level of power consumption for online end-point detection.

Online end-point detection was further developed in research by Betz et al. [9]. Using a third order polynomial approximation and the Simplex method, the turning point of the S-shaped increase in power consumption during stage II (Figure 2.1) was calculated. Through online computation it was possible to identify the turning point for granulations in Loedige M5 and Dionsa P10 high-shear mixers, but the approach failed when granulating in a Loepthien P5 planetary mixer. For all three mixers, the maximum power consumption was found to correspond to 100% saturation and the maximum tensile strength corresponded to 90% saturation, providing a guide for monitoring mixture cohesiveness. In later work, Betz et al. [10] defined a new parameter, TPR, which is equal to the amount of water required to reach the maximum temperature at 130% saturation, divided by the amount of water required to reach the maximum power consumption at 100% saturation. Temperature was selected to reflect interparticle contact and the frictional forces that arise during granulation. The TPR was found to be independent of process fill and could be used to distinguish between two actives of different solubility.

Temperature was also incorporated in research by Holm et al. [11] and Belohlav et al. [12]. Holm et al. [11] identified a non-linear relationship between heat development and power consumption. The relationship was found to be relatively insensitive to formulation and provided an explanation for the relationship between granulation and power consumption. Stress-strain measurements on moist agglomerates suggest that as granules become more saturated they also become more plastic and capable of

absorbing more energy during agitation. The energy absorbed appears in the form of heat due to friction between particles, and corresponds to increases in power consumption and temperature. Belohlav et al. [12] showed power consumption and temperature could be used to detect differences in particle size and shape for granulations using an active ingredient sourced from different suppliers. In addition, it was possible to detect differences in granulations with the same active drawn from different levels of the storage container.

Ritala et al. [13] and Knight et al. [14] both demonstrated an inverse relationship between power consumption and porosity. Knight et al. [14] showed the relationship is due to an increase in surface wetness with decreasing porosity, as more energy is required to overcome the viscous and capillary forces present with wetting. The results agree with findings by Bouwman et al. [15], where torque was shown to increase significantly with size for wet MCC granules, while for dry granules the increase was insignificant. In addition, the increase in torque was shown to decrease when the wet granules were coated with talc, suggesting granule stickiness contributes to the change in torque during granulation.

The effects of binder viscosity and surface tension have been investigated by a number of researchers. Rowe and Sadeghnejad [16] showed power consumption increases with binder viscosity for granulations with microcrystalline cellulose and Ritala et al. [13] showed power consumption was greater for granulations with higher surface tension

binders. These results are in contrast to findings by Pepin et al. [17], demonstrating the effect of binder viscosity is negligible up to 250 mPa·s and power consumption increases with decreasing surface tension due to more deformable granules and consequently increased interparticle friction.

Pepin et al. [18] also developed a method to estimate the over wetting point by relating the spreading energy of a liquid binder to power consumption. The liquid requirement was calculated using the difference between the maximum power consumption at over wetting and the minimum power consumption during dry mixing. A decrease in power consumption was observed with increasing liquid requirement. The decrease was thought to result from a reduction in interparticle friction with increased lubrication because a greater decrease was measured for granulations with smaller particles, where interparticle friction is expected to be greater.

In summary, power consumption monitoring is a relatively simple technique to implement; however, the relationship between power consumption measurements and granulation behaviour is not straightforward and depends on a number of interrelated variables, including formulation properties and liquid addition.

2.2. Near-infrared spectroscopy (NIR)

The near-infrared spectrum results from the absorbance of light with the molecular vibration of hydrogen bonds. Water absorbs strongly in the NIR region, particularly

between 1400 and 1450 nm, where the first overtone of the OH stretching band is found and between 1900 and 2000 nm, where a combination of OH stretching and OH bending bands are found. The wavelength is not exact because the bands are influenced by the chemical and physical state of the water as well as the temperature [19, 20]. In addition, particle size, density and surface texture can affect the amount of back-reflected light [21].

Frake et al. [22] monitored fluidized-bed granulations using a spectrophotometer with a fiber-optic probe positioned in the downward flow of the bed to collect spectra between 1100 and 2500 nm. A peak corresponding to the OH bonds in water was isolated and the second derivative could be used to determine granulation end-point. The relationship was supported by measurements of moisture using loss on drying and Karl Fischer titration. Han [23] also demonstrated a relationship between NIR spectra and Karl Fischer moisture for a fluidized-bed granulation. Measurements were collected through a glass window, however the probe position was found to be problematic in cases where the powder stuck to the window. Rantanen et al. [21, 24] showed NIR can be used to distinguish between dry mixing, spraying and drying for three formulations. They were also able to monitor differences in granule moisture content and detect changes in the rate of granule moistening due to variations in the humidity of the process air. Miwa et al. [25] used offline NIR measurements to predict the amount of water required during granulation. In a later study, the relationship was tested online, using the NIR measurements to stop the fluidized-bed granulation when the predicted

amount of water was reached. The results showed the predicted values corresponded well to achievement of desired granule properties [26].

Jorgensen et al. [27] investigated the potential for using NIR to monitor high-shear granulations by comparing the baseline-corrected water absorbance to measurements of impeller torque. Samples were withdrawn during granulation and NIR measurements were collected at-line. At the optimal liquid volume, a decrease in the slope of the NIR measurements was found to coincide with a plateau in the measured torque, for masses requiring relatively high volumes of binder liquid. In addition, for a granulation with hydrate formation, an increase in the slope of the NIR measurements was found to correspond to an increase in the impeller torque. The NIR features were found to occur slightly before the torque features and could be used online to control granule growth. Rantanen et al. [24] also applied NIR to high-shear granulation, using multivariate analysis techniques to identify three phases: mixing, spraying and wet massing from NIR measurements between 1120 and 1800 nm. Modeling each phase individually, it was possible to determine the extent of mixing, as well as the percentage of water during spraying.

The slope of the NIR spectra is thought to reflect changes in the physical properties of the granules, such as particle size [27]. As particle size increases, the NIR radiation can penetrate deeper into the material, resulting in less back-reflected light and increased absorption. It is difficult to isolate this effect however, because water addition also

affects granule optical properties. For example, water on the granule surface will absorb NIR radiation, reducing the contribution from the granule material at the water wavelengths [28, 29]. Rantanen et al. [28] used multivariate analysis with orthogonal signal correction to remove the effect of water so that information on mean granule size could be extracted from the NIR signal. Luukkonen et al. [29] showed an upward displacement of the absorbance spectra for a high-shear granulation with increasing binder volume that was attributed to an increase in particle size and/or an increase in the amount of liquid at the granule surface. The change in the 1460 nm absorption band over wetting was shown to correlate to bulk density, tablet hardness and median particle size, where the results for bulk density and tablet size were independent of impeller speed.

NIR is a promising technique for granulation monitoring because the measurements are non-destructive and can be collected rapidly online [19]. In addition, the measurements appear to be minimally affected by equipment variables, such as impeller speed [27, 29]. The disadvantages of NIR are the extensive calibrations required prior to use and the complex analysis necessary to isolate features of interest. In addition, the spectra are sensitive to the physical conditions of the sample and the measuring environment [19]. As a result, development is not straightforward and requires some degree of expertise.

2.3. Imaging and focused beam reflectance measurement (FBRM)

Technologies have been also been developed to measure changes in particle size online, as a means of monitoring granule growth. The two main methods that have been developed are imaging and FBRM.

2.3.1. Imaging

Watano and Watano et al. [30-32] used an image processing system to detect end-point for laboratory scale fluidized-bed and high-shear granulations. For the fluidized-bed granulations, images were collected by a CCD camera contained in a stainless steel cylinder along with optical fibers for lighting, a telephoto lens and an air purge unit to prevent powder adhesion. The probe was inserted into the fluidized-bed chamber, above the powder and slit lighting was used to minimize granule overlapping. The collected images were transformed into binary and circle pattern matching was used to segregate any overlapping granules before size and shape were calculated. The particle size measurements were found to agree well with traditional measurements by sieve analysis and it was possible to detect an improvement in granule shape by computing circularity and the aspect ratio. A fuzzy logic control system was also developed using image analysis to determine the amount of power supplied to the pump and consequently increasing or decreasing granule growth. With the control system, granules of the desired size were produced for batches with varying ratios of lactose [30].

For the high-shear granulations, an image probe was installed in the sidewall of the vessel, 19.5 cm from the base, to collect images of granules displaced upwards by the high-speed rotation of the chopper. Comparison with offline measurements confirmed the image probe was able to detect both fine particles and larger granules, as well as detect slow and rapid growth rates. Measurements of granule shape were not accurate at the start of wetting but were shown to agree with offline measurements once significant granule growth began. Online end-point control was attempted using an on-off switch to stop the liquid feed pump based on the image processing data; however, the 10 s lag time for data processing led to over granulation. Instead a fuzzy logic control system was implemented to stop the granulation based on the difference between the current and desired granule size, as well as the rate of change. The revised controller was tested using four target granule sizes [31], two different actives, and various liquid flow rates [32]. More spherical granules were detected at lower spray rates, suggesting the image system could be expanded to also control granule shape [32].

2.3.2. FBRM

An FBRM measurement device consists of a laser beam coupled to the tip of an immersible probe by an optical fiber. The optical fiber is rotated, moving the laser beam in a circular pattern focused on the granular medium [33]. When the beam intersects a particle, the light is scattered and some light is reflected back to a detector. The tangential velocity of the beam is known and can be multiplied by the duration of the

reflected light pulse to determine the particle chord length. It is unlikely the beam will pass directly through the centre of the particle, which is why the measurements are referred to as chord lengths rather than diameters [34]. Thousands of chord lengths can be measured per second to generate a chord length distribution and measure the change in particle count and size during processing [35].

Hu et al. [36] developed an at-line technique where powder samples were withdrawn during fluidized-bed granulation and placed in an oil solution for measurement of the chord-length distribution. The trends in the d10, d50 and d90 size profiles showed good agreement with the trend in wet granule size measured with a laser diffractometer, even though the measurement values were quantitatively different. In addition, the square weighted mean particle size of the dry granules agreed well with the d50 particle size measurements by sieve analysis. As a result, the at-line FBRM method was applied to study granule growth for a new formulation. Measurements of chord length distribution were shown to detect differences in granule growth for a DOE study of binder concentration, spray rate and the ratio of MCC.

For high-shear granulation, Huang et al. [35] used an FBRM probe to collect measurements for nine development batches and eight clinical sub-lots. The FBRM probe was immersed vertically into the bed, 3 to 5 cm above the impeller, through an existing port in the granulator lid and a scraper attached to the probe kept the face clear during granulation. After smoothing, the median moving average of the chord length

distribution showed distinct regions that could be used to characterize the change in particle size during wetting and potentially identify granulation end-point. Further development is required to investigate the relationship between features in the FBRM profile and physical property requirements at granulation end-point and in downstream processes.

One of the main challenges of using FBRM is the positioning of the probe relative to the flow of material. The probe cannot measure anything further than 2 mm away and must be inserted into the material. At greater distances, the laser beam is too wide and particle boundaries cannot be detected as precisely [37]. When Huang et al. [35] adjusted the depth of the probe during high-shear granulation, variability was observed in the wet massing profiles. In addition, material build-up along the wall was found to reduce flow past the probe and resulted in misrepresentative measurements. Huang et al. [35] also identified an increase in measurement noise during the wetting phase and emphasized the need to optimize probe position. The increased noise may be due to the dependence of FBRM measurements on the optical properties of the powder and the surrounding medium. When water is added to a system the index of refraction between the particles and the medium is lessened and the particles may not show up as well [37].

In summary, control of fluidized-bed and high-shear granulations was demonstrated using imaging probes. The disadvantage of imaging is that the probe is large, 20 cm in

length, and equipment modification is required to position the probe inside the vessel. In addition, considerable expertise is required to develop a robust control system. FBRM measurements did not provide an accurate measurement of particle size but were found to represent process changes. The primary limitation appears to be positioning the probe in a location where reliable measurements can be obtained. In addition, further development is required to understand the relationship between the profile trends and physical process behaviour.

2.4. Stress and vibration

A combination of intrusive and non-intrusive stress and vibration sensors have been investigated for monitoring changes in the forces exerted by particles as they are incorporated into granules.

2.4.1. Stress

Ohike et al. [38] inserted a probe with a spherical end into the bed of a high-shear granulator, 10 mm above the impeller blade. A strain gauge was attached to the probe to measure the vibrations during granulation. FFT analysis was performed on the vibration signal, and the change in the elemental strength of the wave at the impeller blade frequency (ESWF) was shown to correspond to the stages of granulation. The change in ESWF was shown to be proportional to changes in the mass median particle

diameter for granulations with raw materials of different size, varying amounts of binder, and different methods of binder addition.

Talu et al. [39] measured stress fluctuations imposed by particles during granulation in a Fluidized Couette Device (FCD). The FCD consisted of two concentric cylinders, where the particles occupied the annulus and the inner cylinder rotated to create shearing. Two stress sensors were mounted in the walls of the vessel, a tangential stress sensor that could only detect impacts from particles larger than 1 mm and a force transducer that measured stresses in the normal direction for particles larger than 500 µm. Preliminary experiments were performed using 500 µm and 4 mm glass beads, followed by granulations with Loctite-495 and PEG binders. The stress fluctuation spectra from 0 to 6 Hz showed an increase in magnitude with increasing granule concentration that was confirmed using a statistical measure known as the S-statistic. The stress measurements were found to be sensitive to particle size, granule concentration and granule strengthening and were independent of changes in bed height and shear rate.

Stress sensors provide a direct measure of granule growth; however they are invasive and require equipment modification. In addition, the size of the sensing element must be large enough to detect an appropriate number of granules at the largest size to avoid bias in the results [39].

2.4.2. Vibration

Early research into vibration as a process monitoring tool was conducted by Staniforth et al. [40] and Staniforth and Quincey [41]. The vibration probe used by Staniforth et al. [40] consisted of an accelerometer positioned behind a slightly concave target plate. The probe was positioned on the inside of the lid of a high-shear granulator and the connection cables were fed in through the fluid addition port. A specific root mean square (RMS) acceleration was associated with ideal granule conditions and could be used to detect end-point for fluid volumes between 14.8 and 16%, as well as accommodate changes in the impeller and chopper speeds. Staniforth and Quincey [41] used a vibration probe to collect measurements for granulations in a planetary mixer. The probe was inserted through the side of the mixing bowl, towards the bottom of the vessel. Peak velocity and peak-to-peak displacement measurements were shown to correspond to changes in size distribution and density during granulation but further development is required for precise process monitoring or end-point control.

More recently, Daniher et al. [42] and Briens et al. [43] measured vibration non-intrusively for granulations in 10 and 25 L high-shear granulators, using an accelerometer positioned on the outside of the bowl wall. For the 10 L granulations, the mean frequency of the vibrations showed sensitivity to the process but with a high level of variability between runs [42]. At the 25 L scale, one-third octave band analysis identified a trend in the 140-180 Hz frequency band. The profile showed an increase in the vibration intensity with binder addition and a transition to a plateau at the

granulation end-point [43]. The difference between the two scales was thought to be due to the mass of material, as greater mass would have a larger impact on the motor and the vibration of the bowl [42].

In general, non-intrusive methods are advantageous because it is easier to consistently position the probe and acquire reproducible measurements without the chance of fowling or disruption of batch flow. With non-intrusive measurements there is an opportunity to further optimize the sensor position, in order to maximize the information in the signal and develop relationships to physical property changes during granulation.

2.5. Acoustic emissions

Acoustic emissions in the ultrasonic and audible ranges have been investigated for non-intrusive monitoring of fluidized-bed and high-shear granulations. For fluidized-bed granulations, acoustic emissions are thought to result from particle-particle and particle-equipment collisions, friction, and fluid turbulence [44]. For high-shear granulation, acoustic emissions have been attributed to particle-particle and particle-equipment collisions, as well as friction [45].

2.5.1. Fluidized-bed granulation

Tsujimoto et al. [44] measured ultrasonic waves for fluidized-bed granulations using an acoustic emissions sensor with a piezoelectric transducer. The sensor was positioned on the outer wall of the lower chamber, 50 mm above the distributor. Microcrystalline cellulose spheres were used to calibrate the sensor at various fluidization conditions and a method was developed for detecting unstable fluidization conditions. Similarly, Matero et al. [46] attached an ultrasonic transducer to the outside of a granulation chamber using silicone grease to optimize contact. A multivariate PCA model suggested a relationship between the acoustic emissions and particle size and PLS models demonstrated an ability to predict granule water content and granule size in most cases.

Briongos et al. [47] measured audible and infrasonic acoustic emissions for fluidized-beds of glass ballotini beads using two condenser microphones positioned on the outside of the vessel chamber, at an angle of 30 degrees from the wall. The first microphone was located just above the distributor and the second was located at the height of the bed surface. The energy in the signal was found to be concentrated below 200 Hz, and focusing on infrasonic frequencies between 0 and 20 Hz was found to minimize the effect of background noise and harmonics. Time, frequency and state space analysis techniques were tested but only state space techniques were able to characterize the full range of fluidized-bed dynamics, including identification of the slugging regime.

2.5.2. High-shear granulation

For high-shear granulations, Whitaker et al. [48], Papp et al. [49] and Gamble et al. [50] collected ultrasonic acoustic emissions using piezoelectric sensors attached to the bottom outer wall of granulator bowl. Whitaker et al. [48] tested 30, 70 and 150 kHz sensors and found the 30 kHz sensor provided the strongest correlations to the physical properties of the granulation. A multivariate PLS model showed the acoustic emissions were correlated to particle size and flow properties, as well as the maximum crushing strength of the final tablets. The quality of the size and flow correlations however, was not maintained after dry screening, restricting the ability to evaluate the final properties of the blend prior to compression. Papp et al. [49] showed the RMS profiles for two laboratory scale granulators were sensitive to changes in the acoustic emissions during water addition and granule growth. Frequency analysis showed new frequencies did not appear with granulation but rather the intensity of the existing peaks changed. In addition, multivariate PLS models demonstrated the acoustic emissions could be used to predict changes in moisture content, as well as the fines, midsized and coarse particle size fractions over granulation. Lastly, Gamble et al. [50] attached two 650 kHz sensors to a laboratory scale high-shear granulator using a silicone sealant. Acoustic emissions were collected for an eleven batch DOE where liquid dose rate, batch size, impeller speed and chopper speed were varied. The results showed it was possible to predict the end-point for nine of the eleven batches, using a multivariate model developed from the acoustic emissions collected for a set of placebo batches. The two batches that failed

corresponded to granulations at different impeller speeds, suggesting a change in granule velocity altered the acoustic frequencies associated with the granulations.

In the audible range, Daniher et al. [42], Briens et al. [43] and Hansuld et al. [Chapter 3] collected acoustic emissions using a condenser microphone suspended at the top of the granulator air exhaust. Daniher et al. [42] compared the signals collected from the air exhaust to signals from microphones attached to the outside of the granulator bowl and the motor. The signals collected from the air exhaust were shown to contain the most relevant information for monitoring granulation. From profiles of mean frequency and the sound pressure level for the 112 to 140 Hz octave band, it was possible to identify the dry mixing, wetting and end-point stages. Briens et al. [43] examined the effect of scale by comparing the 10 L results to acoustic emissions from the air exhaust of a 25 L granulator. The mean frequency profile for the 25 L granulations contained additional features that were thought to represent different mechanisms of granule growth, such as nucleation, growth, and breakage. In addition, the sound pressure level for the 140 to 180 Hz octave band was found to be the most sensitive to granulation, compared to the 112 to 140 Hz range identified for the 10 L granulator. Hansuld et al. [Chapter 3] showed AAEs from the air exhaust can be used to monitor granulations with three different formulations. Physical property measurements were used to define an end-point range and 10 Hz total power spectral density profiles showed a distinct peak and transition to a decline with the achievement of ideal end-point properties.

The primary advantage of acoustic emission monitoring is that the measurements can be acquired without product contact or equipment modification. In addition, the systems are relatively inexpensive to setup [48]. The main challenge is relating the information to relevant physical properties, as the acoustic emissions are not directly related to granulation attributes of interest.

2.6. References

[1] Bier, H.P., Leuenberger, H. & Sucker, H. (1979). Determination of the uncritical quantity of granulating liquid by power measurements on planetary mixers. *Die pharmazeutische inustrie*, *41,* 375-380.

[2] Leuenberger, H., Bier, H.P. & Sucker, H. (1981). Determination of the liquid requirement for a conventional granulation process. *German chemical engineering, 4,* 13-18.

[3] Mackaplow, M.B., Rossen, L.A. & Michaels, J.N. (2000). Effect of primary particle size on granule growth and endpoint determination in high-shear wet granulation. *Powder technology*, *108*, 32-45.

[4] Holm, P., Schaefer, T. & Kristensen, H.G. (1985). Granulation in high speed mixers: Part VI. effects of process conditions on power consumption and granule growth. *Powder technology, 43,* 225-233.

[5] Terashita, K., Watano, S. & Miyanami, K. (1990). Determination of end-point by frequency analysis of power consumption in agitation granulation*. Chemical and pharmaceutical bulletin, 38,* 3120-3123.

[6] Watano, S., Terashita, K. & Miyanami, K. (1992). Frequency analysis of power consumption in agitation granulation of powder materials with sparingly soluble acetaminophen. *Chemical and pharmaceutical bulletin, 40,* 269-271.

[7] Laicher A., Profitlich, T., Schwitzer, K. & Ahlert, D. (1997). A modified signal analysis system for end-point control during granulation. *European journal of pharmaceutical sciences, 5,* 7-14.

[8] Holm, P., Schaefer, T. & Larsen, C. (2001). End-point detection in a wet granulation process. *Pharmaceutical development and technology, 6*, 181-192.

[9] Betz, G., Bürgin, P.J. & Leuenberger, H. (2003). Power consumption profile analysis and tensile strength measurements during moist agglomeration. *International journal of pharmaceutics, 252,* 11-25.

[10] Betz, G., Bürgin, P.J. & Leuenberger, H. (2004). Power consumption measurement and temperature recording during granulation. *International journal of pharmaceutics*, *272,* 137-149.

[11] Holm, P., Schaefer, T. & Kristensen, H.G. (1985). Granulation in high speed mixers: part V. power consumption and temperature changes during granulation. *Powder technology, 43,* 213-223.

[12] Belohlav, Z., Brenkova, L., Hanika, J., Durdil, P., Rapek, P. & Tomasek, V. (2007). Effect of drug active substance particles on wet granulation process. *Chemical engineering research and design*, *85,* 974-980.

[13] Ritala, M., Holm, P., Schaefer, T. & Kristensen, H. (1988). Influence of liquid bonding strength on power consumption during granulation in a high shear mixer. *Drug development and industrial pharmacy*, *14*, 1041-1060.

[14] Knight, P.C., Instone, T., Pearson, J.M.K. & Hounslow, M.J. (1998). An investigation into the kinetics of liquid distribution and growth in high shear mixer agglomeration. *Powder technology*, *97,* 246-257.

[15] Bouwman, A.M., Henstra, M.J., Hegge, J.J.M.E., Zhang, Z., Ingram, A., Seville, J.P.K. & Frijlink, H.W. (2005). The relation between granule size, granule stickiness, and torque in the high-shear granulation process. *Pharmaceutical research*, *22,* 270-275.

[16] Rowe, R.C. & Sadeghnejad, G.R. (1987). The rheology of microcrystalline cellulose powder/water mixes – measurement using a mixer torque rheometer. *International journal of pharmaceutics, 38,* 227-229.

[17] Pepin, X., Blanchon, S. & Couarraze, G. (2001). Power consumption profiles in high-shear wet granulation. I: liquid distribution in relation to powder and binder properties. *Journal of pharmaceutical sciences, 90,* 322-331.

[18] Pepin, X., Blanchon, S. & Couarraze, G. (2001). Power consumption profiles in high-shear wet granulation. II: predicting the overwetting point from a spreading energy. *Journal of pharmaceutical sciences, 90,* 332-339.

[19] Luypaert, J., Massart, D.L. & Heyden, Y.V. (2007). Near-infrared spectroscopy applications in pharmaceutical analysis. *Talanta, 72,* 865-883.

[20] Morisseau, K.M. & Rhodes, C.T. (1995). Pharmaceutical uses of near-infrared spectroscopy. *Drug development and industrial pharmacy, 21,* 1071-1090.

[21] Rantanen, J., Räsänen, E., Tenhunen, J., Känsäkoski, M., Mannermaa, J. & Yliruusi, J. (2000). In-line moisture measurement during granulation with a four-wavelength near infrared sensor: an evaluation of particle size and binder effects. *European journal of pharmaceutics and biopharmaceutics, 50,* 271-276.

[22] Frake, P., Greenhalgh, D., Grierson, S.M., Hempenstall, J.M. & Rudd, D.R. (1997). Process control and end-point determination of a fluid bed granulation by application of near infra-red spectroscopy. *International journal of pharmaceutics*, *151,* 75-80.

[23] Han, S.M. (1998). Direct moisture measurement during granulation using a near-infrared filter instrument. *Pharmacopeial forum, 24*, 6619-6622.

[24] Rantanen, J., Lehtola, S., Rämet, P., Mannermaa, J. & Yliruusi, J. (1998). On-line monitoring of moisture content in an instrumented fluidized bed granulator with a multi-channel NIR moisture sensor. *Powder technology, 99,* 163-170.

[25] Miwa, A., Yajima, T. & Itai, S. (2000). Prediction of suitable amount of water addition for wet granulation. *International journal of pharmaceutics, 195,* 81-92.

[26] Miwa, A., Yajima, T., Ikuta, H. & Makado, K. (2008). Prediction of suitable amounts of water in fluidized bed granulation of pharmaceutical formulations using corresponding values of components. *International journal of pharmaceutics, 352,* 202-208.

[27] Jorgensen, A.C., Luukkonen, P., Rantanen, J., Schaefer, T., Juppo, A.M. & Yliruusi, J. (2004). Comparison of torque measurements and near-infrared spectroscopy in characterization of a wet granulation process. *Journal of pharmaceutical sciences, 93,* 2232-2243.

[28] Rantanen, J., Wikstrom, H., Turner, R. & Taylor, L.S. (2005). Use of in-line near-infrared spectroscopy in combination with chemometrics for improved understanding of pharmaceutical processes. *Analytical chemistry,* 77*,* 556-563.

[29] Luukkonen, P., Fransson, M., Björn, I.N., Hautala, J., Lagerhold, B. & Folestad, S. (2008). Real-time assessment of granule and tablet properties using in-line data from a high-shear granulation process. *Journal of pharmaceutical sciences, 97,* 950-959.

[30] Watano, S. (2001). Direct control of wet granulation processes by image processing system. *Powder technology, 117,* 163-172.

[31] Watano, S., Numa, T., Miyanami, K. & Osako, Y. (2001). A fuzzy control system of high shear granulation using image processing. *Powder technology, 115,* 124-130.

[32] Watano, S., Numa, T., Koizumi, I. & Osako, Y. (2001). Feedback control in high shear granulation of pharmaceutical powders. *European journal of pharmaceutics and biopharmaceutics, 52,* 337-345.

[33] Kail, N., Marquardt, W. & Briesen, H. (2009). Process analysis by means of focused beam reflectance measurements. *Industrial and engineering chemistry research, 48,* 2936-2946.

[34] Heath, A.R., Fawell, P.D., Bahri, P.A. & Swift, J.D. (2002). Estimating average particle size by focused beam reflectance measurement (FBRM). *Particle & particle systems characterization, 19,* 84-95.

[35] Huang, J., Kaul, G., Utz, J., Hernandez, P., Wong, V., Bradley, D., Nagi, A. & O'Grady, D. (2010). A PAT approach to improve process understanding of high shear wet granulation through in-line particle measurement using FBRM C35. *Journal of pharmaceutical sciences, 99,* 3205-3212.

[36] Hu, X., Cunningham, J.C. & Winstead, D. (2008). Study growth kinetics in fluidized bed granulation with at-line FBRM. *International journal of pharmaceutics, 347,* 54-61.

[37] Ruf, A., Worlitschek, J. & Mazzotti, M. (2000). Modeling and experimental analysis of PSD measurements through FBRM. *Particle & particle systems characterizations, 17,* 167-179.

[38] Ohike, A., Ashihara, K. & Ibuki, R. (1999). Granulation monitoring by fast Fourier transform technique. *Chemical and pharmaceutical bulletin, 47,* 1734-1739.

[39] Talu, I., Tardos, G.I. & Ommen, J.R. (2001). Use of stress fluctuations to monitor wet granulation of powders. *Powder technology, 117,* 149-162.

[40] Staniforth, J.N., Walker, S. & Flanders, F. (1986). Granulation monitoring in a high speed mixer/processor using a probe vibration analysis technique. *International journal of pharmaceutics, 31,* 277-280.

[41] Staniforth, J.N. & Quincey, S.M. (1986). Granulation monitoring in a planetary mixer using a probe vibration analysis technique. *International journal of pharmaceutics, 32,* 177-185.

[42] Daniher D. Briens, L. & Tallevi, A. (2007). End-point detection in high-shear granulation using sound and vibration signal analysis. *Powder technology, 181,* 130-136.

[43] Briens, L., Daniher, D. & Tallevi, A. (2007). Monitoring high-shear granulation using sound and vibration measurements. *International journal of pharmaceutics, 331,* 54-60.

[44] Tsujimoto, H., Yokoyama, T., Huang, C.C. & Sekiguchi, I. (2000). Monitoring particle fluidization in a fluidized bed granulator with an acoustic emission sensor. *Powder technology, 113,* 88-96.

[45] Hidaka, J. & Shimosaka, A. (1993). Parameters of radiated sound and state variables in flowing particles. *International journal of modern physics B, 7*, 1965-1974.

[46] Matero, S. Poutiainen, S., Leskinen, J., Järvinen, K., Ketolainen, J., Reinikainen, S., Hakulinen, M., Lappalainen, R. & Poso, A. (2009). The feasibility of using acoustic emissions for monitoring of fluidized bed granulation. *Chemometrics and intelligent laboratory systems, 97,* 75-81.

[47] Briongos, J.V., Aragón, J.M. & Palancar, M.C. (2006). Fluidised bed dynamics diagnosis from measurements of low-frequency out-bed passive acoustic emissions. *Powder technology, 162,* 145-156.

[48] Whitaker, M., Baker, G.R., Westrup, J., Goulding, P.A., Rudd, D.R., Belchamber, R.M. & Collins, M.P. (2000). Application of acoustic emission to the monitoring and end point determination of a high shear granulation process. *International journal of pharmaceutics, 205,* 79-91.

[49] Papp, M.K., Pujara, C.P. & Pinal, R. (2008). Monitoring of high-shear granulation using acoustic emission: predicting granule properties. *Journal of pharmaceutical innovation, 3,* 113-122.

[50] Gamble, J.F., Dennis, A.B. & Tobyn, M. (2009). Monitoring and end-point prediction of a small scale wet granulation process using acoustic emission. *Pharmaceutical development and technology, 14,* 299-304.

Chapter 3

3. Audible acoustics in high-shear granulation: Application of frequency filtering[1]

3.1. Introduction

Regulatory guidance on process analytical technologies (PATs) encourages the pharmaceutical industry to develop innovative tools for monitoring product quality and improving process understanding [1]. High-shear wet granulation is an integral pharmaceutical operation used to reduce segregation, enhance flowability and improve tabletting performance of powders [2, 3]. This is achieved through coalescence of primary particles into larger agglomerates, or granules, by spraying a liquid binder while applying shearing and compaction forces [2, 4]. The process is complex with a large number of critical variables that interact dynamically to influence final product quality, including: binder content, surface tension, viscosity, particle size, humidity, temperature and mixing speed [3, 5]. As a result, process monitoring and control are not straightforward, and to ensure quality there is a need to develop PATs. To date, the following PATs have been investigated for granulation: power consumption/torque monitoring, near-infrared spectroscopy, imaging and vibration sensors [6-8]; however, none of these methods have been adopted in day-to-day pharmaceutical operations.

[1] A version of this chapter has been published, *Int. J. Pharm., 378, 37-44 (see Appendix A for details)*.

3.1.1. Granulation monitoring using acoustic sensors

Recent work with ultrasonic (greater than 20,000 Hz) and audible (20-20,000 Hz) acoustic emission sensors supports their development as PAT tools for granulation monitoring and control [9-12]. Whitaker et al. [9] and Papp et al. [10] attached ultrasonic sensors to the bottom of granulator bowls to detect acoustic emissions from granules contacting the bowl wall near the sensors. Resulting profiles showed acoustic emissions were related to granule size distribution and powder flowability. Audible acoustic emissions (AAEs) differ significantly from ultrasonic because they propagate through air with minimal attenuation [13] and therefore equipment contact is not required for detection. Briens et al. [11] and Daniher et al. [12] showed microphones suspended at the top of PMA-10 and PMA-25 granulator air exhausts were sensitive to granulation of a lactose based placebo formulation, while microphones on the side and bottom of the bowl were unresponsive. The mean frequency profile and root mean square sound pressure levels for one-third octave bands were found to be effective for identifying granulation end-point [11, 12].

3.1.2. Multivariate analysis

Partial least squares discriminant analysis (PLS-DA) is a form of multivariate analysis introduced in this work to assess the frequency content of the AAEs. Multivariate analysis has been recognized in other research for its ability to handle large, noisy and highly correlated datasets without ill-conditioning [14]. In PLS-DA, a response matrix (*Y*) is used to classify each observation in a variable matrix (*X*) using pre-existing knowledge.

The model then seeks to simultaneously describe the structure of the *X* and *Y* matrices, while also explaining the relationship between *X* and *Y*. This is accomplished by projecting each observation into a reduced dimensional space using linear combinations of the original variables. The resulting model can be used to distinguish between the defined classes, such as wetting and end-point [15, 16]. The influence of each *X* variable on the model can be assessed using variable importance to projection (VIP), where a VIP value greater than one indicates above average significance [14, 17]. Work by Chong et al. [17] identified VIP as the preferred method for selecting relevant predictors and suggested the method is relatively insensitive to noise. VIP has mainly been applied in bioinformatics to identify key variables for prediction [18-20] or classification [21, 22].

3.1.3. Objective

The objective was to investigate the use of AAEs for detecting granulation end-point with three different formulations, incorporating physical analysis to explain changes in the resulting profiles. PLS-DA was examined as a method for simplifying the identification of key frequency groups related to granulation stage, i.e. wetting, end-point and over-wetting.

3.2. Materials and methods

3.2.1. Formulation

The platform granule formulation consisted of mannitol (Pearlitol® 160C, Roquette), microcrystalline cellulose (Avicel® PH 101, FMC Biopolymer), hypromellose 2910 (Pharmacoat® 603, Shin-Etsu Chemical Co.) and croscarmellose sodium (AcDiSol®, FMC Biopolymer). Two additional formulations were prepared by replacing 71% of the mannitol with maize starch (Maize Starch B, Roquette) or dextrose anhydrous (Roquette). The purpose of the substitutions was to vary the properties of the formulation by choosing starch to simulate an insoluble active and dextrose to simulate a soluble active. To achieve a 60% bowl fill, the batch sizes were 2.85 kg for mannitol and dextrose and 2.56 kg for starch. Magnesium stearate (HyQual®, Mallinckrodt Inc.) and additional croscarmellose sodium were added prior to tabletting.

3.2.2. Granulation method

Materials for each batch were passed through an 850 µm sieve and granulated in a Niro-Fielder PMA-10 high-shear granulator. The impeller (360 rpm) and chopper (3000 rpm) speeds were constant throughout dry mixing (5 min) and water addition (12.5 – 17 min). Water was added at 80 mL/min (20 psi) through a spray nozzle positioned left-of-center.

3.2.3. Granule analysis

Formulator end-point

The granulation end-point range was determined in duplicate for each formulation by stopping the granulation in 50-100 mL increments and analyzing the granules to determine if end-point had been reached.

Particle size

Granulations were stopped at different extents of binder addition and samples (approximately 20 g) were withdrawn opposite the nozzle and chopper. Samples were tray dried to less than 2% loss on drying (LOD) using a GCA convection oven (80 °C). LOD was determined using a Mettler Toledo Moisture Analyzer and approximately 2 g of sample. Particle size distribution was measured using an ATM Sonic Sifter with a pulse amplitude of 9 and a 5 min sift/pulse setting. The sieve set consisted of 150, 180, 250, 355, 600 and 850 µm sieves and a fines collector.

Flowability

Granulations were stopped at different extents of binder addition and discharged from the granulator. The material was divided in half by weight and one half was dried using a Glatt GPCG-3 fluid-bed dryer (60 °C). Mannitol and starch granules were dried to less than 2% LOD and dextrose granules were dried to less than 3% LOD. The dried granules were passed through a screen with round, 190 µm perforations using a Quadro 197 comil (1500 rpm). A 50 g sample of comilled granules was withdrawn for flowability analysis. Flowability refers to the ease at which a powder flows and was measured by

the avalanche method using a Mercury Scientific Revolution Powder Analyzer. The comilled granules (83 mL) were placed in a disk (25% fill) and rotated at 0.3 rpm. After 30 s of preparation time, images of the avalanching powder were taken at 10 frames per second until a total of 128 avalanches occurred. The change in power (potential energy) for each avalanche and the avalanche time were determined from the digital images and used to assess granule flowability.

Tablet compression for break load testing

Co-milled material was blended with croscarmellose sodium and magnesium stearate in a 10 L bin using a Pharmatech blender. Materials were added separately by first sieving through a 600 μm sieve and then blending for 18 and 3 min, respectively. A Korsch XL100 tablet press, fitted with a B-turret and four alternating oval punches (8.73 by 17.49 mm) was used. The press was operated at 40 rpm and a compression force of 28 kN. For each compression force, a number of tablets were compressed to establish proper operating conditions and then 50 tablets were collected for analysis. Break load was measured across the face of 10 randomly selected tablets using a Holland C50 hardness tester.

3.2.4. Microphone setup and data acquisition

AAEs were collected from five different locations on the granulator, as shown in Figure 3.1. AAEs were acquired at 40,000 Hz using PCB Piezotronics condenser microphones (model 130D20) and conditioned using ICP sensor signal conditioners (PCB Piezotronics).

The data was logged using a National Instruments 16-bit data acquisition system and LabVIEW software. 40,000 Hz was selected to permit full reconstruction of the audible frequency range (20-20,000 Hz) without aliasing (Nyquist sampling theorem) [23].

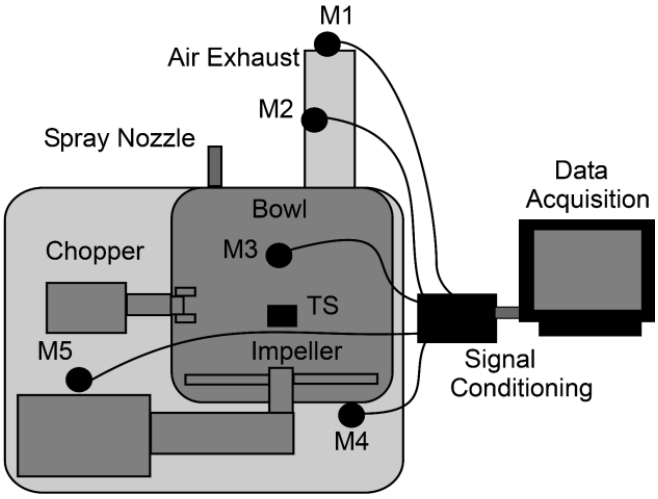

Figure 3.1 Equipment setup and microphone locations (M1-M5) for high-shear granulator.

3.2.5. Signal processing

Fast Fourier transform

All data transformations and calculations were performed using Matlab 6.5. Power spectral density (PSD) was computed by applying fast Fourier transform analysis to 10 s consecutive data segments using the PSD function (Welch's averaged, modified periodogram method). Total power spectral density (TPSD) was determined by summing the PSDs for each time segment over the desired frequency range between 20 and 20,000 Hz. Trend lines were generated in SigmaPlot by aggregating data from five (starch) or six (mannitol and dextrose) runs and applying Loess smoothing. All results shown are for the microphone inside the air exhaust (Figure 3.1).

Multivariate analysis

PLS-DA was used to analyze the frequency content of the acoustic signals using Umetrics SIMCA-P + 11.5 software. The *X* matrix was comprised of TPSDs for 10 Hz increments from 20-20,000 Hz computed over 10 s time segments and the *Y* matrix was formed using ones and zeros to classify each observation as wetting, end-point or over-wet. Classification was based on the formulator end-point range and supporting size, flowability and tablet analyses. The VIP analysis function in SIMCA-P was used to determine which frequency groups were most significant for describing the stages of granulation.

3.3. Results

3.3.1. Definition of end-point range

Table 3.1 summarizes the end-point range defined for each formulation based on formulator, size, flowability and compression analyses.

Table 3.1 End-point range summary

	Mannitol		Starch		Dextrose	
Technique	Lower Limit (mL)	Upper Limit (mL)	Lower Limit (mL)	Upper Limit (mL)	Lower Limit (mL)	Upper Limit (mL)
Formulator	800	900	950	1150	900	1000
Size Distribution[a]	700	1000	950	1250	900	1050
Flowability[a]	700	-	850	1350	850	-
Tablet Hardness[a]	-	1000	950	1250	-	1000
End-point Range	800	900	950	1150	900	1000

Abbreviations: (-) no value

[a] Lower limits were assumed to be greater than the volume reported, and upper limits were assumed to be less than the volume reported.

3.3.2. Size distribution

Granule size distributions were divided into fines (less than 180 µm), midsized (180-600 µm), and large (greater than 600 µm) fractions. Each group was plotted versus binder addition and is shown in Figure 3.2 (A). Lower and upper end-point limits were defined by binder volumes corresponding to between 40 and 10% fines, respectively.

3.3.3. Flowability

Change in flow behaviour with binder content was determined using the avalanche method (Figure 3.2, B). When comparing powders, changes in avalanche power and time define a change in flow properties. For each formulation, Figure 3.2 (B) shows a distinct change in flow properties consistent with the beginning of the formulator defined end-point range (Table 3.1). For starch, an additional change was observed with

over-wetting, between 1250 and 1350 mL, where binder addition exceeded the upper formulator end-point limit.

3.3.4. Tablet break load testing

Tablets were compressed at 28 kN, from granules manufactured with different binder volumes. The resulting break loads are plotted in Figure 3.2 (C). For mannitol, binder volumes up to 950 mL yielded tablets with similar break loads. At 1000 mL, break load decreased significantly indicating weaker tablets and defining 1000 mL as the upper end-point limit. For starch, the break load reached a maximum between 1050 and 1150 mL, consistent with the formulator defined end-point range. For dextrose, the break load reached a maximum at 950 mL and decreased rapidly at higher binder volumes, supporting an upper end-point limit of less than 1000 mL.

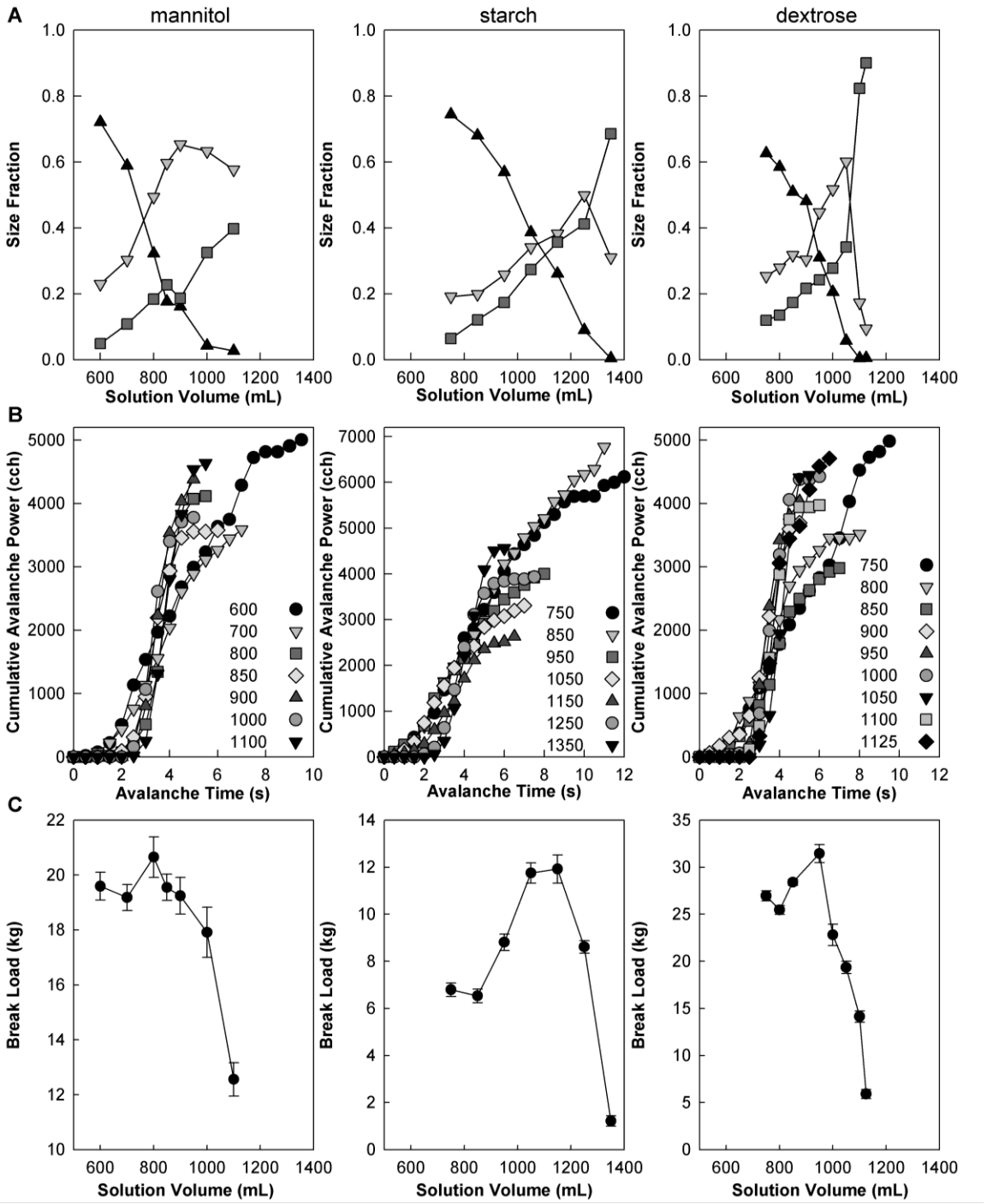

Figure 3.2 A – Size fraction versus solution volume for fines (▲), midsized (▼), and large fractions (■), B – Cumulative total avalanche power versus avalanche time, C – Break load versus solution volume at 28 kN compression force. Formulations: mannitol, starch and dextrose (left to right).

3.3.5. Acoustic results

Microphone location

Microphones were attached to the granulator at five different locations (Figure 3.1) to investigate different sources of sound. The bowl wall targeted particle-equipment contacts, similar to previous ultrasonic work [9, 10]; the motor location was based on research showing impeller power consumption and torque are sensitive to granulation [6]; and the air exhaust targeted AAEs from the mixing and wetting process, in continuation of audible acoustic work by Briens et al. [11] and Daniher et al. [12]. AAEs collected with the microphones on the bowl and motor did not change significantly during granulation (Appendix B). Both air exhaust microphones showed sensitivity to granulation, with profiles for the inside microphone (Figure 3.1, M2) showing higher magnitudes due to closer proximity to granulation AAEs and decreased interference from external AAEs (Appendix B).

TPSD profiles (20-20,000 Hz)

The 20-20,000 Hz TPSD profiles were unique for each formulation and all demonstrated sensitivity to granulation (Figure 3.3). In each case, variability between runs was observed at the start of wetting, likely due to different particle arrangements after dry mixing. Following approximately 600 mL of binder addition, run variability was reduced and TPSD decreased gradually through the respective end-point region for each formulation.

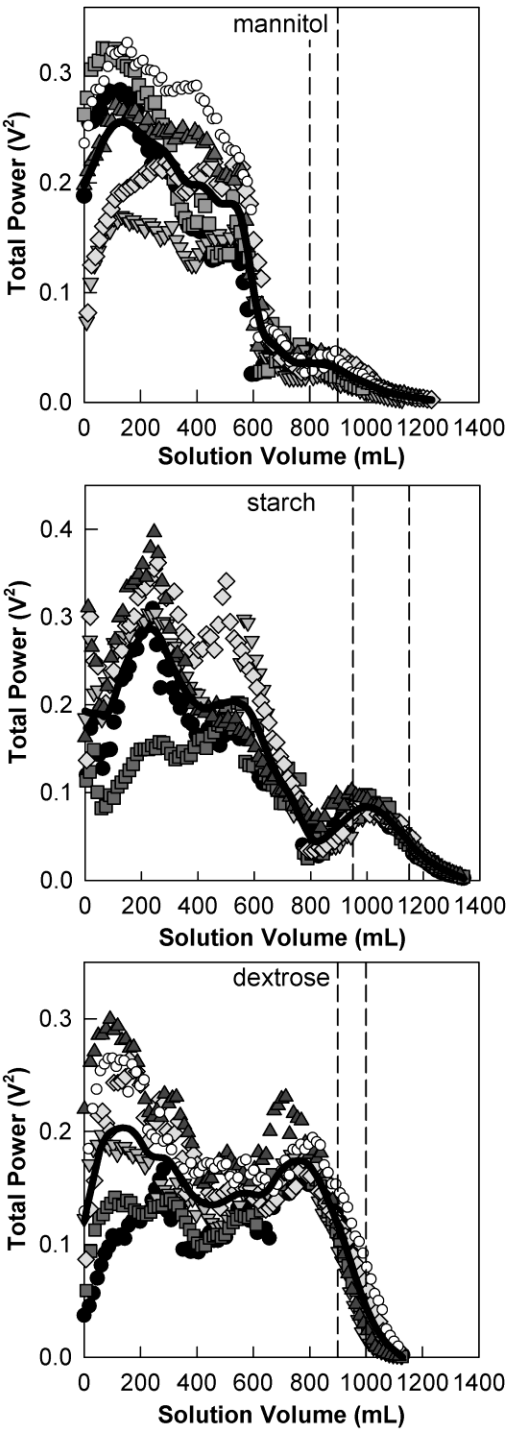

Figure 3.3 Total power versus solution volume from 20-20,000 Hz. Runs defined as Run 1 (●), Run 2 (▼), Run 3 (■), Run 4 (◆), Run 5 (▲), Run 6 (○) (mannitol and dextrose only). End-point range defined by dashed vertical lines (---).

Frequency filtering of the 20-20,000 Hz TPSD profiles

The full frequency TPSD profiles were divided into 50 Hz groups and information relevant to granulation was observed to be concentrated below 250 Hz. The 20 to 250 Hz region was then divided into 10 Hz groups and each TPSD profile was manually examined for (1) reproducibility between runs and (2) distinct maxima and minima; Table 3.2 summarizes the 10 Hz groups that satisfied these criteria and TPSD profiles for select ranges are shown in Figure 3.4.

Table 3.2 Frequency ranges identified manually and by PLS-DA

Mannitol		Starch		Dextrose	
Manual (Hz)	PLS-DA (Hz)	Manual (Hz)	PLS-DA (Hz)	Manual (Hz)	PLS-DA (Hz)
100-110*	100-110[a,]*	-	30-40[b]	-	60-70[b]
110-120	110-120[a]	80-90	80-90[a]	80-90*	80-90[a,]*
-	130-140[b]	100-110*	100-110[a,]*	100-110*	100-110[a,]*
-	150-160[b]	110-120*	110-120[a,]*	110-120	110-120[a]
200-210*	200-210[a,]*	-	130-140[b]	130-140	130-140[a]
-	210-220[b]	-	150-160[b]	210-220	210-220[a]
-	270-280[b]	-	160-170[b]	-	230-240[b]
-	370-380[c]	200-210	200-210[a]	-	250-260[b]
-	450-460[c]	210-220	210-220[a]	-	260-270[b]
		-	250-260[b]	-	270-280[b]
		-	270-280[b]	-	290-300[c]
		-	1370-1380[c]	-	300-310[c]
				-	310-320[c]
				-	2970-2980[c]

Abbreviation: (-) no value
[a] Clear profile.
[b] Noisy trend.
[c] Random noise.
*Total PSD profile shown in Figure 3.4.

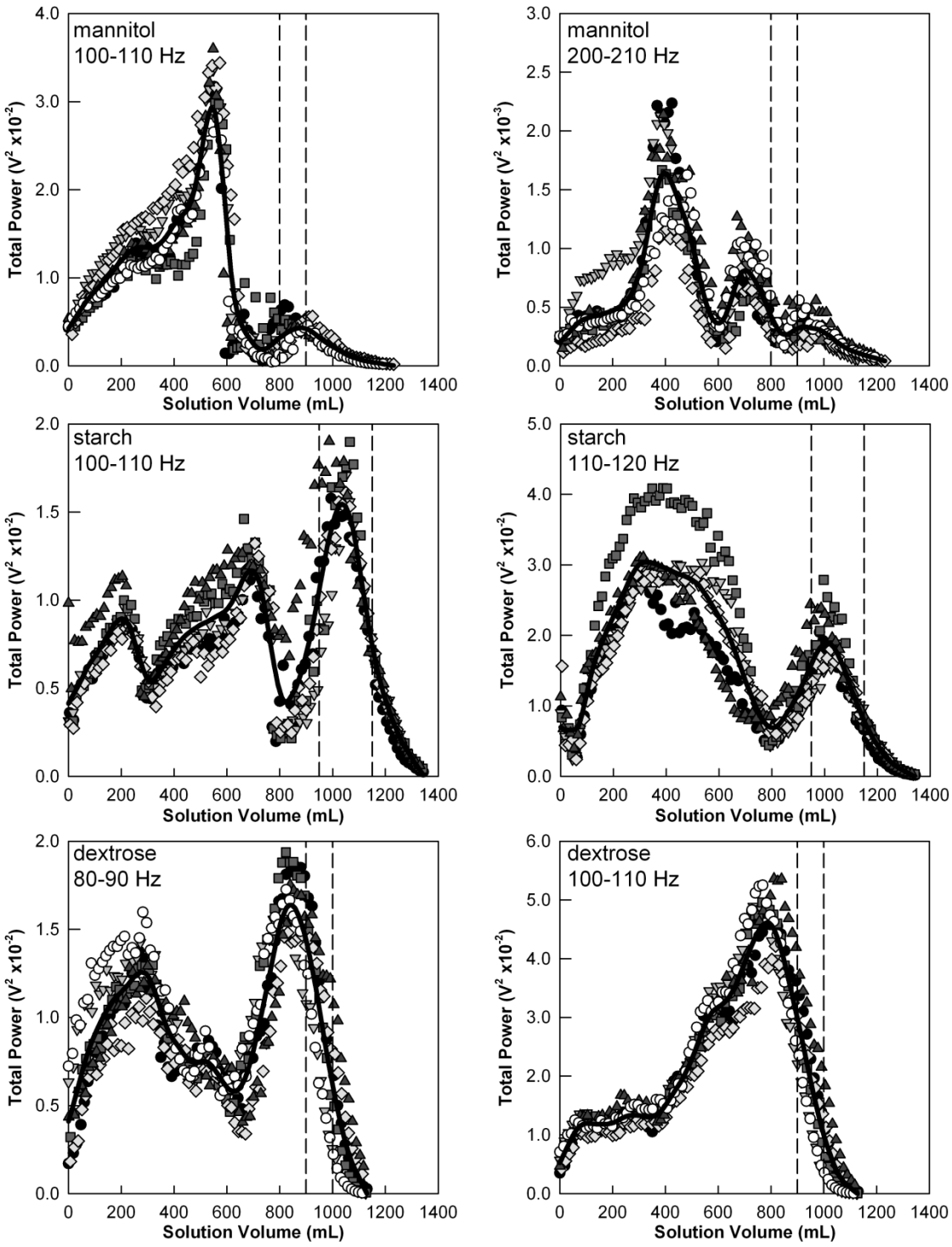

Figure 3.4 Total power versus solution volume. Runs defined as Run 1 (●), Run 2 (▼), Run 3 (■), Run 4 (◆), Run 5 (▲), Run 6 (○) (mannitol and dextrose only). End-point range defined by dashed vertical lines (---).

Frequency filtering using VIP analysis of the PLS-DA models

For each formulation, TPSD data for 10 Hz frequency groups from 20-20,000 Hz was used to generate a PLS-DA model for each run and VIP analysis was performed. If the VIP value for a particular frequency group was greater than one for all runs, it was retained in the PLS-DA model. VIP analysis was then repeated on the refined models to further reduce the total number of 10 Hz frequency groups (Figure 3.5).

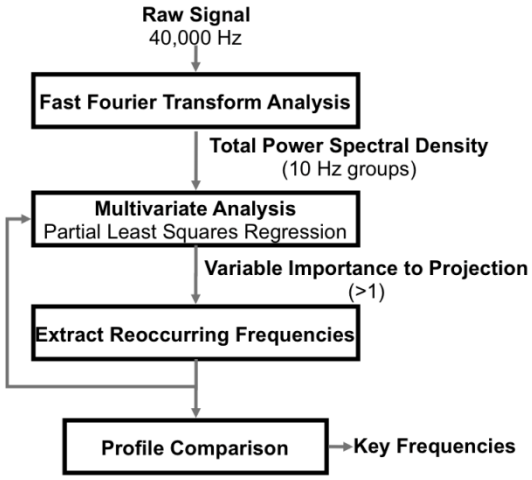

Figure 3.5 PLS-DA method for selection of key frequencies.

The first iteration of the VIP analysis was found to reduce the number of relevant frequency groups by an average of 94 ± 2%, across the three formulations. The second iteration provided an additional 90 ± 2% reduction, for an overall decrease of 99% for each formulation. The final frequency groups are summarized in Table 3.2 and samples of the types of profiles observed for each formulation are shown for dextrose in Figure 3.6. The types of profiles are: clear profiles, with low variability between runs and significant detail throughout binder addition (80-90 Hz); profiles with visible trends but

higher run variability (230-240 Hz); and profiles with no visible relationship to granulation (310-320 Hz). Since not all profile types are ideal for granulation monitoring and control, relevant frequency groups were identified by applying the manual selection criteria outlined previously (Table 3.2).

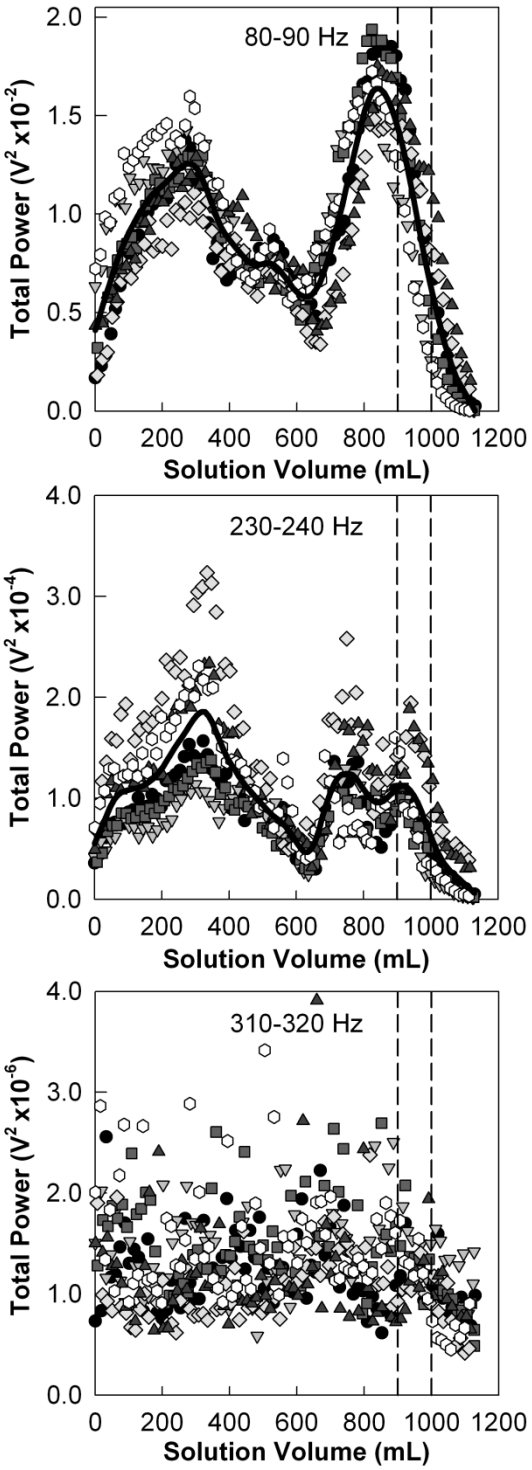

Figure 3.6 Total power versus solution volume for dextrose. Runs defined as Run 1 (●), Run 2 (▼), Run 3 (■), Run 4 (◆), Run 5 (▲), Run 6 (○). End-point range defined by dashed vertical lines (---).

3.4. Discussion

Analysis of the AAEs from the three formulations builds on earlier research using a lactose based placebo formulation [11, 12]. Together these works demonstrate that AAEs collected in granulator air exhausts can be used for end-point detection with multiple formulations. The 10 Hz frequency groups identified for granulation monitoring and control were different for each formulation; VIP analysis showed proof of concept as a rapid approach for identifying significant frequency groups that will facilitate future work with new formulations.

3.4.1. Interpretation of acoustic results using physical property data

The physical property data used to define granulation end-point provided a means of interpreting changes in the AAE profiles. For mannitol and starch, the peaks in the end-point region corresponded to loss of fines and growth in midsized and large granules, a change in flow properties, and ideal tablet properties (Figure 3.2-Figure 3.4). For mannitol, wetting resulted in a predominant increase in midsized granules compared to large (Figure 3.2, A); suggesting large granules formed by granule-granule agglomeration were weak and prone to breakage. For starch, wetting formed large and midsized granules at similar rates, until the material was over-wet and large granules became dominant (Figure 3.2, A). Comparing the TPSD profiles (Figure 3.4) showed the peak in the end-point region was significantly smaller and less pronounced for mannitol than starch, suggesting its intensity is driven by the formation of large granules.

For dextrose, the final peaks occurred prior to end-point and corresponded to dominant fines, flow properties inconsistent with end-point flowability, and suboptimal tablet properties (Figure 3.2-Figure 3.4). The reason for the disparity between dextrose and the other two formulations is unclear but could be the result of a different response to wetting. The reduction in TPSD throughout the end-point region for all formulations is consistent with observations at similar frequencies for fluidized sand grains, where excess moisture is cited as inhibiting sound [24-27]. For dextrose, a different response to wetting could have resulted in AAEs becoming damped before the peak related to growth in large granules was reached. Further studies are required to fully explain these observed differences in TPSD with formulation.

3.4.2. Important features in the 10 Hz TPSD profiles

Physical analysis defined three stages of granulation: 1. wetting, where binder was added to reach end-point; 2. end-point, where binder volumes produced optimal granules; and 3. over-wet, where binder volumes exceeded end-point requirements. Features related to both wetting and end-point stages are critical to the development of AAEs for online use. The 20-20,000 Hz profiles (Figure 3.3) would not be suitable for monitoring the wetting stage, because variability between runs was significant. Breaking the profiles into 10 Hz groups however, was effective for improving run reproducibility and isolating distinct maxima and minima related to granulation stage (Table 3.2, Figure 3.4). Peaks related to end-point would be useful for determining

when to stop a batch, and peaks during wetting would be useful for monitoring batch progress and anticipating end-point.

Mannitol

For mannitol, 10 Hz profiles showed the following early warning signals for end-point control: a local minimum 75 mL prior to end-point (100-110 Hz) and a local maximum 100 mL prior to end-point (200-210 Hz) (Figure 3.4). In addition, monitoring of the wetting stage is supported by distinct and reproducible peaks during the first 500 mL of binder addition in both 10 Hz profiles (Figure 3.4).

Starch

For identifying end-point, the 100-110 Hz and 110-120 Hz profiles (Figure 3.4) accentuated two features in the full frequency profile (Figure 3.3): a local minimum, approximately 150 mL before the end-point and a distinct peak in the end-point region. The minimum could be used to gauge end-point, by signaling the amount of binder remaining. The peak supports online end-point detection, by providing a signal to stop binder addition. Both 10 Hz profiles (Figure 3.4) also show additional local maxima and minima preceding the end-point region that would be suitable for assessing granulation progress.

Dextrose

For dextrose, end-point consistently coincided with the final decrease in TPSD (Figure 3.3, Figure 3.4). The peak preceding the decrease is accentuated in the 10 Hz TPSD

profiles and supports use as an early warning signal (Figure 3.4). The 10 Hz profiles also support monitoring of the wetting stage, using the gradual increase to a maximum (80-90 Hz) or the plateau followed by a gradual increase (100-110 Hz).

Summary

The selected 10 Hz frequency groups (Table 3.2) were different for each formulation, as were the corresponding TPSD profiles (Figure 3.4). Only the starch profiles showed distinct peaks within the defined end-point region; however, early warning peaks 50-100 mL prior to end-point are equally, if not more useful because they would allow time for response with less risk of over-wetting. The profiles were all shown to contain information related to both the wetting and end-point phases, in support of ultrasonic work suggesting granulation does not produce new frequencies but rather alters the acoustic intensity of existing frequencies [10].

3.4.3. Assessment of the PLS-DA method for identification of key frequency groups

The formulation dependence of the key frequency groups poses a challenge for further development of audible acoustics as a PAT tool, since each new formulation would require generation and analysis of nearly 2000 new graphs. The PLS-DA method (Figure 3.5) was developed to simplify the review of all 10 Hz TPSD profiles (Table 3.2). The ability of VIP analysis to identify frequency groups satisfying the manual selection criteria outlined in section 3.3.5. supports the use of the PLS-DA method for rapid frequency selection. VIP analysis also identified frequency groups that did not satisfy

the manual selection criteria, due to the nature of the PLS-DA algorithm. For example, the 230-240 Hz profiles contain features similar to 80-90 Hz (Figure 3.6) but with less defined peaks and higher variability between runs; therefore 230-240 Hz was likely identified because of a correlation with 80-90 Hz. The 310-320 Hz profiles shows no apparent relationship to granulation stage and 310-320 Hz was likely selected for its ability to explain differences between frequency groups, rather than differences between granulation stages. While profiles such as 310-320 Hz still necessitate application of manual selection criteria, the number of frequency groups to assess is considerably less and the method can be easily applied to large datasets.

3.5. Conclusions

Building on proof of concept work by Briens et al. [11] and Daniher et al. [12], AAEs collected from the granulator air exhaust were shown to contain features related to end-point for three different formulations. For each formulation, formulator defined end-point ranges were supported by physical property analysis, allowing for objective interpretation of the acoustic results. A consistent decrease in the TPSD profiles was found to coincide with end-point for each formulation and frequency filtering was used to reduce variability between runs and accentuate features that would be useful for online end-point detection and process monitoring. In addition, PLS-DA demonstrated proof of concept as an objective method for identifying key frequency groups and may

be useful for the development of new formulations or scale-up activities. Overall, the findings support further development of AAEs as a PAT tool.

3.6. References

[1] U.S. Department of Health and Human Services, Food and Drug Administration, Center for Drug Evaluation and Research (CDER) & Center for Biologics Evaluation and Research (CBER). (2008). *Guidance for industry Q8 pharmaceutical development, second revision*. Retrieved from http://www.fda.gov/downloads/Drugs/GuidanceComplianceRegulatoryInformation/Guidances/ucm073507.pdf.

[2] Summer, M. (2002). Powders and granules. In M. Aulton (Ed.), *Pharmaceutics: The science of dosage form design, 2nd edition*. Spain: Elsevier.

[3] Iveson, S.M., Litster, J.D., Hapgood, K. & Ennis, B.J. (2001). Nucleation, growth and breakage phenomena in agitated wet granulation processes: a review. *Powder technology, 177,* 3-39.

[4] Parikh, D.M. (1997). *Handbook of pharmaceutical granulation technology drugs and pharmaceutical sciences, 81,* New York: Marcel Dekker Inc.

[5] Watano, S. (2007). Online monitoring. In A. Salman, M. Hounslow & J. Seville (Eds.), *Handbook of powder technology*, *11*. The Netherlands: Elsevier.

[6] Faure, A., York, P. & Rowe, R.C. (2001). Process control and scale-up of pharmaceutical wet granulation processes: a review. *European journal of pharmaceutics and biopharmaceutics, 52,* 269-277.

[7] Hardy, I.J. & Cook, W.G. (2003). Predictive techniques for the design, optimisation and manufacture of solid dosage forms. *Journal of pharmacy and pharmacology, 55*, 3-18.

[8] Räsänen, E. & Sandler, N. (2007). Near infrared spectroscopy in the development of solid dosage forms. *Journal of pharmacy and pharmacology, 59,* 147-159.

[9] Whitaker, M., Baker, G., Westrup, J., Goulding, P., Rudd, D., Belchamber, R. & Collins, M. (2000). Application of acoustic emission to the monitoring and end point determination of a high shear granulation process. *International journal of pharmaceutics, 204,* 79-91.

[10] Papp, M. Pujara, C. & Pinal, R. (2008). Monitoring of high-shear granulation using acoustic emission: predicting granule properties. *Journal of pharmaceutical innovation*, 3, 113-122.

[11] Briens, L., Daniher, D. & Tallevi, A. (2007). Monitoring high-shear granulation using sound and vibration measurements. *International journal of pharmaceutics, 331,* 54-60.

[12] Daniher, D., Briens, L. & Tallevi, A. (2008). End-point detection in high-shear granulation using sound and vibration signal analysis. *Powder technology*, *181,* 130-136.

[13] Bass, H.E., Campanella, A.J., Chambers, J.P. & Lindsay, R.B. (2008). Sound absorption. *AccessScience, McGraw-Hill Companies*. Retrieved from www.accessscience.com.

[14] Wold, S., Sjöström M. & Eriksson, L. (2001). PLS-regression: a basic tool of chemometrics. *Chemometrics and Intelligent laboratory systems, 58,* 109-130.

[15] Miletic, I., Quinn, S., Dudzic, M., Vaculik, M. & Champagne, M. (2004). An industrial perspective on implementing on-line applications of multivariate statistics. *Journals of process control, 14,* 821-836.

[16] Berrueta, L.A., Alonso-Salces, R.M. & Héberger, K. (2007). Supervised pattern recognition in food analysis. *Journal of chromatography, 1158,* 196-214.

[17] Chong, I. & Jun, C. (2005). Performance of some variable selection methods when multicollinearity is present. *Chemometrics and Intelligent laboratory systems, 78,* 103-112.

[18] Hemmateenejad, B. & Mohajeri, A. (2007). Application of quantum topological molecular similarity descriptors in QSPR study of the o-methylation of substituted phenols. *Journal of computational chemistry, 29,* 266-274.

[19] Musmarra, G., Trovato-Salinaro, A., Scirè, S., Foti, A., Barresi, V., Fortuna, C.G., Strazzulla, G. & Condorelli, D.F. (2007). Identification of genes involved in radiation-induced G_1 arrest. *Journal of chemometrics, 21,* 398-405.

[20] Mohajeri, A., Hemmateenejad, B., Mehdipour, A. & Miri, R. (2008). Modeling calcium channel antagonistic activity of dihydropyridine derivatives using QTMS indices analyzed by GA-PLS and PC-GA-PLS. *Journal of molecular graphics modeling, 26,* 1057-1065.

[21] Sun, H. (2004). Prediction of chemical carcinogenicity from molecular structure. *Journal of chemical information and modeling, 44,* 1506-1514.

[22] Yoo, C. & Gernaey, K.V. (2008). Classification and diagnostic output prediction of cancer using gene expression profiling and supervised machine learning algorithms. *Journal of chemical engineering Japan, 41,* 898-914.

[23] Dodson, M. (1992). Shannon sampling theorem. *Current science, 63,* 253-260.

[24] Sholtz, P., Bretz, M. & Nori, F. (1997). Sound-producing sand avalanches. *Contemporary physics, 38,* 329-342.

[25] Douady, S., Manning, A., Hersen, P. Elbelrhiti, H., Protière, S., Daerr, A. & Kabbachi, B. (2006). Song of the dune as a self-synchronized instrument. *Physical review letters, 97,* 1-4.

[26] Andreotti, B. (2004). The song of dunes as a wave-particle mode locking. *Physical review letters, 93*, 1-4.

[27] Vriend, N.M., Hunt, M.L., Clayton, R.W. & Brennen, C.E. (2007). Solving the mystery of booming sand dunes. *Geophysical research letters, 34,* 1-6.

Chapter 4

4. An investigation of the relationship between audible acoustic emissions and particle size

4.1. Introduction

Acoustic emission monitoring is a non-invasive means of collecting information about a process. It has been applied in the chemical, biochemical and food industries to monitor a diverse range of operations, including gas-liquid mixing and powder flow [1]. An advantage of acoustic emission monitoring is the ability to collect information in real-time and without product contact. In the pharmaceutical industry, acoustic emissions have been investigated as a process analytical technology (PAT) for monitoring batch operations, such as granulation. Granulation processes are complex and depend on a large number of interrelated variables. Acoustic emissions have shown potential to increase process understanding and provide a basis for online monitoring and control [2-6]. For fluidized-bed granulation, Tsujimoto et al. [2] calibrated an acoustic emissions sensor at various fluidization conditions using microcrystalline cellulose spheres of uniform size. The results led to the development of a method for detecting the onset of unstable fluidization conditions. Briongos et al. [3] identified different flow regimes for glass ballotini beads in a fluidized-bed granulator, by applying time, frequency and state space analysis to acoustic emissions. For high-shear granulation, Briens et al. [4] demonstrated the potential for end-point detection using mean frequency and one-third octave band techniques to analyze acoustic emissions collected from 10 and 25 L

PMA granulators. The findings were further developed by Hansuld et al. [5] to show the total power spectral density (TPSD) for 10 Hz frequency groups could be used to develop detailed process signatures for monitoring and control. In addition, Gamble et al. [6] developed a multivariate model for detecting end-point in a small-scale granulator using online data collected from a GranuMet XP acoustic emissions system.

The applications for acoustic emissions are evident but little research has been done to understand the source of generation and why the technology is effective. Early work by researchers such as Leach and Rubin [7-10] and Hidaka and Shimosaka [11] has led to the theory that acoustic emissions are generated by particle-particle and particle-equipment collisions, as well as the friction produced upon contact. Leach and Rubin showed the acoustic frequency is inversely related to particle size and can be used to characterize the shape and width of size distributions for beds of particles [7, 9]. The relationship was initially developed using glass and metallic spheres between 50 μm and 3 cm, and was later extended to rigid particles of irregular shape using gravel [10]. Hidaka and Shimosaka [11] studied acoustic emissions from particle flow, by measuring the impact sound from two spheres colliding on a plate and the flow noise from a group of steel balls moving down an incline. A positive correlation was developed between the acoustic pressure and the macroscopic velocity of the flowing particles. The works support a relationship between acoustic emissions and particle size but further investigation is required to extend the findings to the granulation process.

For fluidized-bed granulation, Tsujimoto et al. [2] showed the mean amplitude of the acoustic emissions is directly proportional to the d50 particle size and Matero et al. [12] utilized multivariate models to demonstrate a predictive relationship between acoustic emissions and particle size. For high-shear granulation, multivariate work by Whitaker et al. [13] showed a positive correlation between the frequency spectrum from the last 20 s of granulation and the mass mean particle size of the granules before dry screening. Similarly, Papp et al. [14] used multivariate techniques to compare final granule properties to the average frequency spectra and waveform data from the last 10 s of granulation. A positive relationship was observed between the acoustic emissions and mean particle size for two pilot-scale granulators. In addition, previous work by Hansuld et al. [5] suggested a correlation between the acoustic intensity and particle size, where an increase in particle size was shown to correspond to a higher TPSD maximum. In all cases, the relationship between acoustic emissions and size is evident but there is an absence of studies to understand the process behaviours responsible for the observed results.

In general, there is considerable research supporting a relationship between granulation acoustic emissions and changes in particle size but further work is required to better understand the origin of the correlation. The following article focuses on understanding the relationship between audible acoustic emissions (AAEs) from granule shearing and particle size. AAEs were generated by rotating dry MCC and sugar spheres in stainless

steel beakers and the effect of particle size was isolated by eliminating other potential sources of AAEs, such as the impeller, moisture content, and changes in density.

4.2. Materials and methods

4.2.1. Materials

Four sizes of MCC spheres (Celphere), 106-212, 150-300, 500-710 and 710-850 µm, and seven sizes of sugar spheres (Paulaur), 177-250, 250-354, 400-500, 500-595, 595-707, 841-1000, 1000-1190 µm were used. The sugar spheres were a generous donation from L.V. Lomas Limited (Brampton).

Wet granules were manufactured from a placebo formulation consisting of dextrose anhydrous (Roquette), mannitol (Pearlitol® 160C, Roquette), microcrystalline cellulose (Avicel® PH 101, FMC Biopolymer), hypromellose 2910 (Pharmacoat® 603, Shin-Etsu Chemical Co.) and croscarmellose sodium (AcDiSol®, FMC Biopolymer), for a total batch size of 1.8 kg.

4.2.2. Shearing MCC and sugar spheres in stainless steel beakers

A Lab-line orbital shaker operating at 350 rpm was used to generate a shearing motion for 0.15 and 1.5 kg of spheres in 1.2 and 12 L Polar Ware beakers, respectively (Figure 4.1). Stainless steel beakers were selected to best match the granulator bowl; however, the beaker surface texture was coarser and the walls were not as thick. To reduce

background noise, the beakers were insulated with foam and sealed with a lid made from 2.5 cm polystyrene insulation. A microphone was positioned above the spheres, secured by a hole in the lid, and a windscreen was used to protect the microphone face from dust (Dalimar Instruments Inc., Richmond Hill). AAEs were collected in triplicate for each sphere size over an acquisition period of three minutes. Attrition was shown to be negligible in these experiments.

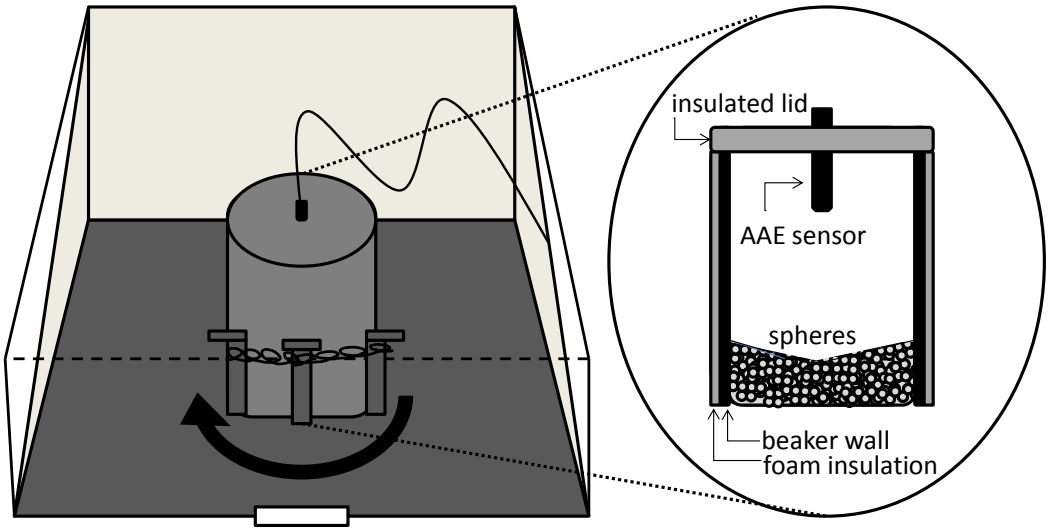

Figure 4.1 Equipment setup for shearing in stainless steel beakers. Arrow indicates direction of platform rotation to induce shearing.

4.2.3. Shearing MCC spheres in a granulator

Three 2.5 kg samples of each MCC sphere size were rotated for three minutes in a Niro-Fielder PMA-10 high-shear granulator at an impeller speed of 350 rpm. AAEs were collected using a microphone positioned inside the air exhaust, 20 cm from the exhaust base.

4.2.4. Shearing wet granules in a stainless steel beaker

Wet granules prepared in a Niro-Fielder PMA-10 granulator were rotated in a 12 L beaker, following the methodology described in section 4.2.2. The granules were prepared by passing the materials through an 850 µm sieve and dry mixing for 5 min at an impeller speed of 350 rpm and chopper setting II. Water was added at 55 mL/min through a spray nozzle positioned right-of-center. Granule size was varied by stopping the batches at different total binder volumes. The total binder was varied between 250 and 750 mL, incrementing by 100 mL per batch. A 20 g sample was withdrawn for each batch and tray dried to less than 2% loss on drying using a GCA convection oven (80 °C). The size distribution of the dry granules was measured using an ATM Sonic Sifter with a pulse amplitude of 9 and a 5 min sift/pulse setting. The sieve set consisted of 150, 180, 250, 355, 600 and 850 µm ATM U.S. standard sieves and a fines collector.

4.2.5. Signal collection

AAEs were collected at 40,000 Hz using a PCB Piezotronics condenser microphone (model 130D20) and conditioned using an ICP sensor signal conditioner (PCB Piezotronics). The signal range was optimized to ±0.5 V for the beaker experiments and ±10 V for the granulator experiments, equating to gains of 10 and 0.5 respectively. A National Instruments data acquisition system and LabVIEW 8.5 software were used for signal collection.

4.2.6. Signal analysis

Total power spectral density (TPSD)

Initial data processing was performed using Matlab 6.5. The AAE data was divided into 10 s segments and the power spectral density was computed to convert each time series into a frequency spectrum. TPSD was determined for each segment by summing the resulting frequency data into 10 Hz groups from 20 to 20,000 Hz.

Multivariate analysis

Principal component analysis (PCA) and orthogonal projection to latent structures by means of partial least squares (OPLS) were used to model the processed AAEs. In PCA, a multidimensional dataset, *X* is represented by a small number of linear relationships, known as principal components. The principal components are orthogonal to each other and together form a plane or hyper-plane. The original data is projected onto the principal components to provide a representation of the systematic variation in the data matrix over a reduced number of dimensions. When the observations are projected into the reduced dimensional space the new coordinates are known as scores and are represented by *t*. The loadings, *p* describe how the original *X* variables are combined to form the new projection coordinates [15].

The difference between PCA and OPLS is the addition of a *Y* variable for OPLS. As a result, the principal components not only describe the relationship between the *X* variables, but also represent the relationship between *X* and *Y*. The first principal component is known as the predictive component and describes the ability to predict *Y*

from *X*. Additional components are known as orthogonal components and describe variability unrelated to *Y*. The scores for *X* are represented by a vector, *t* and the scores for *Y* are represented by a vector, *u*. The weights, *w* and *c*, are used to convert the original variables to the new projection coordinates for the *X* and *Y* matrices, respectively [15]. In this work, PCA and OPLS models were constructed in SIMCA-P+ 11.5 using the 10 Hz TPSDs from 20-20,000 Hz as *X* and mean size as *Y*. The number of principal components was determined by cross validation and unit variance scaling was used for data preprocessing, according to the default approach in SIMCA. In addition, the auto-transformation function was used to achieve a normal distribution in the residuals.

4.3. Results

The relationship between the AAEs and size was explored using PCA and OPLS multivariate models to analyze the 10 Hz TPSDs. AAEs were compared for two types of dry spheres, MCC and sugar, in two vessel sizes. The scores, *t* and *u*, were used to determine whether the 10 Hz TPSDs were predictive of size and the weights, *w* and *c*, were used to determine whether the correlations were positive or negative. The results were compared to OPLS models for MCC spheres in the granulator and wet granules in the 12 L beaker.

4.3.1. MCC and sugar spheres in the 1.2 and 12 L beakers

PCA modeling of AAE data

The PCA scores plots provided a summary of the variation in the original 10 Hz TPSDs using the projection coordinates for the first (*t[1]*) and second (*t[2]*) principal components. For MCC and sugar spheres in the 1.2 and 12 L beakers, the observations separated into groups based on sphere size. Figure 4.2 shows a representative example for MCC spheres in the 1.2 L beaker. The scores plot shows the observations arranged in four groups, one for each sphere size. Observations located close to one another have similar properties; therefore, the PCA scores show the 10 Hz TPSDs were similar for spheres of the same size.

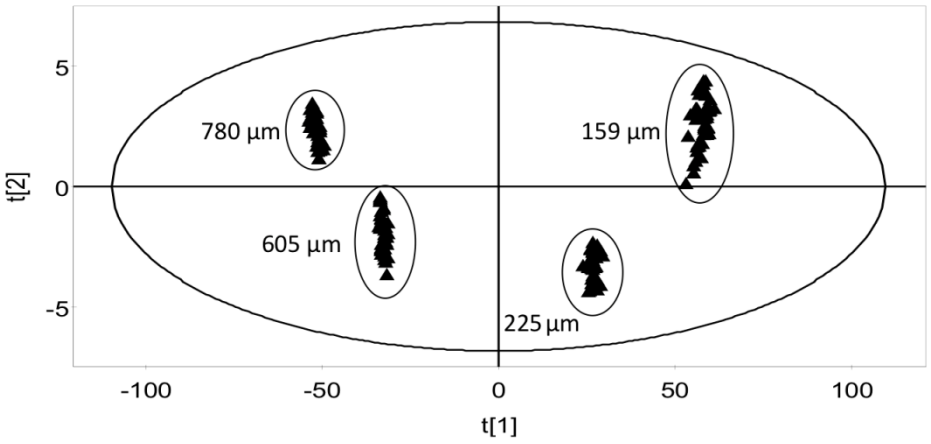

Figure 4.2 PCA scores plot for MCC spheres in the 1.2 L beaker, where *t[1]* and *t[2]* represent the projection coordinates for the first and second principal components, respectively.

OPLS modeling of AAE and size data

Multivariate OPLS models were used to assess the predictive relationship between the 10 Hz TPSDs and size. Figure 4.3 shows the projection coordinates for the 10 Hz TPSDs

(*t[1]*) versus size (*u[1]*), for MCC and sugar spheres in the 1.2 and 12 L beakers. The observations are located along the diagonal and separated into groups based on sphere size, confirming the relationship between size and TPSD proposed in the PCA models. The proximity of the data to the diagonal indicates the relationships are linear and there is a strong ability to predict size from TPSD. The relationship holds for the two different sphere materials and the two vessel sizes.

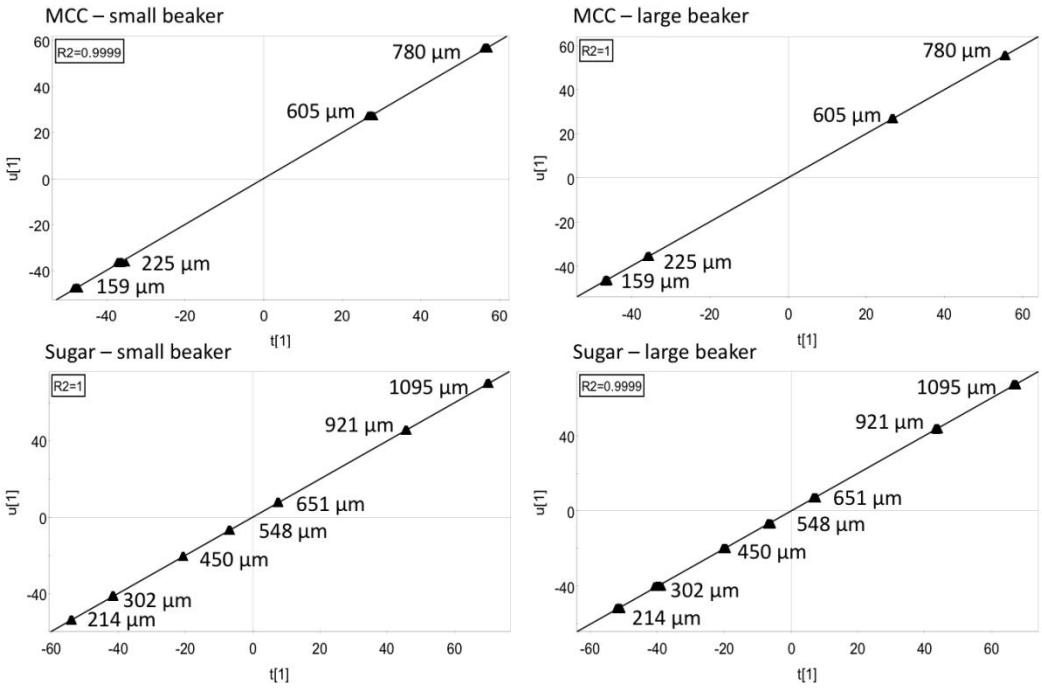

Figure 4.3 Projection coordinates for the TPSDs (*t[1]*) versus projection coordinates for sphere size (*u[1]*), for MCC and sugar spheres in the 1.2 and 12 L beakers. The observations are labeled based on sphere size.

Figure 4.4 summarizes the OPLS weights used to generate the projection coordinates, *t* and *u*. The weights associated with the 10 Hz TPSDs are represented by *w* and the weights associated with size are represented by *c*. The combination, *w*c* allows the

weights for both types of variables to be viewed together, providing information on the correlation structure between the 10 Hz TPSDs and size. Figure 4.4 shows the *w*c* values for the four experiments in a line plot. The *w*c* values for the 10 Hz TPSDs from 20 to 250 Hz are shown first (grey triangles), followed by the single *w*c* value for size (black square). The *w*c* values for the 10 Hz TPSDs are mostly positive. Since the *w*c* value for size is also positive, the majority of the 10 Hz TPSDs are positively correlated to size. The 10 Hz TPSDs that are not positively correlated with size are associated with low frequency groups. The low frequency groups are negatively correlated with size and suggest a difference in sound source compared to the frequency groups that are positively correlated.

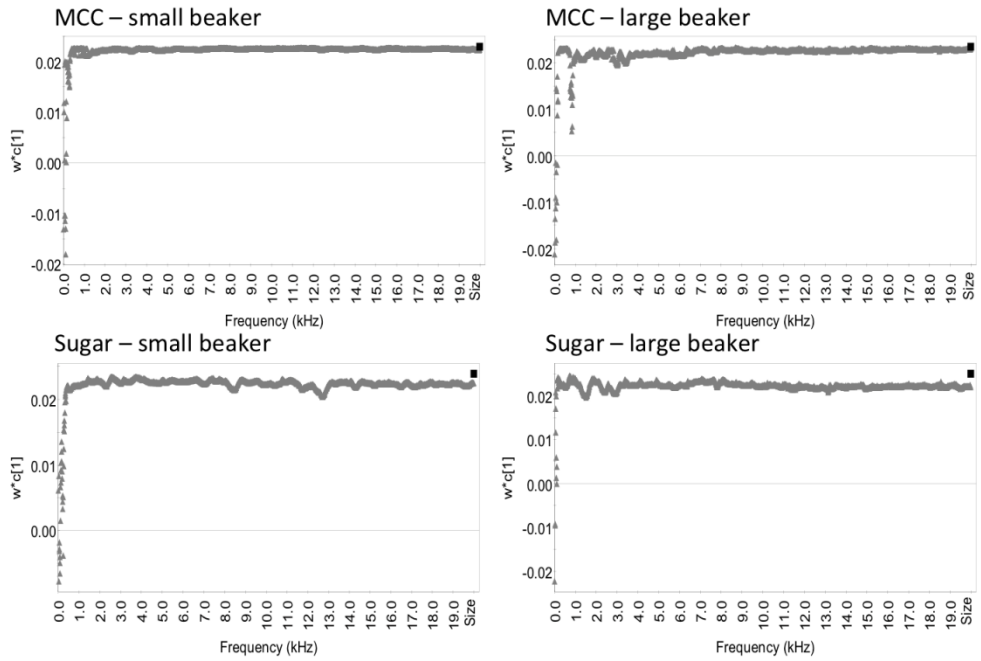

Figure 4.4 OPLS weights (*w*c*) for each 10 Hz TPSD variable (▲) and size (■), where the 10 Hz TPSDs are listed in kHz by starting frequency i.e. 1000-1010 Hz corresponds to 1 kHz.

4.3.2. MCC in the granulator

The relationship observed between the 10 Hz TPSDs and size was extended to the granulator using the MCC spheres. Figure 4.5 summarizes the projection coordinates and associated weights for the resulting OPLS model. The projection coordinates, *t[1]* and *u[1],* show the 10 Hz TPSDs were good predictors of size when the MCC spheres were rotated in the granulator. The relationship is linear, as all observations are located on the diagonal. The weights, summarized in the *w*c* line plot, show the 10 Hz TPSDs were primarily positively correlated with size, except at low frequencies where negative correlations were observed. The correlations are similar to those identified for the spheres in the 1.2 and 12 L beakers (Figure 4.3, Figure 4.4). Additional variability was observed in the *w*c* values for frequency groups below approximately 3.5 kHz, likely due to additional noise from the motor and impeller for the granulator experiments. Overall, the agreement between the OPLS models for the beakers and the granulator suggests the beakers are a good approximation of the shearing motion in the granulator.

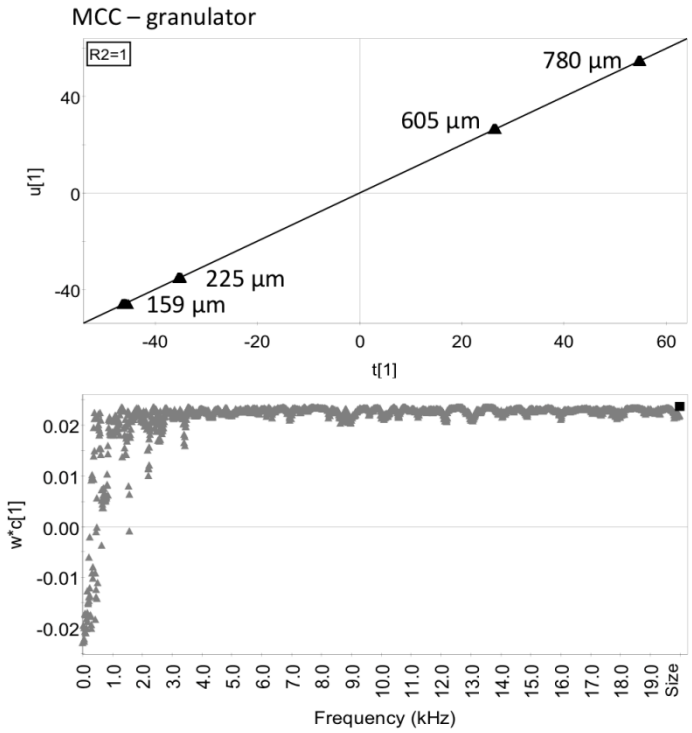

Figure 4.5 Top – Projection coordinates for the TPSDs (*t[1]*) versus projection coordinates for sphere size (*u[1]*), for MCC spheres in the granulator. Bottom – OPLS weights (*w*c*) for each 10 Hz TPSD variable (▲) and size (■), where the 10 Hz TPSDs are listed in kHz by starting frequency i.e. 1000-1010 Hz corresponds to 1 kHz.

4.3.3. Wet granules in the 12 L beaker

The OPLS results in Figure 4.6 examine the relationship between AAEs and size for wet granules in the 12 L beaker. The mean size for the wet granules was approximated from the sieve analysis of the dry granules. The projection coordinates, *t[1]* and *u[1]*, show the 10 Hz TPSDs from the wet granules were good predictors of size. The relationship is linear, even though the growth of granules often starts slowly and increases more rapidly once a critical binder volume has been reached [16]. In the OPLS model, nonlinearities can be identified from the spacing of the observations along the diagonal.

The spacing between samples is tighter towards the start of wetting, where growth was slow, and increases as the binder content increased and granule growth accelerated. The linear relationship suggests multivariate analysis can be used to simplify the expression of complex, nonlinear processes.

The *w*c* values corresponding to the 10 Hz TPSDs are more variable for the wet granules than the spheres (Figure 4.6, Figure 4.4). Strong positive correlations are observed for frequency groups near 0.5, 4 and 7 kHz, and the low frequency groups show negative correlations that are consistent with the results for the dry spheres (Figure 4.4). The *w*c* values associated with the negative frequency groups are closest in magnitude to the *w*c* value for the size variable, indicating a significant negative correlation between the low frequency groups and size. The increased variability in the high frequency weights may be a result of increased heterogeneity in the properties of the wet granules compared to the dry spheres, or frequency damping with the addition of moisture.

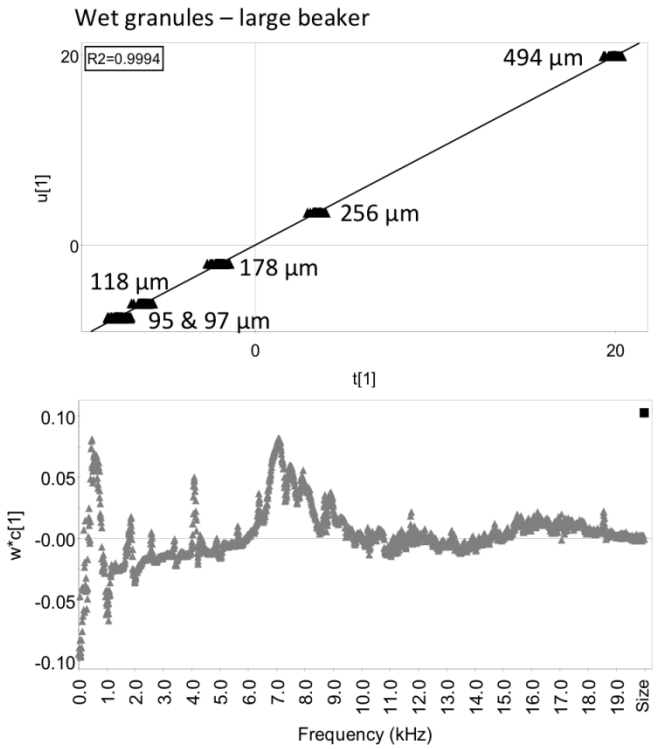

Figure 4.6 Top – Projection coordinates for the TPSDs (*t[1]*) versus projection coordinates for sphere size (*u[1]*), from wet granules in the 12 L beaker. The sizes of the wet granules were approximated using the interpolated d50 sieve size of the dry granules. Bottom – OPLS weights (*w*c*) for each 10 Hz TPSD variable (▲) and size (■), where the 10 Hz TPSDs are listed in kHz by starting frequency i.e. 1000-1010 Hz corresponds to 1 kHz.

4.3.4. Average scores comparison for the low frequency range

The average projection coordinates were compared based on vessel size and fill material, using the low frequency groups that were consistent with negative correlations to size. The range was defined as 20-250 Hz, to encompass the frequency groups previously identified as the most relevant for granulation [5]. The top of Figure 4.7 compares the average OPLS scores for MCC in the 1.2 L beaker, 12 L beaker and granulator. The average scores show an increasing trend with size, independent of

vessel type. The agreement between the scores from the different vessel types suggests the AAEs from particle-equipment interactions were not as significant as the AAEs from particle-particle interactions. The bottom of Figure 4.7 compares the average OPLS scores for MCC spheres, sugar spheres and wet granules in the 12 L beaker versus size. The scores for all three materials show an increasing trend with size. The scores for MCC are parallel to sugar and higher in magnitude. The scores for the wet granules have the highest magnitude and increase at a faster rate. This is likely a reflection of the higher absolute *w*c* weights associated with the low frequency groups for the wet granules compared to the dry spheres. The maximum *w*c* value was approximately 0.1 for the wet granules (Figure 4.6) and 0.02 for the dry spheres (Figure 4.4).

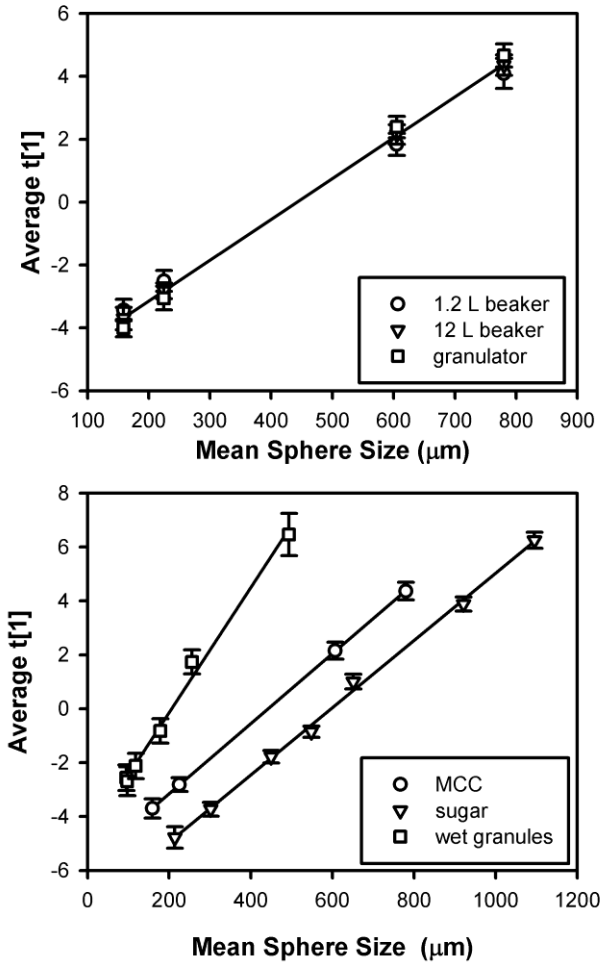

Figure 4.7 Top – Comparison of the average projection coordinates versus size for MCC spheres in the 1.2 L beaker, 12 L beaker and granulator. Bottom – Comparison of the average projection coordinates versus size for MCC spheres, sugar spheres and wet granules in the 12 L beaker. The frequency range for the 10 Hz TPSDs was 20-250 Hz and the size for the wet granules was based on the dry granule sieve size.

4.4. Discussion

The initial PCA modeling of the 10 Hz TPSDs proposed a relationship between AAEs and size, based on the grouping of the observations in the scores plots. OPLS modeling further elucidated the relationship by showing the 10 Hz TPSDs could be used to predict

the size of dry MCC and sugar spheres rotated in 1.2 and 12 L beakers. The majority of the 10 Hz TPSDs were positively correlated with size and some of the low frequency groups were negatively correlated. When the approach was extended to include MCC spheres in the granulator and wet granules in the 12 L beaker, the predictive relationship between AAEs and size was maintained, along with the positive and negative correlations for the various frequency groups.

4.4.1. Positive correlations between AAEs and size

The positive correlations identified between the 10 Hz TPSDs and size support the hypothesis that an increase in particle size contributes to an increase in acoustic intensity. The increase in AAE intensity is believed to be a result of easier flow for surface spheres with increasing size, where the motion of the surface layer primarily results from the transfer of momentum from the vessel wall to the particles and between particles [17]. Momentum transfer is expected to be greater for larger sphere sizes because the mass of the individual spheres is greater. In addition, there would be less contact between large spheres, and consequently lower resistance to motion from interparticle and inertial forces. As a result, the spheres would flow more easily as size increases, with higher flow velocities contributing to greater AAE intensities. The results agree with the theoretical investigation by Hidaka and Shimosaka [11], where acoustic intensity was shown to increase with the macroscopic velocity of the flowing particles.

The positive correlations between the 10 Hz TPSDs and size for the dry spheres suggest AAEs could be used to monitor size for applications with dry powder, such as roller compaction and dry granulation. For both processes, granule size determines whether output is recycled as feed or advanced to downstream operations [18]. By using AAEs to assess particle size in real-time, process efficiency and product quality could be optimized. In addition, the positive correlations provide support for relationships between size and acoustic emissions developed using process data. For example, the positive relationship between the intensity of the maximum TPSD and size observed in an earlier study of high-shear granulation [5]; the positive correlation between final granule size and acoustic emissions identified by Whitaker et al. [13] and Papp et al. [14]; and the increase in the mean amplitude of the acoustic emissions with bed holdup and particle size reported by Tsujimoto et al. [2]. In all three cases, the correlations between size and acoustic emissions were developed using data from granulation processes, where a number of variables were changing simultaneously. Since the variables in the investigations were uncontrolled, there exists the possibility an unmeasured variable was responsible for the observed change in both size and acoustic emissions. The beaker experiments were designed to reduce the potential for an unknown variable and provide insight into one aspect of the AAEs from granulation. As such, the findings demonstrate the sensitivity of AAEs to changes in particle size and provide support for correlations developed using process data.

4.4.2. Negative correlations between AAEs and size

Considering the entire 20-20,000 Hz range, there are relatively few frequency groups with negative correlations to size for the dry spheres. Although the number of negative correlations is small, the associated *w*c* values indicate the negative correlations are as significant as the positive correlations (Figure 4.4). Extraction of meaningful information from noise is a primary capability of multivariate analysis [15]; therefore the source of the negative correlations was considered important for a complete understanding of the AAEs generated during rotation.

The negative correlations identified for the low frequency groups are thought to correspond to a different sound source than the flow of surface particles previously discussed. For the low frequency groups, the decrease in AAE intensity with particle size is believed to result from a reduction in interparticle friction near the base of the vessel, where particle motion is primarily due to the driving force exerted by the impeller [17]. As sphere size increases there would be less contact between larger spheres, and a reduction in interparticle friction would lead to a decrease in AAEs. Interparticle friction is expected to be more significant near the bottom of the vessel due to higher velocities of rotation and the additional weight imposed by particles resting on top of the bottom layer. Research by Saito et al. [19] showed particle velocity is approximately proportional to rotation speed near the source of agitation and significantly less at the surface. The frequencies associated with motors and equipment are typically lower;

therefore, it follows that the frequencies describing the interactions of particles heavily influenced by the equipment would also be lower.

Negative correlations between acoustic emissions and particle size do not appear to be as common in literature, likely because the primary focus of investigations has been on higher frequencies, consistent with the positive correlations identified in the previous section (4.4.1). The low frequency correlations explore a different aspect of the acoustic emissions and may explain the common decrease that has been observed in the 10 Hz TPSD profiles with end-point and over wetting [5]. Towards end-point, moisture on the outside of the granule surface would lead to a decrease in interparticle friction with increasing granule size, resulting in the observed decrease in AAEs. The results suggest different mechanisms of AAE generation dominate at different times throughout the granulation process and provide evidence that AAEs are sensitive to the physical transitions that occur during granulation.

4.4.3. Scale independence for MCC spheres in the 1.2 L beaker, 12 L beaker and granulator

An unexpected result of the OPLS analysis was the similarity in the projection coordinates between the beakers and the granulator (Figure 4.7). The results for the 1.2 and 12 L beakers were expected to be similar because the mass of the spheres was scaled with volume; however, differences in wall thickness and surface texture between the beakers and the granulator were expected to impact AAEs from particle-equipment contacts. Since no major differences were detected, the findings suggest the AAEs were

primarily generated by interactions between particles, rather than the particles and the equipment. As such, the combination of AAEs and multivariate analysis may be useful for applications where the vessel surface or scale changes. In pharmaceutical operations, it is often desired to maintain consistent physical properties when batches are scaled-up during development and again from development to production. A model relating AAEs to particle size could be used to help reduce the time required to achieve a consistent product at a new scale.

4.4.4. Interpretation of average OPLS scores for dry spheres versus wet granules

A comparison of the average OPLS scores showed a greater increase in the projection coordinates with particle size for the wet granules compared to the dry spheres (Figure 4.7). The average OPLS scores correspond to the 20-250 Hz region and therefore represent negative correlations between the 10 Hz TPSDs and size. The difference is thought to be a result of a greater reduction in interparticle friction with increasing size for wet granules. The increase in size coincides with an increase in moisture content and consequently granule cohesion. Cohesion has been observed to lubricate granules and decrease friction between particles [20]. Therefore, as particle size increases for wet granules, interparticle friction would be reduced by two factors: reduced contact between particles and lubrication from water addition. As a result, the AAEs arising from friction would decrease at a faster rate, reflected by the increased magnitude of the average projection coordinates.

The linear relationship shown for the wet granule projection coordinates suggests the potential to use multivariate techniques to simplify the interpretation of complex, non-linear processes (Figure 4.6). Particle size is a critical variable to monitor in granulation because excess fines can affect flow in downstream processes and too many oversized granules may lead to weak tablets with poor uniformity. By developing an OPLS model with AAEs from granulation, it may be possible to track granule growth online. This would provide the opportunity to monitor a critical variable in high-shear wet granulation and introduce an online quality control measure to a process with high variability.

4.5. Conclusions

In this work, a series of controlled experiments were performed to investigate the relationship between particle size and AAEs from granule shearing. Multivariate PCA and OPLS models showed a strong ability to predict size from the 10 Hz TPSDs of the AAEs, for MCC and sugar spheres rotated in 1.2 and 12 L beakers. The relationship was extended to granulation by rotating MCC spheres in a high-shear granulator and wet granules in the 12 L beaker. In both cases, the predictive ability of the AAEs was maintained. The results showed the correlation to size was positive for the majority of the 10 Hz frequency groups, with some negative correlations for low frequency groups. The positive correlations were thought to relate to the motion of granules near the surface and the negative correlations were associated with interparticle friction from

particles rotating at high velocities near the base of the vessel. The findings provide support for the empirical correlations developed using complex process data, and demonstrate potential for monitoring dry and wet processes that depend on size. Future work should involve similar controlled experiments to investigate other critical process variables that may influence AAEs, such as density and moisture content.

4.6. References

[1] Boyd, J.W.R. & Varley, J. (2001). The uses of passive measurement of acoustic emissions from chemical engineering processes. *Chemical engineering science, 56,* 1749-1767.

[2] Tsujimoto, H., Yokoyama, T., Huang, C.C. & Sekiguchi, I. (2000). Monitoring particle fluidization in a fluidized bed granulator with an acoustic emission sensor. *Powder technology, 113,* 88-96.

[3] Briongos, J.V., Aragón, J.M. & Palancar, M.C. (2006). Fluidised bed dynamics diagnosis from measurements of low-frequency out-bed passive acoustic emissions. *Powder technology, 162,* 145-156.

[4] Briens, L., Daniher, D. & Tallevi, A. (2007). Monitoring high-shear granulations using sound and vibration measurements. *International journal of pharmaceutics, 331,* 54-60.

[5] Hansuld, E.M., Briens, L., McCann, J.A.B. & Sayani, A. (2009). Audible acoustics in high-shear wet granulation: Application of frequency filtering. *International journal of pharmaceutics, 378,* 37-44.

[6] Gamble, J.F., Dennis, A.B. & Tobyn, M. (2009). Monitoring and end-point prediction of a small scale wet granulation process using acoustic emission. *Pharmaceutical development and technology, 14,* 299-304.

[7] Leach, M.F. & Rubin, G.A. (1977). Particle size determination from acoustic emissions. *Powder technology, 16,* 153-158.

[8] Leach, M.F. & Rubin, G.A. (1978). Particle size distribution characterization from acoustic emissions. *Powder technology, 19,* 157-167.

[9] Leach, M.F. & Rubin, G.A. (1978). Analysis of Gaussian size distribution of rigid particles from their acoustic emissions. *Powder technology, 19,* 189-195.

[10] Leach, M.F. & Rubin, G.A. (1978). Size analysis of particles of irregular shape from their acoustic emissions. *Powder technology, 21,* 263-267.

[11] Hidaka, J. & Shimosaka, A. (1993). Parameters of radiated sound and state variables in flowing particles. *International journal of modern physics B, 7,* 1965-1974.

[12] Matero, S., Poutiainen, S., Leskinen, J., Jarvinen, K., Ketolainen, J., Reinikainen, S., Hakulinen, M., Lappalainen, R. & Poso., A. (2009). The feasibility of using acoustic emissions for monitoring of fluidized bed granulation. *Chemometrics and intelligent laboratory systems, 97,* 75-81.

[13] Whitaker, M., Baker, G.R., Westrup, J., Goulding, P.A., Rudd, D.R., Belchamber, R.M. & Collins, M.P. (2000). Application of acoustic emission to the monitoring and end point determination of a high shear granulation process. *International journal of pharmaceutics, 205,* 79-91.

[14] Papp, M.J., Pujara, C.P. & Pinal, R. (2008). Monitoring of high-shear granulation using acoustic emission: predicting granule properties. *Journal of pharmaceutical innovation, 3,* 113-122.

[15] Eriksson, L., Johansson, E., Kettaneh-Wold, N., Trygg, J., Wikström, C. & Wold, S. (2006). *Multi- and megavariate data analysis Part I basic principles and applications, 2nd edition*. Sweden: Umetrics.

[16] Iveson, S.M., Litster, J.D., Hapgood, K. & Ennis, B.J. (2001). Nucleation, growth and breakage phenomena in agitated wet granulation processes: a review. *Powder technology, 117,* 3-39.

[17] Sato, Y., Nakamura, H. & Watano, S. (2008). Numerical analysis of agitator torque and particle motion in a high shear mixer. *Powder technology, 186,* 130-136.

[18] Sherrington, P.J. & Oliver, R. (2006). Granulation. In A.S. Goldberg (Ed.), *Monographs in powder science and technology*. London: Heyden.

[19] Saito, Y., Fan, X., Ingram, A. & Seville, J.P.K. (2011). A new approach to high-shear mixer granulation using positron emission particle tracking. *Chemical engineering science, 66*, 563-569.

[20] Darelius, A., Lennartsson, E., Rasmuson, A., Björn, I.N. & Folestad, S. (2007). Measurement of the velocity field and frictional properties of wet masses in a high shear mixer. *Chemical engineering science, 62,* 2366-2374.

Chapter 5

5. Monitoring quality attributes for high-shear wet granulation with audible acoustic emissions

5.1. Introduction

Granulation is a complex process and product quality depends on the consistency of the raw material inputs, process conditions, and equipment operation. Quality attributes are interrelated and minor variations during processing can lead to a suboptimal product. As a result, product quality is difficult to determine online and a series of offline tests are typically used. This process is expected to change however, as recent regulatory guidance documents recommend an upstream shift in quality testing [1]. The ICH Q8 guidance document encourages the development of online measurement systems for monitoring critical attributes related to product quality and process end-point. The intent is to increase process knowledge such that adjustments can be made during operation to overcome variability and manufacture a product of consistent quality.

Technologies for collecting online measurements are known as process analytical technologies, or PATs. Impeller torque [2-4], near-infrared spectroscopy (NIR) [5], acoustics and vibration [6-9], focused-beam reflectance measurement (FBRM) [10], and imaging [11] are some of the PATs currently being explored for monitoring high-shear granulation. The following work focuses on audible acoustic emissions (AAEs). In

comparison to other techniques, AAE systems are inexpensive to set up and the signals contain a high volume of information that can be related to the granulation process [6, 9]. In addition, data collection is non-invasive and does not require contact between the sensor and the equipment. The current equipment setup uses the granulator air exhaust to suspend the sensor, eliminating the challenge of maintaining consistent contact between the sensor and the vessel with a couplant or adhesive. Furthermore, by positioning the sensor inside the exhaust, AAE detection is not limited to localized contacts between the particles and the equipment but instead reflects a variety of particle interactions within the granulator [Chapter 4].

In order to use PATs to improve product quality and increase process knowledge, it is necessary to relate the online measurements to critical quality attributes. According to Pottmann et al. [12], particle size distribution and bulk density form the basis of all quality attributes for granulation. In high-shear granulation, correlations have been developed between acoustic emissions and particle size but there do not appear to be any correlations for bulk density. Papp et al. [8] demonstrated a positive relationship to particle size using the average frequency spectra and waveform data from the last 10 s of granulation. Similarly, Whitaker et al. [7] showed the frequency spectrum from the last 20 s of granulation was related to the mass mean particle size of the granules before dry screening. Whitaker et al. also mentioned a relationship between acoustic emissions and density but did not provide any experimental investigation. The correlations developed by Papp et al. [8] and Whitaker et al. [7] suggest an opportunity

to further investigate the origin of the relationship between acoustic emissions and changes in size and density.

Acoustic emissions from granulation are thought to be the result of particle-particle and particle-equipment collisions, as well as friction [13-15]. Leach and Rubin [13, 14] showed the acoustic frequency from rotating glass and metallic spheres can be used to characterize the shape and width of the particle size distribution and Hidaka and Shimosaka [15] demonstrated a positive relationship between the acoustic pressure and the macroscopic velocity of flowing particles. More recently, a relationship between AAEs and particle size was identified by rotating MCC spheres, sugar spheres and wet granules of specific sizes in stainless steel beakers [Chapter 4]. The following work expands on existing research to demonstrate a relationship between AAEs and changes in particle size and density during high-shear wet granulation for use in online monitoring of product quality.

5.2. Materials and methods

5.2.1. Materials

The base formulation for the granulations consisted of mannitol (Pearlitol® 160C, Roquette), cornstarch (NF, National Starch and Chemical Co.), microcrystalline cellulose (Avicel® PH 101, FMC Biopolymer), hypromellose 2910 (Pharmacoat® 603, Shin-Etsu Chemical Co.) and croscarmellose sodium (AcDiSol®, FMC Biopolymer) for a total batch

size of 1.8 kg. Three additional formulations were created by replacing Avicel PH101 with three alternate grades, donated by FMC Biopolymer. The properties of the four Avicel grades are summarized in Table 5.1.

Table 5.1 Summary of Avicel grades

Avicel Grade	Particle Size (μm)	Bulk Density (g/cc)
PH101	50	0.26-0.31
PH102	100	0.28-0.33
PH301	50	0.34-0.45
PH302	100	0.35-0.46

5.2.2. Methods

High-shear wet granulation

For each granulation, the materials were passed through an 850 μm sieve and added to a Niro-Fielder PMA-10 high-shear granulator for 5 min of dry mixing at an impeller speed of 350 rpm and chopper setting II. Water was introduced at 55 mL/min through a spray nozzle positioned right-of-center until approximately 800 mL were added and the batch was considered over wet.

Collection of AAEs

AAEs were collected at 40,000 Hz using two PCB Piezotronics condenser microphones (model 130D20). The microphones were positioned at the top of the air exhaust and on the inside, 20 cm from the exhaust base (Figure 5.1). The signals were conditioned using ICP sensor signal conditioners (PCB Piezotronics) and acquired using a National

Instruments data acquisition system and LabVIEW 8.5. The signal range was optimized to ±10 V, equating to a gain of 0.5.

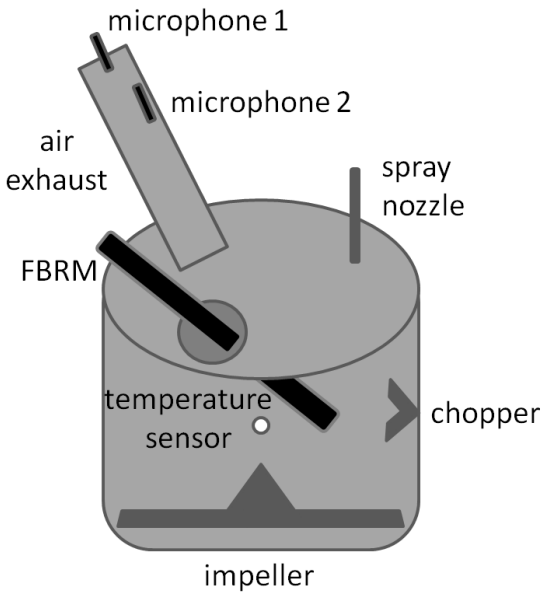

Figure 5.1 Equipment configuration for granulations.

DOE investigation and granulations for multivariate analysis

Eight batches were granulated in random order according to a full two factor DOE with replicates (Table 5.2). The two factors, size (A) and density (B), were varied by changing the grade of Avicel used in the formulation. In addition, three granulations were completed outside of the DOE framework using the base formulation, to provide additional AAEs for multivariate analysis. Granulation and acoustic collection followed the procedures outlined in the previous two sections.

Table 5.2 DOE summary

DOE	Size (A)	Density (B)
1 – Avicel PH102	100	Low
2 – Avicel PH302	100	High
3 – Avicel PH301	50	High
4 – Avicel PH302	100	High
5 – Avicel PH101	50	Low
6 – Avicel PH301	50	High
7 – Avicel PH102	100	Low
8 – Avicel PH101	50	Low

Granulation with density and particle size measurement

For each formulation, four additional batches were granulated according to the procedure outlined previously, stopping every 100 mL to measure the tap and bulk densities of the wet granules and withdraw a sample (approximately 20 g) for particle size analysis. The starting sample point was incremented by 25 mL for each batch, to increase the data resolution from 100 to 25 mL. Tap and bulk density were measured by filling a graduated cylinder to 100 mL with powder, recording the mass and tapping the cylinder 500 times using a Vankel tap density machine. The powder volume was measured before and after tapping to compute the bulk and tap densities, respectively. The densities were measured in triplicate, returning the powder to the granulator bowl after measurement. The samples removed for size analysis were tray dried to less than 2% loss on drying at the end of each batch, using a GCA Convection oven (80 °C). The particle size distributions of the dried granules were measured using an ATM Sonic Sifter with a pulse amplitude of 9 and a 5 min sift/pulse setting. The sieve set consisted of 150, 180, 250, 355, 600 and 850 µm ATM U.S. standard sieves and a fines collector.

Three size fractions were defined: fines – less than 180 µm, midsized – 180-600 µm, and large – greater than 600 µm.

Particle size data was also acquired online using an FBRM D600 Lasentec® probe (Mettler-Toledo) and FBRM Control Interface software (Mettler-Toledo, version 6.7.0). The probe was positioned using a stainless steel holder, manufactured to fit the granulator viewport. The face of the probe was submerged near the chopper, where there was good batch movement and the powder was less likely to stick (Figure 5.1). The FBRM provided a measure of particle size known as a chord length distribution. The chord length distribution is based on the backscattering of light that occurs when a focused laser beam intersects a particle. The duration of the reflection is multiplied by the velocity of the scanning beam to determine the chord length. For this work, a scan speed of 4 m/s was used with a 2 s sampling period and the electronics were configured for "coarse" particle sizes. The measurements were divided into fines (<150 µm) and large (>150 µm) fractions and the number of counts per second were computed based on a square weight distribution.

Signal analysis

The AAEs were divided into 10 s segments and the time series data was transformed into frequency data by computing the power spectral density for each segment in Matlab 6.5. The TPSD was determined by summing the transformed data for each segment into 10 Hz groups from 20 to 20,000 Hz. The matrix was later reduced to 20 to

250 Hz, based on previous results identifying this range as the most relevant for high-shear wet granulation [9].

The 10 Hz TPSDs were sampled every minute to form the responses for the DOE analysis (Stat-Ease Design Expert 6). DOE analysis relates experimental factors (size and density) to measured responses (10 Hz TPSDs), using a regression approach to fit coefficients to a polynomial model. The importance of each factor is determined from the regression coefficients and an analysis of variance (ANOVA). The analysis considers each factor individually and in combination, based on a 5% level of significance. If the effect of a factor is shown to depend on the level of another factor then it is known as an interaction. Interaction effects override main effects and factors involved in an interaction can no longer be considered individually.

The 10 Hz TPSDs from the three batches completed outside of the DOE were analyzed in Umetrics SIMCA P+ 11.5, using multivariate projection to latent structures by means of partial least squares (PLS) and orthogonal projection to latent structures by means of partial least squares (OPLS). PLS is a method for relating two spaces of information, *X* and *Y*. The *X* space was comprised of the 10 Hz TPSD measurements from 20 to 250 Hz and the *Y* space consisted of the following physical property measurements: tap and bulk density; the fraction of fines, midsized and large granules measured by sieving; and the distribution of fines and large granules measured by FBRM. Both sieve and FBRM size measurements were included to capture the dry and wet granule size distributions.

The procedure followed by SIMCA to develop the models involves simultaneously fitting a straight line, known as a principal component, to each space and projecting the original data points onto the lines. The projection coordinates are linear combinations of the original data, known as scores and are formed using the weights *w* and *c*, for the *X* and *Y* spaces respectively. The components are oriented such that the scores approximate the data in *X* and *Y*, and provide an understanding of the correlation between the two. Additional components may be added but the most significant variability is captured in the first component [16].

OPLS is a method for relating information in a matrix, *X* to a single variable, *Y*. The *X* space consisted of the 10 Hz TPSD measurements from 20 to 250 Hz and the *Y* space consisted of a single size or density measurement. As a result, several models were required to represent all of the physical property measurements. The procedure followed by SIMCA involves fitting a single principal component to the *X* space with the objective of describing the predictive relationship between *X* and a single *Y*. Additional components may be added to describe other sources of variability that are not related to the predictive relationship [16]. For both PLS and OPLS, the data was pre-processed by centering and scaling to unit variance, according to the standard procedure in SIMCA. In addition, the auto-transformation function was used to achieve a normal distribution in the variables.

5.3. Results

The capability of AAEs as a PAT tool for monitoring changes in critical physical properties during granulation was evaluated. A DOE was used to determine whether changes in size and density had a significant effect on granulation AAEs, and multivariate PLS and OPLS models were used to assess the potential for monitoring changes in size and density online. Size and density were selected based on their importance to granule quality and because they could be varied according to a DOE methodology.

5.3.1. DOE investigation of the effect of size and density on AAEs

The DOE varied size and density in a controlled manner using four grades of Avicel. The investigation showed size and density had a significant effect on the 10 Hz TPSDs computed from the AAEs. The significance primarily corresponded to a consistent decrease in the 10 Hz TPSD profiles during the latter half of wetting. In previous work, the decrease was shown to relate to the achievement of ideal granule properties and the transition to over wetting [9]. In the following section, the results for the 100-110 Hz frequency group are presented as a representative example. Measurements of density and particle size distribution throughout granulation are also included to validate the experimental approach.

5.3.2. 100-110 Hz TPSDs

Figure 5.2 shows the average 100-110 Hz TPSD profiles for granulations with each Avicel grade. The profiles all follow the same trend, a gradual increase to a maximum followed by a steady decrease. The magnitudes are similar until the decrease begins, at which point the profiles are observed to separate based on size and density. The largest separation is related to density, with the two high density blends corresponding to greater TPSD magnitudes than the two low density blends. The profiles are further separated based on size, with higher magnitudes observed for blends with smaller sized Avicel. The decrease appears to start sooner for the high density blends and towards the end of wetting the profiles become aligned, whereas the profiles for the low density blends show an increase in separation. Earlier work showed end-point corresponds to the peak and the beginning of the decrease [9]; therefore, the results suggest the high density blends granulated faster and the alignment may represent similar over wet states. In general, the findings suggest the AAEs were sensitive to changes in size and density during the latter half of wetting, where different magnitudes were observed for the decrease in the 100-110 Hz TPSD.

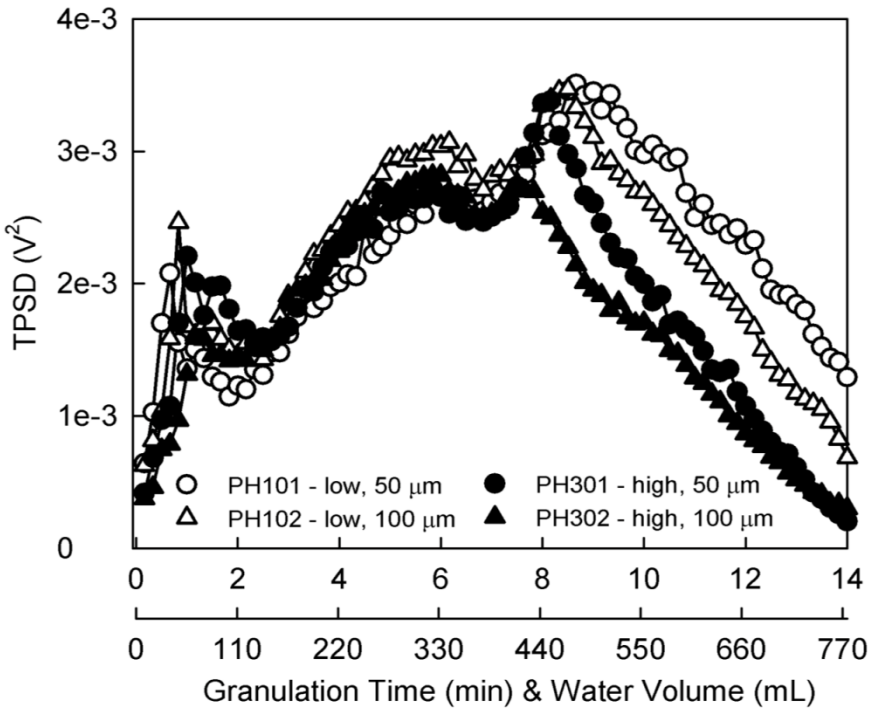

Figure 5.2 100-110 Hz TPSD versus time and water volume, for DOE granulations with four grades of Avicel. Each profile represents the average 100-110 Hz TPSD from two runs. The granulation conditions are summarized in the legend as follows: Avicel grade – density, particle size.

5.3.3. DOE analysis of the 100-110 Hz TPSDs

The DOE analysis of the 100-110 Hz TPSDs confirmed the decrease during the latter half of wetting was significantly affected by changes in size and density. Figure 5.3 shows the DOE plots for minutes 9 to 14, illustrating the effect of changing the levels of size (A) and density (B) on the 100-110 Hz TPSD. For minutes 9 to 12, size and density were observed to be independent effects. The DOE plots show that increasing size or increasing density caused a decrease in the 100-110 Hz TPSD. The effect of density was more significant, as it was identified consistently for minutes 9 through 12, whereas size was not identified for minutes 10 or 11. In addition, the decrease in TPSD was observed

to be greater when density was increased, compared to size. The results agree with the 100-110 Hz TPSD profiles, where greater separation was observed based on density (Figure 5.2). For minutes 13 and 14, the DOE analysis identified a significant interaction between size and density. The DOE plots show the change in TPSD with increasing size was more significant for granulations with low density Avicel grades. The results agree with the 100-110 Hz TPSD profile, where separation was only observed between the low density profiles at the end of wetting (Figure 5.2).

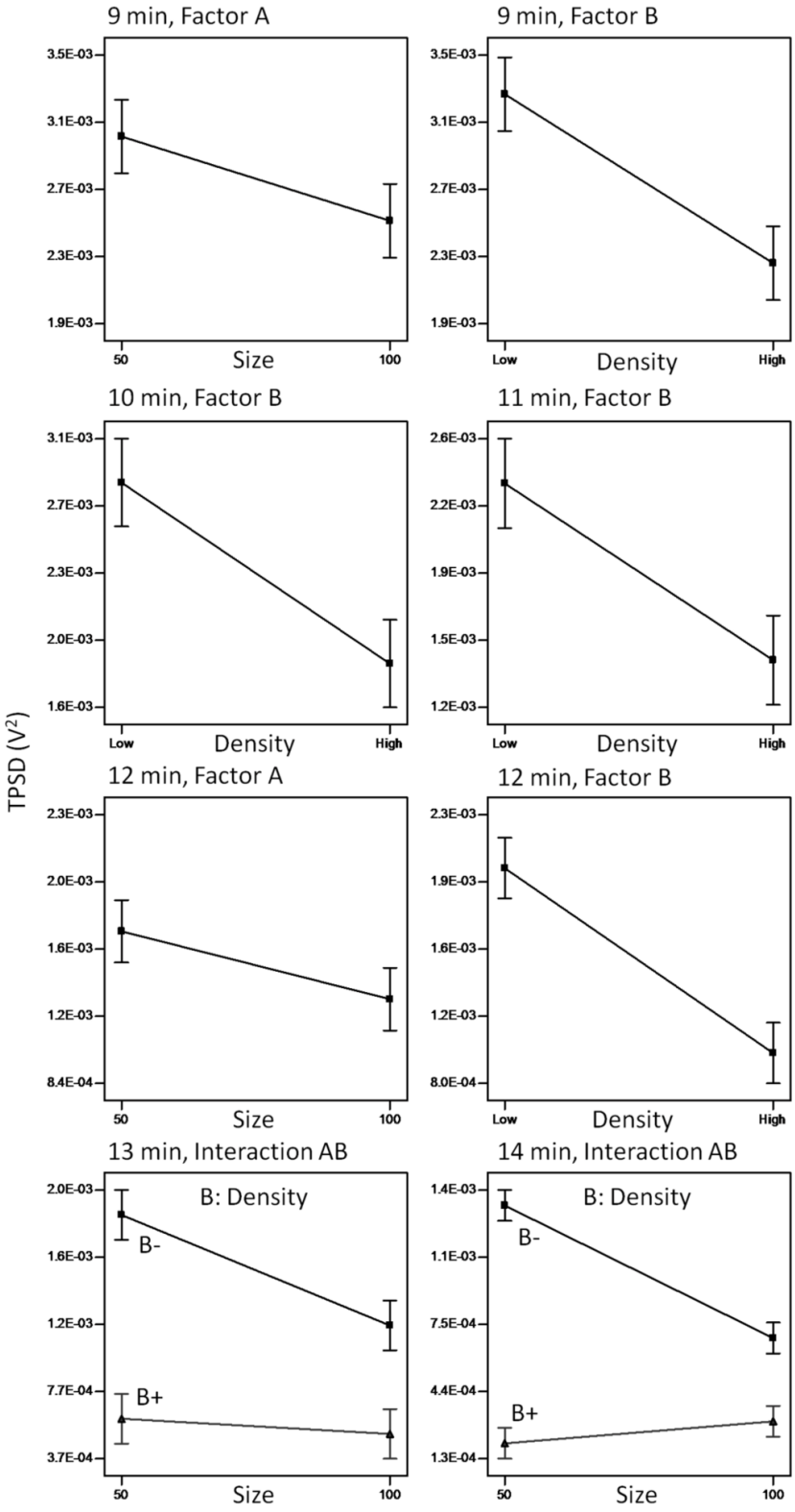

Figure 5.3 DOE plots showing the significant factors and interactions affecting the decrease in the 100-110 Hz TPSD from minutes 9 to 14. The two factors are size (A) and density (B).

5.3.4. Density and particle size measurements

Density and particle size measurements were collected for granulations with each Avicel grade. Figure 5.4 summarizes the changes in tap and bulk density, as well as the fines, midsized and large size fractions throughout wetting. The trend in each physical property is observed to be the same for all four Avicel grades and the separation between datasets confirms it was possible to alter the size and density of the granulations by varying the raw material properties. The profiles show an increase in bulk and tap density, a decrease in fines, and an increase in the fraction of midsized granules when the Avicel density was increased from low to high, and when size was increased from 50 to 100 μm. The changes support the DOE findings, showing increases in size and density contributed to a statistically significant decrease in TPSD magnitude (Figure 5.2, Figure 5.3). For the large size fraction, the trend is not as clear and higher fractions appear to correspond to granulations with small sized Avicel rather than large sized Avicel. The difference between the large size fraction and the fines and midsized fractions suggests layering may have taken place during granulations with the small sized Avicel blends. Layering is a mechanism of granule growth that occurs when fine particles adhere to the surface of large pre-existing granules, increasing their overall size [17]. Thus, a layering mechanism would explain the higher fraction of large granules observed with small sized Avicel. Overall, the measurements validate the experimental approach, by showing it was possible to introduce controlled changes to the size and density of the granulation by altering the properties of the raw material.

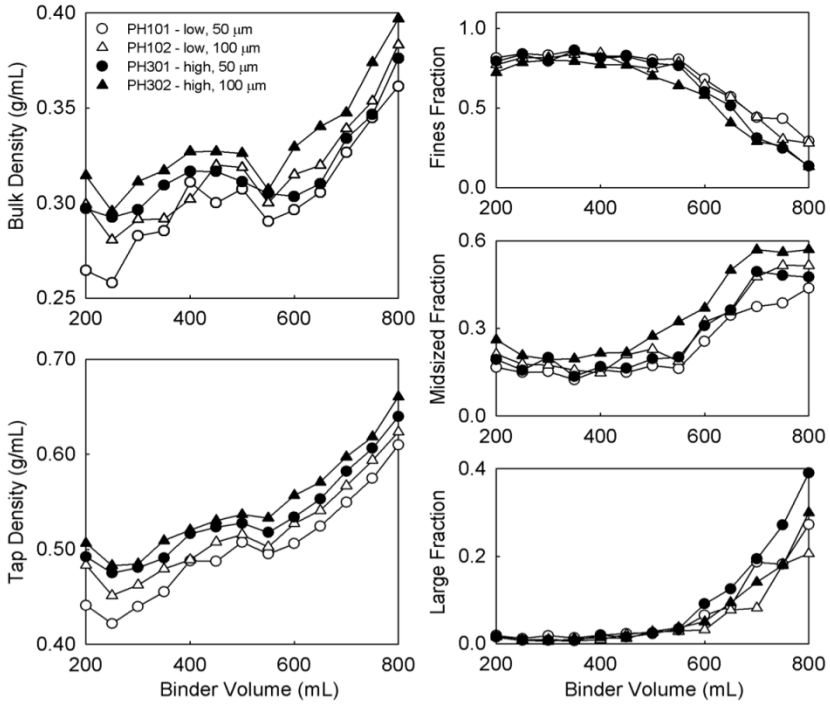

Figure 5.4 Changes in density (tap and bulk) and size (fines, midsized and large fractions) over binder volume (mL). The granulation conditions are summarized in the legend as follows: Avicel grade – density, particle size.

5.3.5. Multivariate analysis of the 10 Hz TPSDs

After establishing that the AAEs were in fact sensitive to changes in size and density during granulation, multivariate analysis was investigated as an approach for monitoring these changes online. A PLS model was generated initially to examine the overall relationship between the 10 Hz TPSDs and measurements of size and density. OPLS models were then used to examine the predictive relationships between the 10 Hz TPSDs and each physical property measurement, on an individual basis.

Figure 5.5 shows the correlation structure between the 10 Hz TPSDs and measurements of size and density using a *w*c* plot of the first two principal components from the PLS model; where, *w* represents the weights associated with the 10 Hz TPSDs and *c* represents the weights associated with the physical properties. The representation of each physical property measurement by the 10 Hz TPSDs can be visualized by drawing an imaginary line from the measurement through the origin, and then projecting each 10 Hz TPSD onto the line. The positions of the projected variables relative to the origin represent the strength and direction of the correlations, where the groups furthest from the origin correspond to the strongest correlations [16]. Figure 5.5 (A) shows an example for the midsized sieve fraction (SM). The frequency groups located on the same side of the origin as the midsized sieve fraction represent positive correlations, such as 150-160 Hz and 210-220 Hz, and the frequency groups on the opposite side represent negative correlations, such as 100-110 Hz and 40-50 Hz. The overall arrangement of the variables shows different combinations of 10 Hz TPSDs are needed to represent different physical properties. For example, if an imaginary line was drawn through tap density (TD) instead of the midsized sieve fraction (SM), the frequency groups associated with the strongest positive and negative correlations would change. Figure 5.5 (B) shows the frequency groups in the bottom left quadrant have a strong negative correlation to tap density, whereas for the midsized sieve fraction the strongest negative correlations were observed for frequency groups in the top left quadrant.

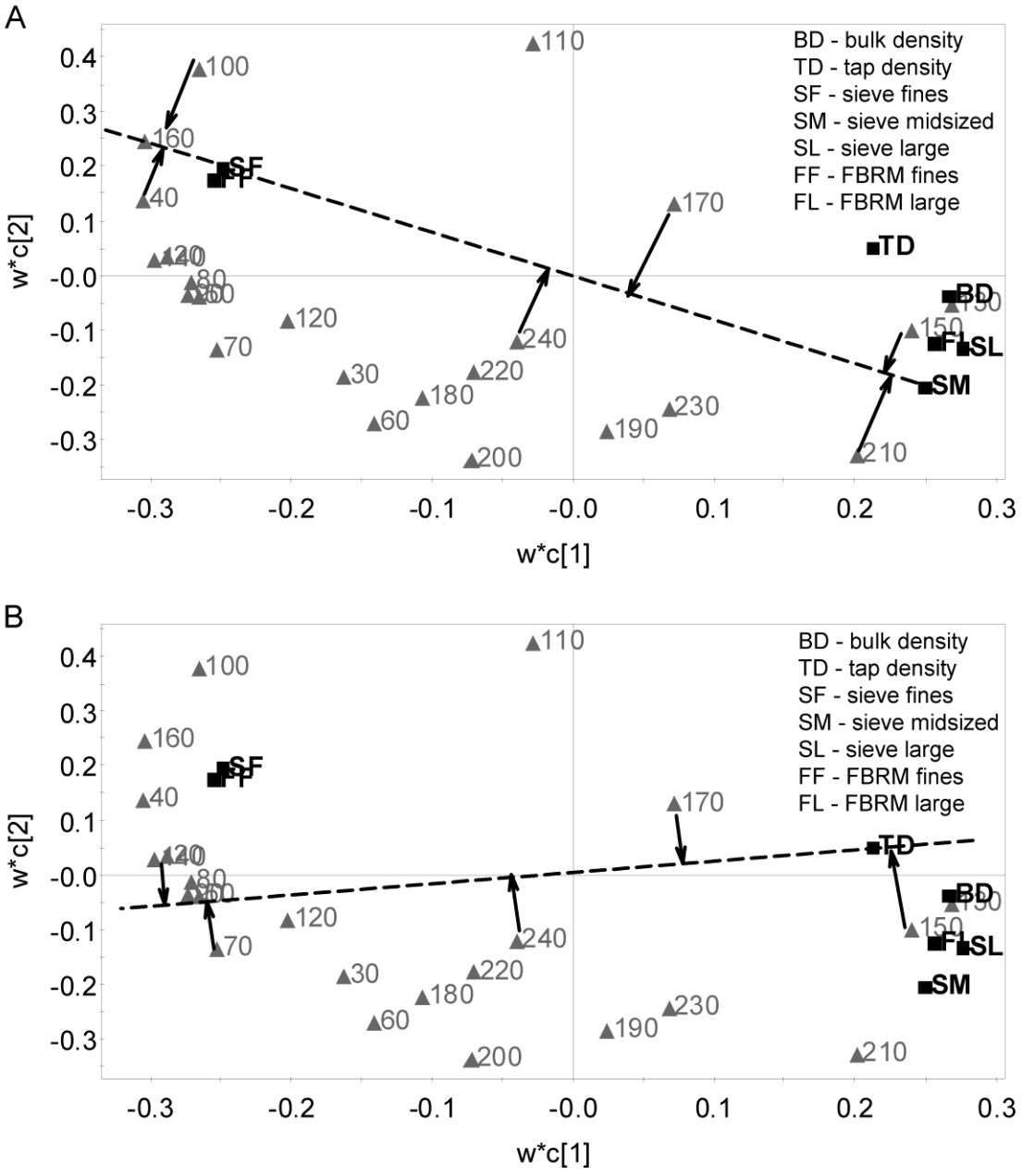

Figure 5.5 PLS weights (*w*c*) for the first and second principal components, where *w* represents the weights associated with the 10 Hz TPSDs and *c* represents the weights associated with the measurements of size and density. The 10 Hz TPSDs are listed by starting frequency, i.e. 100 corresponds to 100-110 Hz.

The arrangement of the variables in the PLS model suggests the physical property measurements can be described using different combinations of 10 Hz frequency groups. To further examine the predictive relationships between the 10 Hz TPSDs and

each physical property measurement, OPLS models were developed. The OPLS scores summarize the information in the 10 Hz TPSDs that is relevant for predicting each property. In Figure 5.6, the OPLS scores are compared to the original size and density measurements. The profiles for the OPLS scores are observed to be unique based on the measured physical property and the trends agree with the original measurements. As such, the results support the use of OPLS scores to follow changes in size and density online. The scores representing the sieve size measurements are similar to the scores for the FBRM measurements, suggesting either method could be used to measure changes in particle size. The OPLS scores for bulk density and the large sieve fraction do not agree as well with the original data, and it is thought that the linear projection method used by OPLS may have smoothed out some of the more abrupt transitions in the original data.

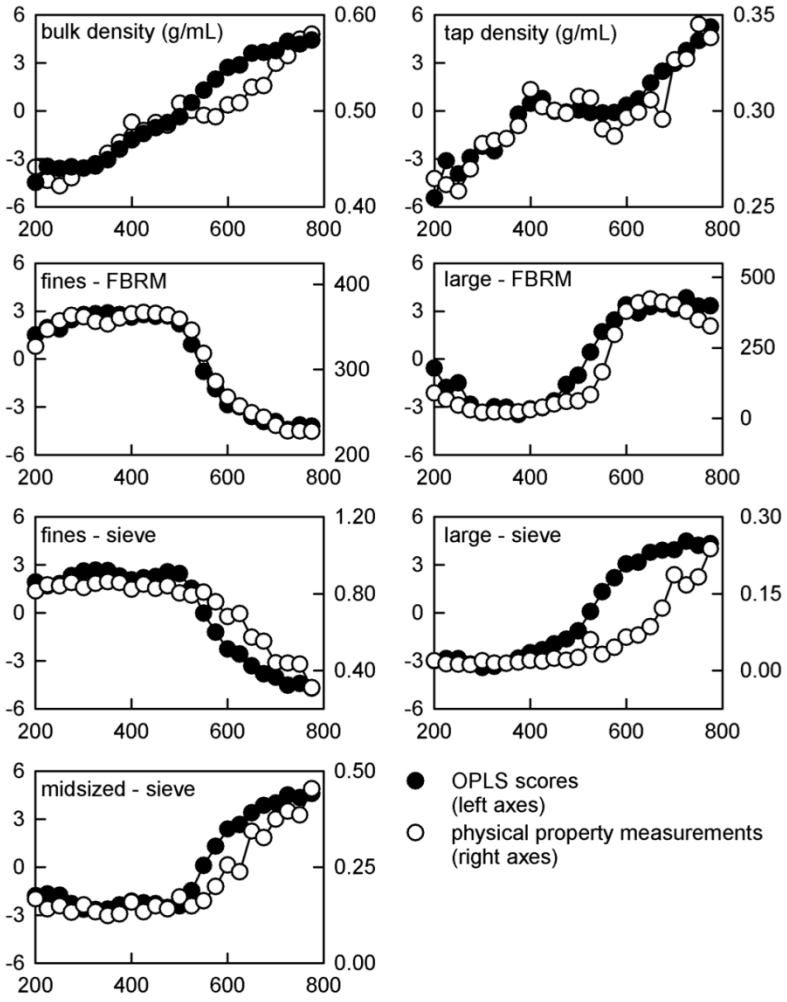

Figure 5.6 OPLS scores and physical property measurements versus binder volume (mL).

5.4. Discussion

The DOE analysis showed changes in size and density have a significant effect on the AAEs generated during high-shear wet granulation. More specifically, increases in density and particle size during wetting contribute to the decrease in the 10 Hz TPSDs consistently observed with end-point and over wetting [9]. The results support the development of AAEs for online prediction of size and density. As such, multivariate

models were developed using the 10 Hz TPSDs, and the resulting OPLS scores were shown to represent changes in size and density throughout wetting. The following discussion explores the relationship of the AAEs to changes in size and density, as well as potential applications for the multivariate results.

5.4.1. Relating AAEs to size and density

While correlations between AAEs and physical properties can be used to develop models for online prediction, they do not prove the existence of causal relationships between properties. In other words, a correlation does not provide evidence that a change in factor A caused a change in response Y, or a change in size caused a change in TPSD. As such, an error term is always included to account for the possibility that an unmeasured variable was truly responsible for the observed relationship [18]. By applying a DOE methodology, however, it was possible to design a rigorous investigation where size and density were systematically varied, such that a distinction could be made between significant effects and measurement error. As a result, it was possible to quantify the influence of each factor on the measured responses and therefore establish that the AAEs generated by the granulations were directly affected by changes in size and density.

The decrease in the 100-110 Hz TPSD began at approximately 500 mL and coincided with an increase in tap and bulk density, a decrease in fines, and an increase in the fractions of midsized and large granules (Figure 5.2, Figure 5.4). The results suggest the

decrease in TPSD coincides with the onset of granule growth and densification. Granule growth requires a critical amount of liquid to be present at the surface [17] and the liquid is thought to create a lubrication effect that reduces interparticle friction, a primary source of acoustic emissions [13, 19]. As the granules grow and become denser, more liquid would be squeezed to the surface and the decrease in interparticle friction would result in a decrease in TPSD. Therefore, the decrease in TPSD is believed to result from the increased presence of liquid on the granule surface with growth and densification. The results are consistent with earlier work, where a negative relationship was identified between AAEs and size for wet granules rotated in a stainless steel beaker [Chapter 4]. The results are also similar to those for shearing sand grains, where AAEs generated by interparticle friction were thought to be reduced when humidity increased and liquid coated the grain surface [20]. In addition, findings for fluidized-bed granulation showed a decrease in acoustic emissions coincided with the presence of additional moisture among particles during agglomeration [21]. The moisture was thought to reduce interparticle friction from particle-particle and particle-wall collisions, resulting in lower acoustic intensity.

The multivariate PLS model showed the 10 Hz TPSDs were correlated differently to measurements of size versus density. The frequency groups that were the most significant in relation to size were not the same as the ones that were the most significant in relation to density. The results are expected because granule growth and densification do not occur uniformly throughout the granulator, and therefore shear

rate and particle velocity depend on axial and radial location [22, 23]. As a result, a specific frequency group may be more representative of granule densification or granule growth, depending on the location in the granulator where the corresponding sound was generated. For example, AAEs resulting from interactions close to the surface, where the liquid is first introduced and coalescence begins, would more likely be related to changes in size. Alternatively, AAEs from interactions near the base of the granulator, where the impeller is located and densification is more pronounced, would be more representative of changes in density. The results require further investigation, as granule behaviour at different locations in the mixer is complex and not completely understood.

5.4.2. Applications

Establishing relationships between online measurements and physical property changes is a critical step in PAT development, as the ICH Q8 guidance encourages the use of PAT tools to monitor attributes related to product quality [1]. For complex processes, such as granulation the relationship between online measurements and physical properties is not always obvious and additional effort is required to verify the effectiveness of PAT tools. Research using both audible [6, 9] and ultrasonic [8, 24] acoustics has identified a decrease in acoustic intensity with increasing binder volume; however, there has been little attempt to understand the reason for the decrease. The DOE analysis presented in this work (Figure 5.2-Figure 5.4) shows the decrease in AAEs is affected by increases in size and density with binder addition. Size and density are both critical variables that

affect downstream processing and product quality in high-shear granulation [12]. Particle size distribution and density impact granule flowability and compaction properties during tabletting, as well as the uniformity and disintegration of the final product [25]. As a result, a PAT tool capable of monitoring changes in size and density is highly desirable. AAEs were shown to measure both properties, offering an advantage over other PAT technologies that are only capable of measuring one or the other.

The trends in the OPLS scores show how AAEs could be used to monitor changes in size and density online during granulation (Figure 5.6). An online monitoring system would reduce product development times because a process could be adjusted in real-time to achieve the desired product attributes, rather than relying on a multi-batch trial and error procedure using offline measurements. Online monitoring would also increase process flexibility because parameters could be adjusted during operation to account for minor variations in process inputs and achieve consistent product quality. In addition, it may be possible to use AAEs to assist in scale-up and product transfers, as the sensors are small and can be easily transferred from one piece of equipment to another. The portability of the equipment offers an advantage over other techniques where the probe is inserted directly into the granulation, such as FBRM. In these cases, the probe would need to be repositioned at each scale and the larger size would be difficult to accommodate in smaller units.

5.5. Conclusions

PAT technologies should demonstrate an ability to monitor changes in critical attributes related to product quality. For complex processes, such as high-shear granulation it can be difficult to demonstrate a relationship between online measurements and quality attributes because there are a high number of interrelated variables. AAEs have shown potential for monitoring the high-shear granulation process but the relationship between the AAEs and product quality attributes is not fully understood. The results from this work further develop the capabilities of AAEs as a PAT tool. DOE analysis showed increases in size and density contribute significantly to the decrease in acoustic TPSD observed with end-point and over wetting, demonstrating a relationship between the AAEs and product quality attributes. In addition, multivariate OPLS scores were shown to predict changes in size and density using the 10 Hz TPSDs from 20 to 250 Hz, in support of online monitoring. Future work should involve the development the OPLS scores for online use to assist in new product development and achievement of consistent product quality.

5.6. References

[1] U.S. Department of Health and Human Services, Food and Drug Administration, Center for Drug Evaluation and Research (CDER), Center for Biologics Evaluation and Research (CBER). (2008). *Guidance for industry Q8 pharmaceutical development, second revision*. Retrieved from http://www.fda.gov/downloads/Drugs/GuidanceComplianceRegulatoryInformation/Guidances/ucm073507.pdf.

[2] Laicher A., Profitlich, T., Schwitzer, K. & Ahlert, D. (1997). A modified signal analysis system for end-point control during granulation. *European journal of pharmaceutical sciences, 5,* 7-14.

[3] Holm, P., Schaefer, T. & Kristensen, H.G. (1985). Granulation in high speed mixers: Part VI. effects of process conditions on power consumption and granule growth. *Powder technology, 43,* 225-233.

[4] Betz, G., Bürgin, P.J. & Leuenberger, H. (2004). Power consumption measurement and temperature recording during granulation. *International journal of pharmaceutics*, *272,* 137-149.

[5] Miwa, A. & Makado, K. (2009). A method for predicting the amount of water required for wet granulation using NIR. *International journal of pharmaceutics, 376,* 41-45.

[6] Briens, L., Daniher, D. & Tallevi, A. (2007). Monitoring high-shear granulation using sound and vibration measurements. *International journal of pharmaceutics, 331,* 54-60.

[7] Whitaker, M., Baker, G.R., Westrup, J., Goulding, P.A., Rudd, D.R., Belchamber, R.M. & Collins, M.P. (2000). Application of acoustic emission to the monitoring and end point determination of a high shear granulation process. *International journal of pharmaceutics, 205,* 79-91.

[8] Papp, M.K., Pujara, C.P. & Pinal, R. (2008). Monitoring of high-shear granulation using acoustic emission: predicting granule properties. *Journal of pharmaceutical innovation, 3,* 113-122.

[9] Hansuld, E.M., Briens, L., McCann, J.A.B. & Sayani, A. (2009). Audible acoustics in high-shear wet granulation: Application of frequency filtering. *International journal of pharmaceutics, 378,* 37-44.

[10] Huang, J., Kaul, G., Utz, J., Hernandez, P., Wong, V., Bradley, D., Nagi, A. & O'Grady, D. (2010). A PAT approach to improve process understanding of high shear wet granulation through in-line particle measurement using FBRM C35, *Journal of pharmaceutical sciences, 99,* 3205-3212.

[11] Watano, S. (2001). Direct control of wet granulation processes by image processing system. *Powder technology, 163,* 164-172.

[12] Pottmann, M., Ogunnaike, B.A., Adetayo, A.A. & Ennis, B.J. (2000). Model-based control of a granulation system. *Powder technology, 108,* 192-201.

[13] Leach, M.F. & Rubin, G.A. (1978). Analysis of Gaussian size distribution of rigid particles from their acoustic emissions. *Powder technology*, *19*, 189-195.

[14] Leach, M.F. & Rubin, G.A. (1977). Particle size determination from acoustic emissions. *Powder technology, 16,* 153-158.

[15] Hidaka, J. & Shimosaka, A. (1993). Parameters of radiated sound and state variables in flowing particles. *International journal of modern physics B, 7*, 1965-1974.

[16] Eriksson, L., Johansson, E., Kettaneh-Wold, N., Trygg, J., Wikström, C. & Wold, S. (2006). *Multi- and megavariate data analysis Part I basic principles and applications, 2nd edition*. Sweden: Umetrics.

[17] Iveson, S.M., Litster, J.D., Hapgood, K. & Ennis, B.J. (2001). Nucleation, growth and breakage phenomena in agitated wet granulation processes: a review. *Powder technology, 117,* 3-39.

[18] Box, G.E.P., Hunter, W.G. & Hunter, J.S. (1978). *Statistics for experimenters: an introduction to design, data analysis and model building*. New York: John Wiley & Sons Inc.

[19] Darelius, A., Lennartsson, E., Rasmuson, A., Björn, I.N. & Folestad, S. (2007). Measurement of the velocity field and frictional properties of wet masses in a high shear mixer. *Chemical engineering science, 62,* 2366-2374.

[20] Sholtz, P., Bretz, M. & Nori, F. (1997). Sound-producing sand avalanches. *Contemporary physics, 38,* 329-342.

[21] Tsujimoto, H., Yokoyama, T., Huang, C.C. & Sekiguchi, I. (2000). Monitoring particle fluidization in a fluidized bed granulator with an acoustic emission sensor. *Powder technology, 113,* 88-96.

[22] Sato, Y., Nakamura, H. & Watano, S. (2008). Numerical analysis of agitator torque and particle motion in a high shear mixer. *Powder technology, 186,* 130-136.

[23] Saito, Y., Fan, X., Ingram, A. & Seville, J.P.K. (2011). A new approach to high-shear mixer granulation using positron emission particle tracking. *Chemical engineering science, 66*, 563-569.

[24] Gamble, J.F., Dennis, A.B. & Tobyn, M. (2009). Monitoring and end-point prediction of a small scale wet granulation process using acoustic emission. *Pharmaceutical development and technology, 14,* 299-304.

[25] Cameron, I.T. & Wang, F.Y. (2007). Process systems engineering applied to granulation. In A.D. Salman, M.J. Hounslow & J.P.K. Seville (Eds.), *Handbook of powder technology,1st edition.* The Netherlands: Elsevier.

Chapter 6

6. The effect of process parameters on audible acoustic emissions from high-shear granulation

6.1. Introduction

The complexity and lack of understanding surrounding pharmaceutical processes has lead to an industry-wide reliance on offline testing to determine whether a product satisfies quality requirements. The recent ICH Q8 regulatory guidance document recommends an upstream shift in quality testing, where in-process analysis and controls are utilized to improve product consistency and reduce the need for end product testing [1]. Adoption necessitates increased knowledge of the process and the product, as well as an in-depth understanding of the associated sources of variability. It is recommended to use a design space approach to study the interaction of input variables and process parameters in relation to product quality. The design space is a subset of the knowledge space, which represents all that is known about the process, including failure conditions. It refers to the set of operating situations that lead to a final product with acceptable quality attributes. From a regulatory standpoint, operation is acceptable anywhere within the design space but a process can be further optimized to define a target range for normal operation, known as the control space. The design space is useful for identifying process variables that need to be controlled and optimizing process parameters. The ultimate goal is to generate knowledge of product performance under a variety of operating conditions and develop a robust process

where variability in materials, process parameters and equipment can be accommodated.

The ICH Q8 guidance recommends the use of process analytical technology (PAT) tools to acquire information on product quality throughout manufacturing [1]. In previous work, audible acoustic emissions (AAEs) were demonstrated as a PAT tool for monitoring high-shear wet granulation and detecting end-point with three different formulations [2]. The method of detection was non-intrusive and involved suspending a microphone inside the granulator air exhaust. The air exhaust location was later shown to be sensitive to a variety of particle interactions generated by granule shearing [Chapter 4]. The results are in contrast to work by other researchers, where acoustic sensors were placed in contact with the granulator bowl and only local granule-equipment collisions were detected [3, 4]. The AAEs detected in the air exhaust were also shown to reflect changes in size distribution and density during granulation and could be related to final properties, such as granule flow and tablet hardness [2, Chapter 5]. As such, AAEs provide a means of measuring the combined effect of several variables that is consistent with a design space approach.

In design space development, systematic methods such as design of experiment (DOE) and multivariate analysis are encouraged to simplify the interpretation of a large number of variable interactions [1]. DOE allows the maximum amount of information to be extracted in the fewest number of experiments and utilizes statistical measures to

increase the likelihood of separating important effects from measurement error. The rigorous approach allows a distinction to be made between correlative and causal relationships, and permits assessment of complex relationships such as variable interactions and nonlinear effects [5]. Multivariate analysis is advantageous for extracting meaningful relationships from a large number of collinear variables and can also accommodate missing data points. For a review of multivariate applications in the pharmaceutical industry see Gabrielsson et al. [6]. DOE and multivariate analysis can be combined to take advantage of the DOE experimental design structure and the rigorous data analysis possible with multivariate techniques. In their review, Gabrielsson et al. [6] cited the combination of DOE and multivariate analysis as the preferred approach for advancing the robustness of pharmaceutical processing. In practice, Huang et al. [7] combined the two approaches to evaluate the effects of water volume, wet massing time and lubrication time on blend flow, compressibility and tablet dissolution for a high-shear wet granulation process. The results were used to develop a design space for the process and optimize blend flow. Multivariate and DOE analysis were also combined by Gamble et al. [8] to develop a model for identifying end-point using acoustic emissions from granulation. The acoustic signals were acquired for an eleven batch DOE varying liquid dose rate, impeller speed, chopper speed and batch size. End-point was successfully identified for all but two batches, where a change in impeller speed appeared to alter the final granule properties.

The following article develops AAEs as a PAT tool for monitoring granulation progress towards acceptable product quality. A DOE approach was used to systematically introduce minor variations in three process variables: impeller speed, total binder volume and spray rate, and the results were analyzed using both DOE and multivariate approaches.

6.2. Materials and methods

6.2.1. Formulation

The formulation for the granulations consisted of cornstarch (NF, National Starch and Chemical Co.), mannitol (Pearlitol® 160C, Roquette), microcrystalline cellulose (Avicel® PH 101, FMC Biopolymer), hypromellose 2910 (Pharmacoat® 603, Shin-Etsu Chemical Co.) and croscarmellose sodium (AcDiSol®, FMC Biopolymer) for a total batch size of 1.8 kg.

6.2.2. Methods

<u>High-shear wet granulation</u>

Ten batches were granulated in random order according to a full three factor DOE with two center point replicates (Table 6.1). The three factors were: impeller speed, total binder volume and spray rate. Each factor was varied between a high level and a low level based on the established end-point range for the formulation and typical operating

conditions for the granulator. The two center points were included to check for significant curvature in the responses.

Table 6.1 DOE summary

DOE	Impeller Speed (rpm)	Total Binder Volume (mL)	Spray Rate (mL/min)
1	300	650	45
2	420	650	45
3	300	700	45
4	420	700	45
5	300	650	65
6	420	650	65
7	300	700	65
8	420	700	65
9	360	675	55
10	360	675	55

The materials for each batch were passed through an 850 μm sieve and added to a Niro-Fielder PMA-10 high-shear granulator for 5 minutes of dry mixing. The material was granulated according to the DOE specifications (Table 6.1) using a chopper speed of 3000 rpm and 30 s of wet massing. AAEs were collected at 40,000 Hz, using a PCB Piezotronics condenser microphone located at the top of the air exhaust (model 130D20). The signals were conditioned using ICP sensor signal conditioners (PCB Piezotronics) and acquired using a National Instruments data acquisition system and LabVIEW 8.5 software. The signal range was optimized to ±10 V, equating to a gain of 0.5. At the end of wetting, the bulk and tap densities of the granules were measured three times by filling a 100 mL graduated cylinder with powder, determining the mass, and tapping 500 times with a Vankel tap density machine. The mass was divided by the volume before and after tapping to determine the bulk and tap densities, respectively.

Drying and blending

A 100 g sample of granules was tray dried in a GCA convection oven (80°C) and the remainder of the batch was dried in a Glatt GPCG-3 fluid-bed drier (60°C) to less than 2% loss on drying. The size distributions of the tray and fluid-bed dried granules were measured three times using an ATM Sonic Sifter with 150, 180, 250, 355, 600 and 850 µm ATM U.S. standard sieves and a fines collector. The remaining fluid-bed dried granules were passed through an 850 µm sieve and added to a 10 L Pharmatech bin blender. Croscarmellose sodium and magnesium stearate were passed through a 600 µm sieve and blended with the granules for 18 min and 3 min, respectively. Flowability was measured according to the avalanche method for three 100 cc samples. Each sample was placed in a disk and rotated at 0.6 rpm using a Mercury Scientific Revolution Powder Analyzer. Images were collected at 10 fps for 200 avalanches, based on a 65% avalanche threshold. The change in power (potential energy) for each avalanche and the avalanche time were computed from the images and used to assess granule flowability.

Tabletting

A Korsch XL100 tablet press, fitted with a B-turret and four oval alternating punches (8.73 by 17.49 mm) was operated at 20 rpm and 100 tablets were collected at compression forces of 10, 15, 20 and 25 kN. Break load was measured across the face of 10 randomly selected tablets from each compression force, using a Holland C50 hardness tester. Friability was measured in triplicate by rotating ten tablets at 25 rpm

for 4 min in a SOTAX FT-1 Friabilator and measuring the change in total weight. Additionally, disintegration was measured for 6 tablets using a SOTAX DT-2 disintegration tester. Contact sensor discs were placed on top of each tablet to detect when the tablet had completely disintegrated.

Signal analysis

The AAEs were divided into 10 s segments and the time series data was transformed into frequency data by computing the power spectral density for each segment using Matlab 6.5. TPSD was determined by summing the transformed data for each segment into 10 Hz groups from 20 to 20,000 Hz. Based on previous findings, the range was reduced to 20 to 250 Hz to focus on the most relevant content for high-shear wet granulation [2].

Stat-Ease Design-Expert 6 software was used to analyze the DOE results. The experimental factors consisted of the three process variables (Table 6.1), and the responses consisted of the final physical property measurements for size, density, flowability, tablet hardness, friability and disintegration, as well as the 10 Hz TPSDs sampled every minute from minute 1 to 9, and every 100 mL from 100 to 600 mL. It was not possible to sample any further because there would have been data missing for the DOE runs completed the fastest i.e. runs with high spray rate or low total binder volume. Where necessary, the responses were transformed using a mathematical function such as a logarithm or inverse, to maintain a normal distribution in the residuals. DOE analysis uses a regression approach to relate experimental factors to

measured responses by fitting coefficients to a polynomial model. The regression coefficients represent the importance of each factor to the model and an analysis of variance (ANOVA) is used identify significant effects, based on a 5% level of significance. The analysis considers each factor individually and in combination with the other factors. If the effect of a factor is found to depend on the level of one or more of the other factors it is known as an interaction. An interaction effect overrides a main effect, such that a factor involved in an interaction can no longer be considered individually.

The 10 Hz TPSD responses were also analyzed in Umetrics SIMCA P+ 11.5, using multivariate projection to latent structures by means of partial least squares (PLS). PLS is a method for relating two matrices of information, *X* and *Y*. In this case, the *X* matrix consisted of the three process factors (Table 6.1) and the *Y* matrix consisted of the 10 Hz TPSD responses for each DOE run. The PLS procedure followed by SIMCA involves first pre-processing the data by centering and scaling to unit variance. The *X* and *Y* observations are then plotted in two separate spaces of dimensions *N* and *M*, where *N* and *M* correspond to the number of variables in each matrix (Figure 6.1, A). When plotted, the observations form two clusters, one in the *X* space and another in the *Y* space (Figure 6.1, B). A straight line, known as a principal component, is fit to each cluster and the original data points are projected onto the lines. The projection coordinates are known as scores and are represented by a vector, *t* for the *X* space and *u* for the *Y* space. The lines are oriented to approximate the shape of each cluster and maximize the correlation between *t* and *u*. The first component describes the most

significant variability but additional components may be added to further represent the relationship between *X* and *Y*. For two or more components, the observations are projected onto a plane or hyper-plane formed by the principal components, instead of a straight line (Figure 6.1, C). In SIMCA, a cross validation procedure is used to determine the optimal number of components. The final relationship between the original data points and the new projection coordinates can be described using the following equations:

$$X = 1\underline{x}' + TP' + E \qquad (1)$$

$$Y = 1\underline{y}' + UC' + F \qquad (2)$$

Where $1\underline{x}'$ and $1\underline{y}'$ represent the variable averages after pre-processing, *T* and *U* are the scores matrices, *P'* and *C'* are the transposed loadings matrices, and *E* and *F* are the residuals. The correlation structure between *X* and *Y* can be visualized by plotting the score vectors, *t* and *u*, for each principal component (Figure 6.1, D). The score vectors are connected by the relationship $u_i = t_i + h_i$, where h_i is a residual. When there is perfect matching between *X* and *Y* the points will all be located on the 45° line passing through the origin [9].

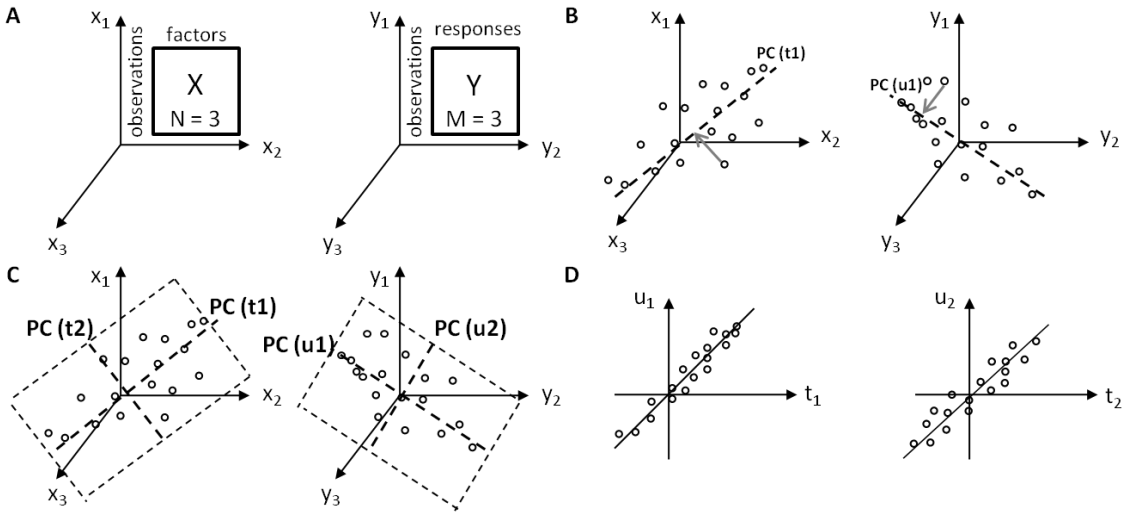

Figure 6.1 Description of the multivariate PLS analysis procedure. A – Describes how the observations for *X* and *Y* are each represented in a multivariate space with one axis for each variable. B – Describes the fitting of the first principal components to the *X* and *Y* data and the projection of the original data onto the lines to form the scores for the X-space, *t1* and the scores for the Y-space, *u1*. C – Describes the projection of the data onto a plane when two principal components are used. D – Provides a visualization of the correlation between *X* and *Y* based on the respective scores, *t* and *u*. Adapted from [9].

6.3. Results

The DOE investigation looked at the effect of minor variations in three process variables believed to be important for controlling granule quality: impeller speed, total binder volume and spray rate. The impact on quality was assessed by measuring the physical properties of intermediate products as well as the final tablets. The measured properties were based on a previous granulation study using the same formulation [2] and attributes commonly measured during product development.

6.3.1. Summary of physical property responses

The quality of the final tablets was acceptable for all DOE runs, satisfying the criteria for a design space. Table 6.2 shows the measured physical properties for the wet granules, dry granules and tablets; tablet measurements are only shown for the compression force where the largest difference was observed between runs. The percent relative standard deviation (%RSD) was computed for each physical property to show the degree of variation across ten batches. Tablet friability, break load, disintegration, and the fractions of midsized and large granules exhibited the greatest %RSD; while the fraction of fines by fluid-bed drying, density and flow differed by less than 5%. A comparison of the 10 DOE runs suggests the process conditions for DOE 3 and DOE 7 were the most favourable. The resulting tablets exhibited high break loads at 25 kN and the lowest number of friability failures at 15 kN. In addition, the size factions for the dried granules were consistent with the desired distribution for this formulation: low fines, high midsized granules and an average number of large granules. Both granulations were manufactured at low impeller speed and high binder volume but a low spray rate was used for DOE 3 and a high spray rate was used for DOE 7. This suggests impeller speed and binder volume were the most important conditions for achieving optimal physical properties and the effect of spray rate was relatively insignificant.

Table 6.2 Summary of physical property measurements for the granules and tablets

DOE	1	2	3	4	5	6	7	8	9	10	%RSD
Fines tray dried	0.56	0.58	0.52	0.56	0.65	0.6	0.57	0.56	0.59	0.59	**6**
Midsized tray dried	0.31	0.28	0.34	0.29	0.25	0.24	0.31	0.30	0.29	0.26	**11**
Large tray dried	0.12	0.14	0.14	0.14	0.10	0.16	0.13	0.14	0.12	0.14	**12**
Fines fluid-bed dried	0.82	0.84	0.77	0.80	0.80	0.83	0.76	0.79	0.81	0.80	**3**
Midsized fluid-bed dried	0.16	0.09	0.15	0.12	0.16	0.10	0.17	0.13	0.13	0.13	**20**
Large fluid-bed dried	0.02	0.07	0.08	0.09	0.05	0.07	0.06	0.08	0.06	0.07	**30**
Bulk density (g/cc)	0.32	0.33	0.33	0.34	0.31	0.31	0.32	0.33	0.32	0.32	**3**
Tap density (g/cc)	0.54	0.55	0.56	0.57	0.53	0.53	0.55	0.55	0.54	0.53	**2**
Flow avalanche time (s)	4	4	3.7	3.9	4.5	4.2	3.9	4	3.9	4	**5**
Flow break energy (Pa)	156	159	155	164	157	152	150	159	156	157	**2**
Friability failures	3	3	0	3	3	3	1	3	2	2	**46**
Break load at 15 kN (kg)	11.09	11.61	13.45	12.30	11.05	11.87	13.58	13.53	12.79	13.42	**8**
Disintegration at 25 kN (min)	4:34	4:51	5:02	5:06	5:07	4:58	5:15	5:33	5:40	5:44	**7**

6.3.2. DOE analysis of the AAE responses

DOE analysis of the 10 Hz TPSDs showed that both the time and volume-based responses were significantly affected by changes in the three process variables. The following sub-sections present examples for two frequency ranges, 110-120 Hz and 130-140 Hz, respectively selected for their relevance to granulation monitoring and end-point detection.

110-120 Hz

The 110-120 Hz TPSD profiles for each DOE run are shown in Figure 6.2 versus time and binder volume. The profiles all follow the same general trend: a sudden decrease, followed by a steady increase to a plateau (or a more gradual increase), a second steady increase to a maximum, and a final decrease. The features in the time-based profiles appear extended or compressed in the horizontal direction, depending on whether the spray rate was high or low. When the data is plotted by volume instead of time, the features are aligned and the only difference is the TPSD magnitude. The magnitude appears to depend on impeller speed, with higher intensities corresponding to runs at lower impeller speed. Some vertical separation is also observed based on spray rate, particularly for the time-based profiles. In general, the profiles are grouped in pairs according to impeller speed and spray rate, and the length of each profile varies with the amount of total binder volume. The one exception is DOE 7, where the TPSD magnitude is higher than that of its proposed pair, DOE 5.

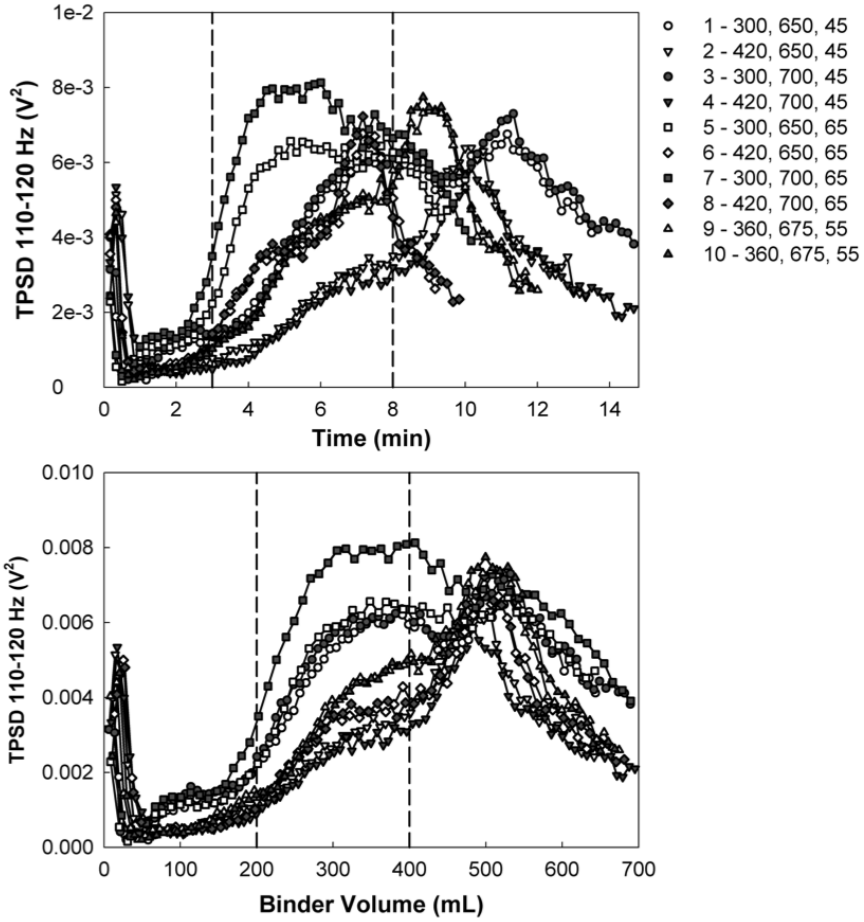

Figure 6.2 110-120 Hz TPSD versus time (top) and versus binder volume (bottom) for each DOE run. Run conditions are listed in the legend as follows: DOE # - impeller speed (rpm), total binder volume (mL), spray rate (mL/min). The dashed lines define the region where the process factors show significant linear relationships to the TPSD response.

The DOE analysis identified significant linear relationships between minutes 3 and 8 and volumes 200 and 400 mL for the 110-120 Hz TPSD responses. For the time-based responses, the analysis showed impeller speed and spray rate were linearly related to TPSD between minutes 3 and 6. Figure 6.3 provides a representative description of the two independent relationships using the DOE plots for minute 6. DOE plots show the linear effect of changing the level of a factor from low to high. The two dots represent

the center points and describe how closely the linear approximation represents the data. For single factor plots the centre points should be close to the linear approximation and for interactions they should be centrally located between the two linear approximations. The DOE plots for minute 6 show that increasing the impeller speed caused a decrease in TPSD and increasing the spray rate caused an increase in TPSD. The relationships establish that the differences in TPSD magnitude observed in Figure 6.2 are statistically significant and a direct result of changes in impeller speed and spray rate. For minutes 7 and 8, a significant interaction was identified between impeller speed and spray rate in relation to TPSD. The DOE plots show the TPSD did not change with spray rate for runs at low impeller speed, but at high impeller speed there was a significant decrease in TPSD for runs at low spray rate (Figure 6.3). This agrees with the separation in the TPSD profiles for runs at 420 rpm, compared to the overlap observed for runs at 300 rpm between minutes 7 and 8 (Figure 6.2) and suggests the TPSD is sensitive to differences in granulation rate.

The results for the volume-based responses were similar from 200 to 400 mL. Figure 6.3 provides a representative description of the relationship using the DOE plots for 300 mL. The plots show that increasing the impeller speed caused a decrease in TPSD and increasing the spray rate caused an increase in TPSD. The relationships agree with the time-based results for minute 6 and correspond to approximately the same point in processing. There were no interactions observed, likely because the profile trends were more aligned when the results were considered based on binder volume. In general,

the DOE analysis showed the increase in TPSD during wetting was affected by impeller speed and spray rate, with the highest TPSD corresponding to runs at low impeller speed and high spray rate.

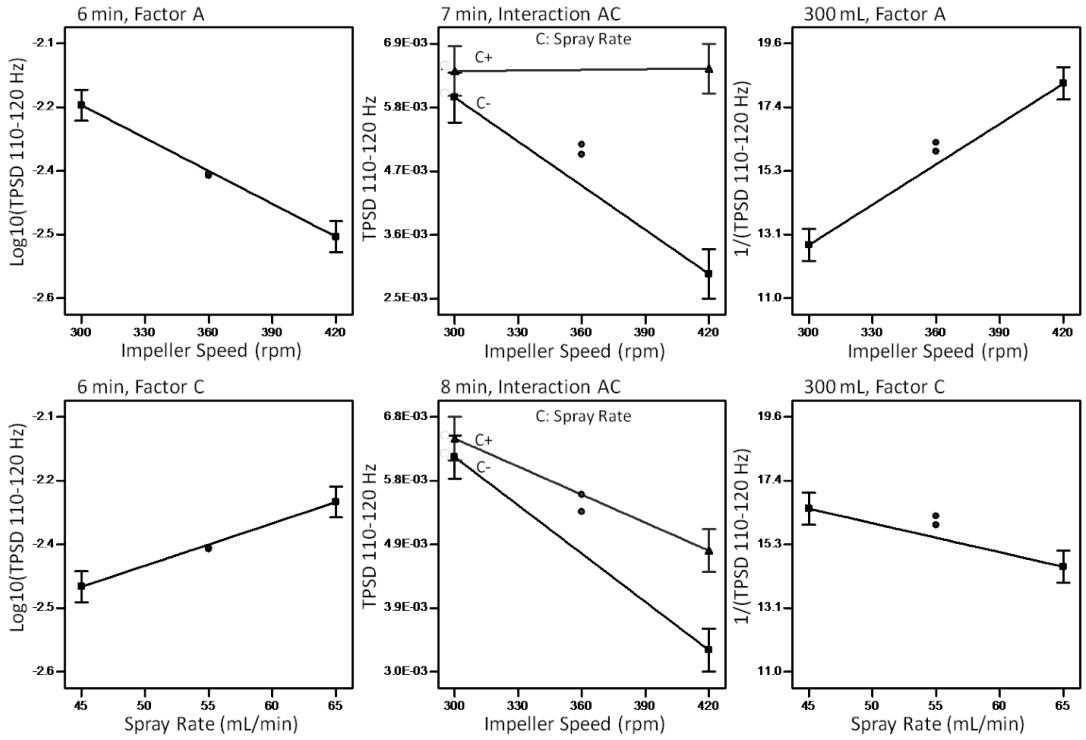

Figure 6.3 DOE plots for significant factors and interactions affecting the 110-120 Hz TPSD throughout granulation. The three factors are the effect of impeller speed (A), total binder volume (B) and spray rate (C). For the results at 6 min and 300 mL, logarithm and inverse transforms were used to achieve a normal distribution in the residuals.

130-140 Hz

Figure 6.4 shows the progression of the 130-140 Hz TPSD over time (top) and binder addition (bottom). Similar to the 110-120 Hz range (Figure 6.2), all profiles show a sharp decrease at the initial onset of wetting. The profiles then exhibit a delay, followed by a rapid increase in TPSD. Depending on the extent of granulation, the increase is followed

by a plateau and a decrease. The magnitude of the rapid increase appears to depend on impeller speed, with runs at high impeller speed corresponding to greater intensities. Similar to 110-120 Hz, the profiles align when the results are plotted versus binder volume. Arranged this way, the relationship between intensity and impeller speed is more apparent and additional separation is observed based on spray rate. For the low impeller speed, runs at low spray rate correspond to higher magnitudes than runs at high spray rate and for the high impeller speed, a relatively flat local maximum is observed between 300 and 400 mL.

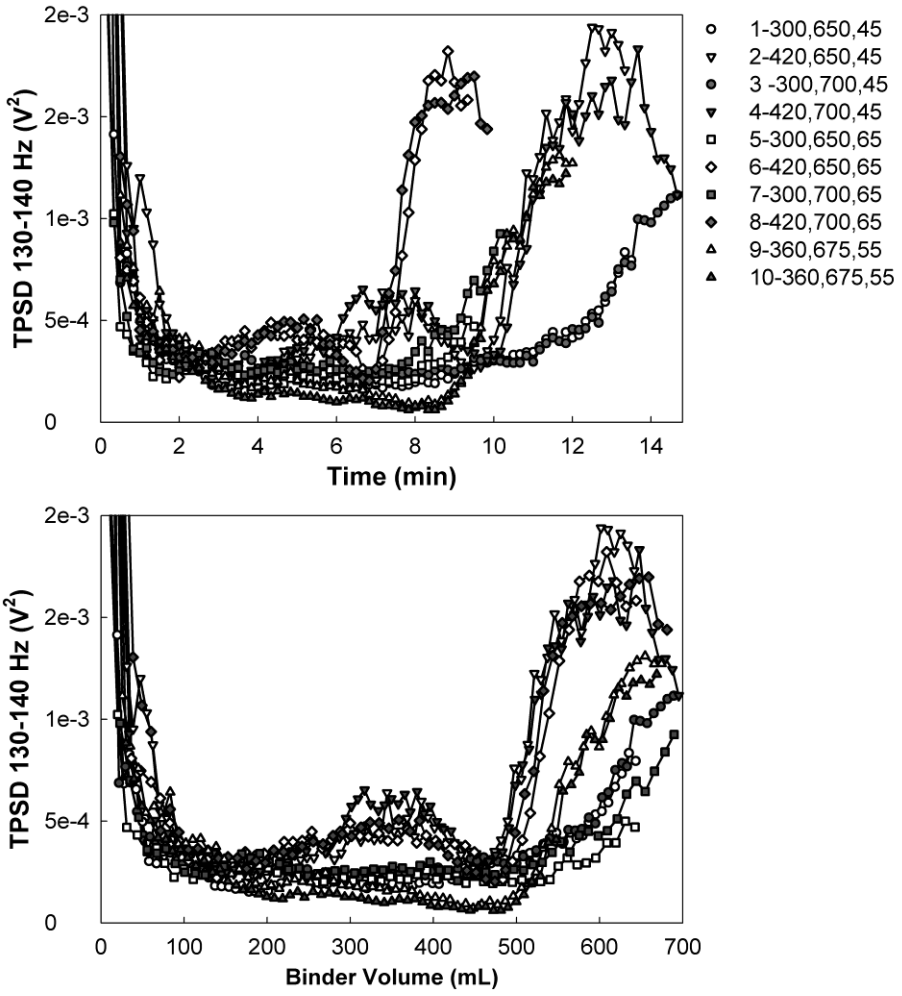

Figure 6.4 130-140 Hz TPSD versus binder volume for each DOE run. Run conditions are listed in the legend as follows: DOE # - impeller speed (rpm), total binder volume (mL), spray rate (mL/min).

For the 130-140 Hz range, the DOE analysis was the most relevant towards the end of wetting, where the TPSD increased (Figure 6.4). Figure 6.5 shows the significant process effects and interactions identified for the TPSD responses 50 mL and 30 s prior to the end of wetting, and at the end of wetting. The DOE plots show the significant effects were impeller speed and the interaction between impeller speed and total binder volume. The general trend was an increase in TPSD with increasing impeller speed. The

interactions indicate the increase in TPSD with impeller speed was more significant for runs at low binder volume, due to differences in granulation rate. Runs at low binder volume granulated the slowest and were still increasing in TPSD during the final stages of wetting, while runs at high binder volume were reaching a plateau or showing a decrease in TPSD that is consistent with over wetting (Figure 6.4).

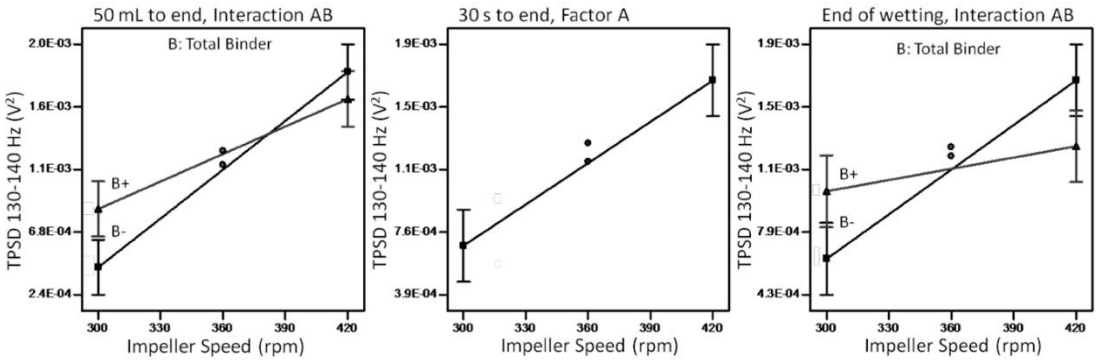

Figure 6.5 DOE plots for significant factors affecting the 130-140 Hz TPSD at 50 mL to the end of wetting, 30 s to the end of wetting and the end of wetting. The three factors are the effect of impeller speed (A), total binder volume (B) and spray rate (C).

6.3.3. Multivariate PLS analysis of AAE responses

Multivariate PLS modeling allowed for the simultaneous analysis of the relationships between the three process variables and the 10 Hz TPSDs, rather than considering each 10 Hz response separately. Figure 6.6 shows how well the 10 Hz TPSDs correlated to the process variables by comparing their respective projection coordinates, *t* and *u*. For the first principal component, the location of the projection coordinates *t[1]* and *u[1]* close to the 45° line demonstrates good matching between the process variables and the 10 Hz TPSD data. The R^2 value indicates 99% of the variability in the 10 Hz TPSDs

described by the first principal component can be explained by changes to the process parameters. The observations are separated into three groups according to impeller speed, indicating impeller speed was the primary source of variability in the 10 Hz TPSDs. Figure 6.6 also shows the relationship between the projection coordinates for the second principal component, *t[2]* and *u[2]*. Again the observations are located close to the 45° line and the R^2 value indicates 97% of the change in TPSD described by the second principal component can be explained by changes in the process variables. The data is separated into three groups according to spray rate; therefore spray rate is the second most significant source of variability.

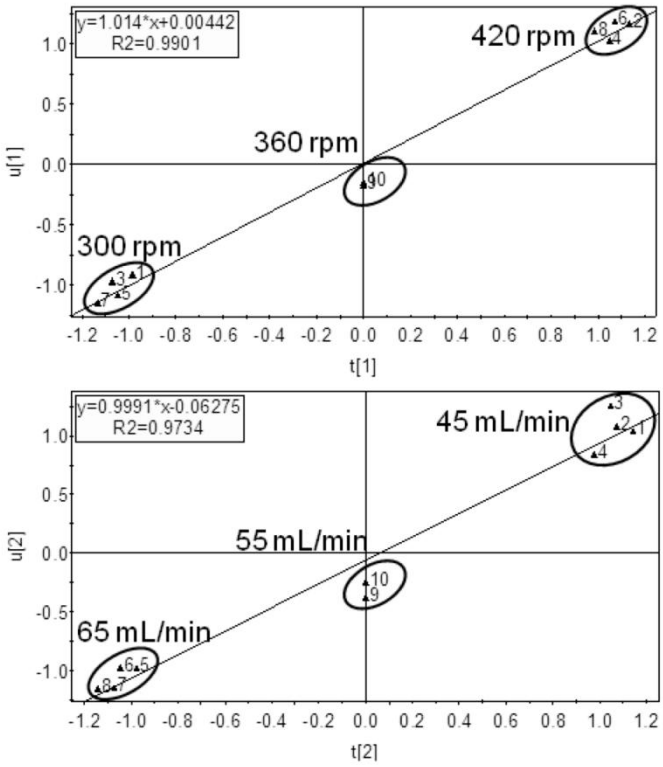

Figure 6.6 Correlation between the observations projected onto the first [1] and second [2] principal components, where *t* represents the projection coordinates for the process variables (*X*) and *u* represents the projection coordinates for the 10 Hz TPSDs (*Y*).

6.4. Discussion

The results show the DOE successfully varied three process parameters in a manner consistent with design space development. The quality of the final product was acceptable in all cases and the process could be optimized by moving in the direction of low impeller speed and high total binder volume. The changes in process conditions were detectable by AAEs and demonstrated to be statistically significant. The results support the use of acoustics to optimize operating conditions and monitor batch progress towards target final properties, thereby reducing the need for offline analysis and testing. The following discussion will further explore the application of AAEs to process monitoring and end-point control.

6.4.1. Summary of DOE physical properties analysis

The results from the DOE analysis of the physical property responses can be used for process optimization and knowledge building. Figure 6.7 summarizes the results according to a series of common process objectives, such as decreasing the fraction of fines or increasing tablet break load. Tablet disintegration was not included because there were either large amounts of curvature or no significant effects. This was not a concern, since the tablets all dissolved rapidly, in under 6 minutes (Table 6.2). For each process objective, an asterisk was used to identify the most significant effect or interaction, except in cases where two effects were similar. As an example, reading across, the first row shows the fines fraction was reduced by operating at low impeller

speed or high total binder volume, and the effect of total binder volume was more significant than the effect of impeller speed. The results are logical because at low impeller speed there would be less attrition and at high binder volume a greater number of fines would be incorporated into agglomerates. As another example, the second last row shows tablet friability was reduced by operating at high total binder volume and low spray rate, or low impeller speed and low spray rate. Since there is no asterisk, both combinations had similar effects on friability.

The summary provides statistical evidence of the importance of impeller speed and total binder volume to product quality. In agreement with Table 6.2, the chart suggests low impeller speed and high total binder volume were the preferred run conditions, and the effect of spray rate was relatively insignificant. Low impeller speed satisfied the process objectives for all three size fractions, and high total binder volume was the most significant factor for three of the seven objectives, including increasing break load for tablets compressed at 25 kN. In addition, the combination of low impeller speed and high binder volume produced tablets with optimal break loads for compression forces of 10, 15 and 20 kN. The opposing factor levels, high impeller speed and low binder volume, were identified less frequently and coincided with objectives that varied minimally across the ten batches, such as density and flow.

The summary also provided statistical support for the relative unimportance of spray rate in achieving the desired product attributes. Spray rate was only significant for

increasing granule density and flow, two properties with low %RSD (Table 6.2), and was never the most significant factor. As such, the results statistically confirm the hypothesis that low impeller speed and high total binder volume were favourable and spray rate was relatively insignificant, in terms of the measured physical properties. The chart format was useful for assessing the overall impact on product quality from changes made during granulation and identifying the most significant sources of variability. In the future, it would be possible to use the chart to decide which process conditions to use based on the desired product attributes.

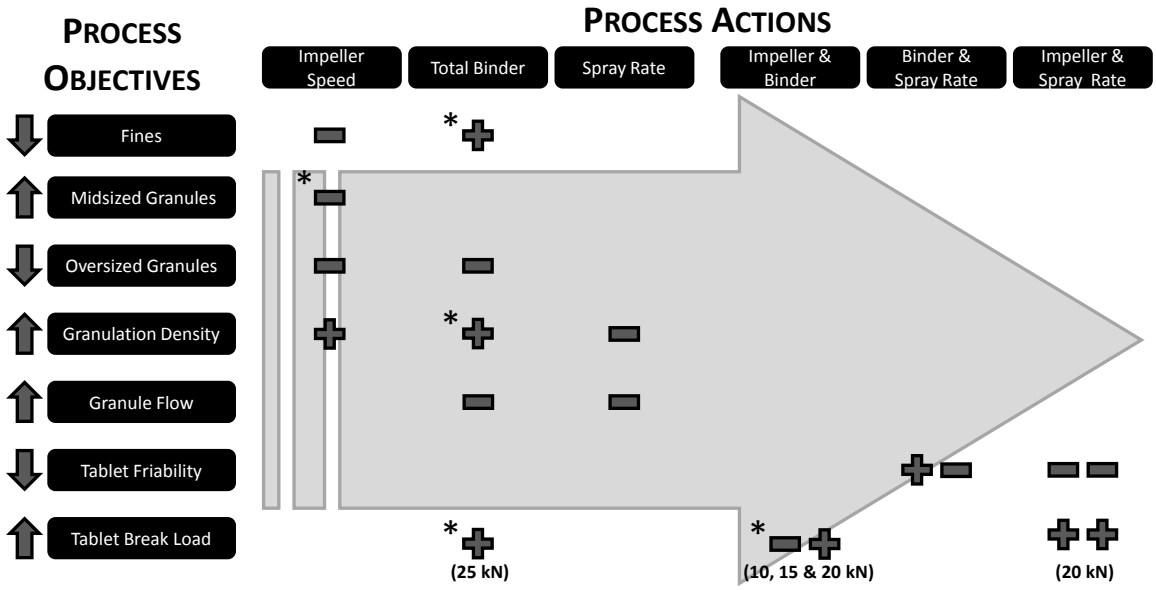

Figure 6.7 Sample of how DOE results can be used to achieve various process objectives. The + and - symbols refer to the high and low levels for each process variable, and the most significant effect is identified by an asterisk. If no asterisk is shown then both actions are of similar significance. The size fractions correspond to the fluid-bed dried samples and density encompasses the results for both tap and bulk measurements.

6.4.2. Detection of process changes from AAEs

The AAEs detected by the air exhaust microphone were sensitive to changes in all three process conditions: impeller speed, total binder volume and spray rate. The position of the microphone allowed for collection of AAEs that were representative of the complete granulation process and therefore effective for detecting changes in process conditions. Impeller speed and spray rate were found to be significant in relation to wetting, while impeller speed and total binder volume were significant in terms of end-point. Statistical significance does not necessarily imply process significance, and the physical property measurements (Table 6.2) were used to assess the impact of the process changes in terms of product usability. The following section further investigates the relationship between the changes in process conditions and the 10 Hz TPSD responses.

Impeller speed

The importance of changes in impeller speed to final product quality was demonstrated by the physical property measurements. The results show impeller speed has a significant effect on the granule size distribution and density (Figure 6.7), which is expected since impeller rotation is known to affect the rate of granule growth and consolidation [10]. AAEs were shown to be an effective method for monitoring changes in impeller speed and would therefore be useful for optimizing particle size distribution and density. Vertical separation in the 110-120 and 130-140 Hz TPSDs profiles was greatest between runs at different impeller speeds (Figure 6.2, Figure 6.4) and the DOE

and PLS analyses both identified impeller speed as the most significant process factor affecting TPSD (Figure 6.3, Figure 6.5, Figure 6.6).

The impeller speed corresponding to the highest TPSD magnitude was observed to depend on frequency. For 110-120 Hz, the DOE runs at 300 rpm corresponded to the highest TPSD, whereas for 130-140 Hz the highest magnitude was observed for runs at 420 rpm (Figure 6.2, Figure 6.4). Similar discrepancies were also observed for other 10 Hz frequency groups (Appendix C). The change in magnitude with impeller speed is thought to reflect a change in the granule shearing motion, resulting in a different dominant frequency and harmonics. The results are consistent with findings for sheared sand grains, where the sound frequency was observed to increase with increased shearing velocity due to a change in the relative motion of the moving grains [11]. The AAEs from shearing sand grains are harmonic in nature, consisting of one dominant frequency and several higher harmonics [12], and are believed to be similar to AAEs generated during high-shear granulation [2].

The direct relationship between AAEs and granule shearing explains why impeller speed was repeatedly identified as the most significant process variable. The velocity profile for shear flow has been shown to vary with impeller speed, particularly near the bottom of the vessel, in close proximity to the agitation source [13, 14]. A change in impeller speed is therefore thought to affect the frequency and velocity of particle collisions, resulting in a change in the AAEs. The results agree with a DOE study by Gamble et al.

[8], where a model for detecting granulation end-point from acoustic emissions failed when the impeller speed was changed. The failure was attributed to a change in the granule velocity with impeller speed that affected the acoustic frequency of the granules. The results enforce the need to monitor a number of frequencies, rather than focusing on a single range as some researchers have done. A model with complete frequency information will be more robust and better equipped to accommodate necessary changes in process parameters during the development process. A robust model would also satisfy the ICH Q8 objectives, which emphasize movement towards flexible operation, where parameters can be adjusted in-process to accommodate variability that may affect product quality.

Spray Rate

Spray rate was shown to have the next most significant effect on the AAEs, after impeller speed. The DOE analysis of the 110-120 Hz range identified spray rate as a significant variable (Figure 6.3) and the PLS model showed separation based on spray rate in the second principal component (Figure 6.6). The results suggest spray rate affected the AAEs generated during wetting. This is likely because the introduction of binder increased granule cohesiveness, which has been shown to increase the momentum transfer to particles and consequently particle surface velocity [15, 16]. The results suggest the increase in granule cohesiveness had an effect on granule shearing and consequently the generation of AAEs. The relationship between surface velocity and spray rate is expected because the surface particles would be the first affected by

the water droplets, just as granules close to the impeller would be the first affected by a change in impeller speed.

The effect of spray rate was relatively insignificant in relation to the final stages of granulation. The measured physical properties were not significantly affected by spray rate and neither were the 10 Hz TPSDs from the end of wetting. This could be because the AAEs associated with spray rate became damped towards the end of wetting, due to the lubrication effect created by liquid at the granule surface. When granules become dense, liquid from the pores is squeezed to the surface and a film develops on the outside of the granules. In previous work, the presence of liquid on the granule surface was shown to contribute to a decrease in AAEs during the latter half of wetting [2, Chapter 4, Chapter 5] and for shearing sand grains AAEs were observed to decrease with an increase in humidity [17].

The difference between volume and time-based sampling was the most evident in relation to spray rate (Figure 6.2, Figure 6.4). The horizontal separation in the time based profiles with spray rate agrees with results by Briens et al. [18]. The alignment observed when the data was plotted versus volume instead of time demonstrates the majority of the spray rate effect was due to differences in the amount of binder added, rather than the rate of binder addition. The results suggest the total amount of binder is more important to granule growth than the rate of addition and are consistent with a DOE study of high-shear granulation by He et al. [19], where total water was shown to

be more important than fluid addition rate and wet massing time. In addition, the findings suggest it may not be necessary to control the rate of water addition during granulation, as long as the total volume requirement is met.

Total binder volume

Differences in total binder volume only affected the AAEs related to the end of wetting. The DOE results showed total binder volume was significant in relation to the final granule properties (Figure 6.7) and the increase in the 130-140 Hz TPSD profile towards the end of wetting (Figure 6.4). The increase in the 130-140 Hz TPSD occurred 500 mL into binder addition and coincided with a decrease in the 110-120 Hz TPSD profile (Figure 6.2). As such, the increase is thought to correspond to granule densification and the presence of liquid on the granule surface. Surface liquid increases granule cohesion and stickiness and is believed to reduce granule shearing, resulting in a more collective bulk motion. The collective motion differs from the surface motion detected in the 110-120 Hz range and is therefore represented by a different acoustic frequency. It is not present until the granules reach a dense, agglomerated state, and is therefore consistent with the relative absence of AAEs in the 130-140 Hz range prior to 500 mL. Overall, the results suggest the 10 Hz frequencies respond to changes in the granular motion with wetting in addition to changes in process conditions.

The significance of binder volume towards the end of wetting illustrates its critical effect on the granulation process, in relation to AAEs and final granule properties. The percent variation between the center point and the high and low extremes was only ±4%, in

comparison to ±17% and ±18% for impeller speed and spray rate, respectively. The range for total binder volume was purposely reduced because results from an earlier study of granulation end-point showed changes in total binder volume rapidly affected critical final properties, such as particle size and tablet hardness [2]. Introducing greater variability would have resulted in failed batches, which is inconsistent with the design space approach. Instead, the results reinforce the critical sensitivity of the granulation process to binder volume and the opportunity to significantly alter the granulation outcome through its control.

6.4.3. Application to pharmaceutical development and process control

The dynamic features of the TPSD profiles support online monitoring of AAEs to determine whether an adjustment in process conditions is needed to achieve the desired physical properties. The features in the 110-120 and 130-140 Hz TPSD profiles support both process monitoring and end-point detection (Figure 6.2, Figure 6.4). The horizontal shift in the time-based profiles was consistent with the rate of binder addition and the vertical shift in the volume-based profiles was primarily related to impeller power. For 130-140 Hz, the plateau towards the end of wetting was consistent with end-point and acceptable product quality. The results support the development of a process signature using the AAEs that would become the target for future batches [2]. For each granulation, the AAEs could be compared to the target profile to facilitate the achievement of optimal product quality. This interactive approach would reduce

development times for new products and result in more flexible processes capable of accommodating variability in raw material properties and processing conditions.

The results from the multivariate PLS model support use in online process control. The first component scores are suitable for monitoring impeller speed and the second component scores are suitable for monitoring binder volume through the control of spray rate. The scores can be used to define the design space, by establishing upper and lower limits for operation. By computing the scores online at regular intervals throughout granulation, a feedback control system could be implemented where impeller speed and spray rate are adjusted to achieve consistent product quality. Such a system would reduce development times for new products and help achieve consistent quality when a process is scaled-up from development to manufacturing. Further runs are necessary to define the scores associated with failure conditions outside the design space and to increase the number of observations used to construct the model, as ten runs are insufficient for online prediction.

6.5. Conclusions

The complexity of the high-shear granulation process makes it unpredictable in the sense that minor changes in raw material inputs or processing conditions can affect product quality. Rather than follow a set manufacturing procedure that does not allow for these variations, it is desirable to design a more robust process where a range of operating conditions are acceptable. The result is a more flexible operation, where

minor variations can be accommodated by adjusting the process parameters. In order for this technique to work, a method is required for monitoring batch quality throughout granulation.

The findings presented here support the development of AAEs as a PAT technology for monitoring changes in process conditions to achieve a desired product quality. DOE and multivariate PLS analyses showed AAEs from high-shear wet granulation were sensitive to changes in impeller speed, spray rate and total binder volume. Impeller speed and spray rate were significant in relation to granulation wetting, and impeller speed and total binder were the most relevant approaching granulation end-point. Future work should involve integration of a classification system for new data points and adaptation into an online system using either the TPSD profiles or the multivariate scores. Such a system would provide a quantitative method for process optimization that would reduce development times and help build process knowledge to benefit development activities as well as scale-up and product transfers.

6.6. References

[1] U.S. Department of Health and Human Services, Food and Drug Administration, Center for Drug Evaluation and Research (CDER), Center for Biologics Evaluation and Research (CBER). (2008). *Guidance for industry Q8 pharmaceutical development, second revision*. Retrieved from http://www.fda.gov/downloads/Drugs/GuidanceComplianceRegulatoryInformation/Guidances/ucm073507.pdf.

[2] Hansuld, E.M., Briens, L., McCann, J.A.B. & Sayani, A. (2009). Audible acoustics in high-shear wet granulation: application of frequency filtering. *International journal of pharmaceutics, 378,* 37-44.

[3] Whitaker, M., Baker, G.R., Westrup, J., Goulding, P.A., Rudd, D.R., Belchamber, R.M. & Collins, M.P. (2000). Application of acoustic emission to the monitoring and end point determination of a high shear granulation process. *International journal of pharmaceutics, 205,* 79-91.

[4] Papp, M.K., Pujara, C.P. & Pinal, R. (2008). Monitoring of high-shear granulation using acoustic emission: predicting granule properties. *Journal of pharmaceutical innovation, 3,* 113-122.

[5] Box, G.E.P., Hunter, W.G. & Hunter, J.S. (1978). *Statistics for experimenters: an introduction to design, data analysis and model building*. New York: John Wiley & Sons Inc.

[6] Gabrielsson, J., Lindberg, N. & Lundstedt, T. (2002). Multivariate methods in pharmaceutical applications. *Journal of chemometrics, 16,* 141-160.

[7] Huang, J., Kaul, G., Cai, C., Chatlapalli, R. & Hernandez-Abad, P. (2009). Quality by design case study: An integrated multivariate approach to drug product and process development. *International journal of pharmaceutics, 382,* 23-32.

[8] Gamble, J.F., Dennis, A.B. & Tobyn, M. (2009). Monitoring and end-point prediction of a small scale wet granulation process using acoustic emission. *Pharmaceutical development and technology, 14,* 299-304.

[9] Eriksson, L., Johansson, E., Kettaneh-Wold, N., Trygg, J., Wikström, C. & Wold, S. (2006). *Multi- and megavariate data analysis Part I basic principles and applications, 2nd edition*. Sweden: Umetrics.

[10] Litster, J., Ennis, B. & Liu, L. (2004). *The science and engineering of granulation processes.* The Netherlands: Kluwer Academic Publishers.

[11] Douady, S., Manning, A., Hersen, P., Elbelrhiti, H., Protière S., Daerr, A. & Kabbachi, B. (2006). Song of the dunes as a self-synchronized instrument. *Physical review letters, 97,* 1-4.

[12] Vriend, N.M., Hunt, M.L., Clayton, R.W., Brennen, C.E., Brantley, K.S. & Ruiz-Angulo, A. (2007). Solving the mystery of booming sand dunes. *Geophysical research letters, 23,* 1-6.

[13] Sato, Y., Nakamura, H. & Watano, S. (2008). Numerical analysis of agitation torque and particle motion in a high shear mixer. *Powder technology, 186,* 130-136.

[14] Saito, Y., Fan, X., Ingram, A. & Seville, J.P.K. (2011). A new approach to high-shear mixer granulation using positron emission particle tracking. *Chemical engineering science, 66*, 563-569.

[15] Litster, J.D., Hapgood, K.P., Michaels, J.N., Sims, A., Roberts, M. & Kameneni, S.K. (2002). Scale-up of mixer granulators for effective liquid distribution. *Powder technology, 124,* 272-280.

[16] Plank, R., Diehl, B., Grinstead, H. & Zega, J. (2003). Quantifying liquid coverage and powder flux in high-shear granulators. *Powder technology, 134,* 223-234.

[17] Sholtz, P., Bretz, M. &Nori, F. (1997). Sound-producing sand avalanches. *Contemporary physics, 38,* 329-342.

[18] Briens, L., Daniher, D. & Tallevi, A. (2007). Monitoring high-shear granulation using sound and vibration measurements. *The international journal of pharmaceutics, 331,* 54-60.

[19] He, X., Lunday, K.A., Li, L. & Sacchetti, M.J. (2008). Formulation development and process scale up of a high shear wet granulation formulation containing a poorly wettable drug. *Journal of pharmaceutical sciences, 97,* 5274-5289.

Chapter 7

7. General discussion and conclusions

Granulation is a common step in the manufacture of pharmaceutical solid dosage forms. The objective of granulation is to improve the properties of fine powders through size enlargement to facilitate downstream unit operations, such as tabletting. Granule growth is complex, depending on a number of mechanisms and the transition to rapid growth and over wetting often occurs quickly [1]. As a result, granulation behaviour is difficult to predict, for both new and existing formulations, and variations in raw material properties, process conditions, or equipment can lead to changes in product quality. This is a concern for the pharmaceutical industry, as product quality is essential for drug safety and effectiveness. During development, batches are scaled from bench-top to manufacturing units, and production changes hands from scientists to plant operators. As a result, it is important to completely understand each product and how it behaves under different conditions. The development of quantitative systems for process monitoring and end-point detection would help control product quality and reduce the time and effort required for product development and scale-up. A variety of technologies have been investigated, however a disconnect between the tools developed and regulatory objectives appears to be hindering widespread adoption of any one technique.

The objective of this work was to develop AAEs as a PAT for high-shear granulation, with attention to the recommendations provided by the FDA and other regulatory bodies [2]. The ICH Q8 guidance document emphasizes the importance of developing technologies that improve process understanding and increase manufacturing flexibility. As a result, demonstration of a correlation between online measurements and granulation end-point is only the first step in PAT development. The work presented in this thesis demonstrates the robustness of AAEs as a technology for monitoring granulation and detecting end-point by 1) relating the AAEs to critical quality attributes, such as particle size and density 2) investigating the effect of process parameters, such as impeller speed, spray rate, and total binder volume on the AAEs and 3) using controlled experiments to better understand the source of the AAEs and why the technology is effective. The incorporation of DOE and multivariate analysis techniques provided an effective means of extracting relevant information from the AAEs and understanding relationships to the granulation process and final product quality.

This thesis builds on proof-of-concept work by Daniher et al. [3] and Briens et al. [4], demonstrating AAEs collected from the air exhaust of a high-shear granulator can be related to process end-point. The air exhaust location is unique to AAE collection and cannot be applied to ultrasonic acoustic emissions, as ultrasonic waves attenuate significantly in air [5]. The findings presented in this work suggest the air exhaust location is favourable because the information collected is directly related to particle interactions and reflects the collective granulation process (Chapter 4). The relationship

between AAEs and particle-particle interactions was demonstrated by rotating MCC and sugar spheres of known size in stainless steel beakers, and rotating MCC spheres in a high-shear granulator. The beaker experiments made it possible to isolate AAEs from particle-particle and particle-equipment interactions, by removing the effects of the impeller and binder addition. Using multivariate PCA and PLS models, it was possible to establish a relationship between AAEs and sphere size, confirming that AAEs are related to particle behaviour. In addition, the similarity between the AAEs for MCC in the beaker and the granulator suggested the dominate source of AAEs is particle-particle interactions, rather than particle-equipment interactions. Multivariate analysis of the AAEs showed the sound from the spheres was generated by two different sources (Chapter 4). Low frequency emissions, negatively correlated with size, were thought to result from interactions between particles near the base of the vessel, and high frequency emissions, positively correlated with size, were thought to reflect particle interactions at the surface. The results for the low frequencies support the observed decrease in AAEs with granulation end-point and over wetting [6], while the positive relationships for high frequencies support correlations developed in the ultrasonic range [7, 8].

The results from the beaker experiments suggest AAEs are sensitive to different types of particle interactions. Granulation depends on a number of complex interactions; therefore, the ability to detect different behaviours would be useful for understanding the complete process. TPSD analysis of AAEs from high-shear granulation showed

unique trends could be identified when the profiles were divided into 10 Hz groups (Chapter 3) and multivariate analysis confirmed a relationship to physical property changes (Chapter 5). A PLS model showed different combinations of 10 Hz TPSDs were predictive of changes in size versus changes in density during granulation, suggesting densification and growth do not occur uniformly throughout the granulator. In a separate study, a PLS model was generated using the 10 Hz TPSDs from granulations completed under different process conditions (Chapter 6). The resulting model showed the variability in the 10 Hz TPSDs represented by the first principal component was related to changes in impeller speed, while the variability represented by the second principal component was related to changes in spray rate. The results suggest the AAEs are information-rich and reflect the complexity of particle behaviour during granulation. The findings are in contrast to other PATs, where measurements reflect a localized area in front of the probe and may not be representative of the complete process.

In addition to the unique features identified in the 10 Hz TPSD profiles, a common decrease in acoustic intensity was shown to coincide with granulation end-point and over wetting (Chapter 3). The decrease was consistently observed, independent of changes in formulation, raw material properties and process parameters and agrees with ultrasonic acoustic emissions profiles for fluidized-bed [9] and high-shear granulations [8, 10]. Despite its common occurrence, there has been relatively little research into the source of the decrease. In this work, a DOE approach was used to investigate the effect of changes in size and density on the granulation AAEs (Chapter 5).

The results from the DOE analysis showed increases in size and density contribute significantly to the decrease. The relationship to size was also identified in the beaker experiments, where low frequency groups were shown to be negatively correlated to size for sugar spheres, MCC spheres and wet granules (Chapter 4). The findings confirm AAEs are useful for understanding physical changes that occur during granulation and offer an explanation for the consistent decrease during the latter half of wetting.

Multivariate analysis was used throughout this work to extract meaningful information from large amounts of data and simplify understanding of a complex process. A routine was developed utilizing the VIP parameter to identify frequencies with relevant information for monitoring granulation (Chapter 3). The combined results for three formulations showed the most relevant information was concentrated below 250 Hz. The findings are similar to the range identified by Daniher et al. [3] for high-shear granulation and Briongos et al. [11] for fluidized-bed granulation. The VIP routine greatly simplified subsequent analysis of the AAEs by reducing the number of frequency groups considered from 1998 to 23. In later work, multivariate analysis was used to simplify understanding of the AAEs by establishing relationships to quality attributes and process parameters (Chapter 5, Chapter 6). Predictive relationships were identified between the OPLS scores and measurements of particle size distribution, bulk density and tap density (Chapter 5). The scores profiles were shown to be unique for each measurement and online computation would provide a means of evaluating changes in real-time using AAEs. Measurements of size and density are valuable because both

variables have been identified as critical to granule quality [12], yet they are difficult to measure online. There are currently no technologies capable of isolating changes in density, and existing PATs for measuring particle size require equipment modification or product contact. AAEs provide a method for measuring both properties non-intrusively, using a single sensor. Multivariate scores were also shown to be sensitive to changes in impeller speed, spray rate and total binder volume (Chapter 6). The results suggest impeller speed and spray rate could be adjusted online to achieve target granule properties, using multivariate scores plots to monitor the changes.

In summary, the findings provide support for the adoption of AAEs as a PAT technology for high-shear granulation. The demonstrated relationship of AAEs to particle-particle interactions and changes in size and density confirm the information acquired is relevant to the granulation process. As a result, AAEs can be used with confidence to understand and accommodate process variability during product development and manufacturing. The results support the initiatives outlined in the ICH Q8 guidance to build process knowledge and increase manufacturing flexibility using PATs [2]. With improved process knowledge, it would be possible to adjust operating parameters in real-time to achieve the desired product quality, rather than relying on offline testing. In addition, AAEs could be used to reduce development times for new products. AAEs were demonstrated to be sensitive to impeller speed and spray rate; therefore, these parameters could be adjusted during granulation to achieve target profiles for critical properties such as particle size and density. Having quantitative, real-time information

would reduce the dependence on offline measurements, such that processes could be optimized in fewer iterations. It would also be easier to identify the root cause of product issues because it would not be necessary to trace offline measurements back through each stage of processing. Quantitative measurements may also be valuable for assisting scale-up operations and product transfers, where it is desirable to maintain consistent product attributes. Since AAE sensors are small and portable they would be easy to move from one unit to another to compare information on quality attributes. Overall, the work demonstrates AAEs provide a robust measure of the complex interactions known to occur during granulation and with the use of multivariate analysis techniques it is possible to extract relevant information to increase process understanding and assist in optimization and control. Future work should focus on the development of online systems for measuring changes in critical quality attributes and detecting end-point at both development and manufacturing scales.

7.1. References

[1] Iveson, S.M., Litster, J.D., Hapgood, K. & Ennis, B.J. (2001). Nucleation, growth and breakage phenomena in agitated wet granulation processes: a review. *Powder technology, 117,* 3-39.

[2] U.S. Department of Health and Human Services, Food and Drug Administration, Center for Drug Evaluation and Research (CDER) & Center for Biologics Evaluation and Research (CBER). (2008). *Guidance for industry Q8 pharmaceutical development, second revision*. Retrieved from http://www.fda.gov/downloads/Drugs/GuidanceComplianceRegulatoryInformation/Guidances/ucm073507.pdf.

[3] Daniher D. Briens, L. & Tallevi, A. (2007). End-point detection in high-shear granulation using sound and vibration signal analysis. *Powder technology, 181,* 130-136.

[4] Briens, L., Daniher, D. & Tallevi, A. (2007). Monitoring high-shear granulation using sound and vibration measurements. *International journal of pharmaceutics, 331,* 54-60.

[5] Bass, H.E., Campanella, A.J., Chambers, J.P. & Lindsay, R.B. (2008). Sound absorption. *AccessScience, McGraw-Hill Companies*. Retrieved from www.accessscience.com.

[6] Hansuld, E.M., Briens, L., McCann, J.A.B. & Sayani, A. (2009). Audible acoustics in high-shear wet granulation: application of frequency filtering. *International journal of pharmaceutics, 378,* 37-44.

[7] Whitaker, M., Baker, G.R., Westrup, J., Goulding, P.A., Rudd, D.R., Belchamber, R.M. & Collins, M.P. (2000). Application of acoustic emission to the monitoring and end point determination of a high shear granulation process. *International journal of pharmaceutics, 205,* 79-91.

[8] Papp, M.K., Pujara, C.P. & Pinal, R. (2008). Monitoring of high-shear granulation using acoustic emission: predicting granule properties. *Journal of pharmaceutical innovation*, *3,* 113-122.

[9] Tsujimoto, H., Yokoyama, T., Huang, C.C. & Sekiguchi, I. (2000). Monitoring particle fluidization in a fluidized bed granulator with an acoustic emission sensor. *Powder technology, 113,* 88-96.

[10] Gamble, J.F., Dennis, A.B. & Tobyn, M. (2009). Monitoring and end-point prediction of a small scale wet granulation process using acoustic emission. *Pharmaceutical development and technology, 14,* 299-304.

[11] Briongos, J.V., Aragón, J.M. & Palancar, M.C. (2006). Fluidised bed dynamics diagnosis from measurements of low-frequency out-bed passive acoustic emissions. *Powder technology, 162,* 145-156.

[12] Pottmann, M., Ogunnaike, B.A., Adetayo, A.A. & Ennis, B.J. (2000). Model-based control of a granulation system. *Powder technology, 108*, 192-201.

Appendices

Appendix A: Copyright permissions for Chapter 3.

For an article published with Elsevier the author retains the right to publish the manuscript, in full or in part, in a thesis or dissertation. The version of the article included in this thesis differs from the published article in some of the language and wording but the overall content is the same.

Appendix B: TPSD profiles for other microphone positions.

Top – The TPSD profiles for the microphones attached to the bowl wall and the motor show minimal change throughout water addition and would be difficult to use for precise process monitoring and control.

Bottom – The TPSD profiles for the microphones suspended at the top and inside of the air exhaust are more detailed and distinct maxima and minima features can be identified for process monitoring and control. The trend in TPSD over wetting for the microphone inside the air exhaust matches the trend for the microphone at the top of the air exhaust, differing only in magnitude.

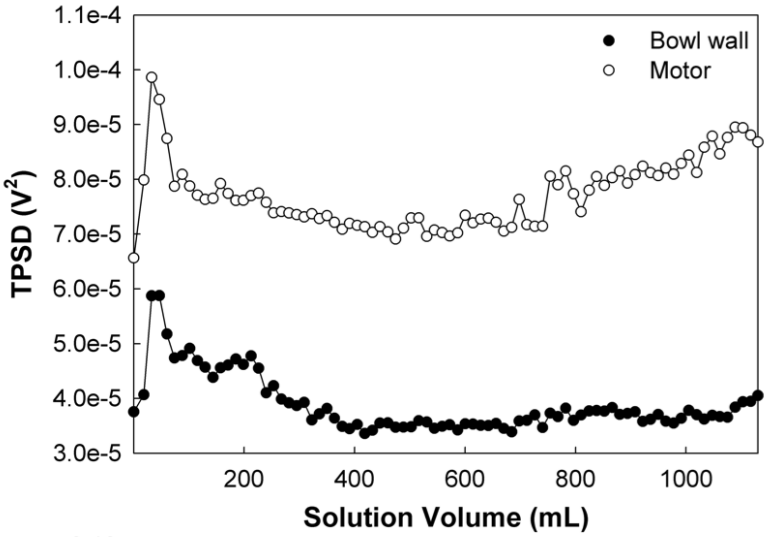
1.1e-4
1.0e-4
9.0e-5
8.0e-5
7.0e-5
6.0e-5
5.0e-5
4.0e-5
3.0e-5
TPSD (V²)
Bowl wall
Motor
200
400
600
800
1000
Solution Volume (mL)

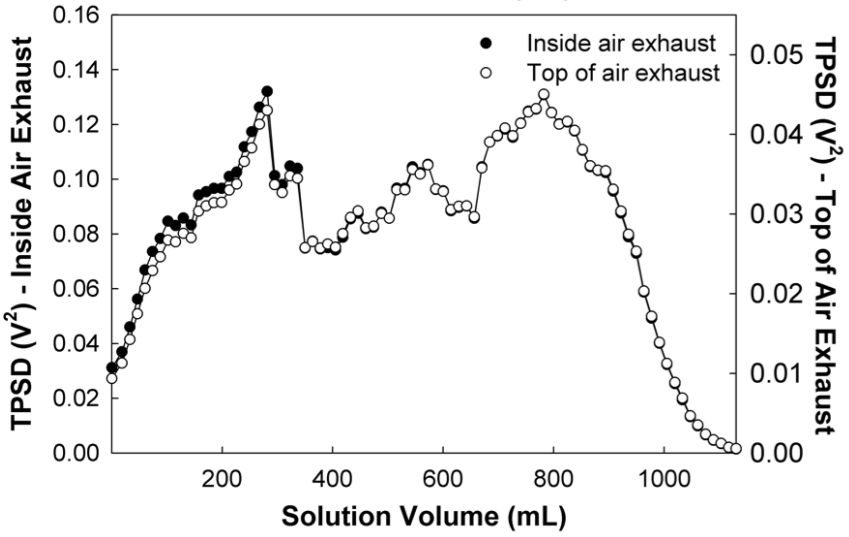
0.16
0.14
0.12
0.10
0.08
0.06
0.04
0.02
0.00
TPSD (V²) - Inside Air Exhaust
Inside air exhaust
Top of air exhaust
0.05
0.04
0.03
0.02
0.01
0.00
TPSD (V²) - Top of Air Exhaust
200
400
600
800
1000
Solution Volume (mL)

Appendix C: Supplementary 10 Hz profiles in support of impeller speed dependence.

The following three plots are further examples of how the maximum TPSD magnitude corresponds to different impeller speeds depending on the frequency range examined. In the top plot, for 130-140 Hz, runs at 420 rpm exhibit the highest magnitude; in the middle plot, for 200-210 Hz, runs at 360 rpm exhibit the highest magnitude; and in the bottom plot, for 220-230 Hz, runs at 300 rpm exhibit the highest magnitude.

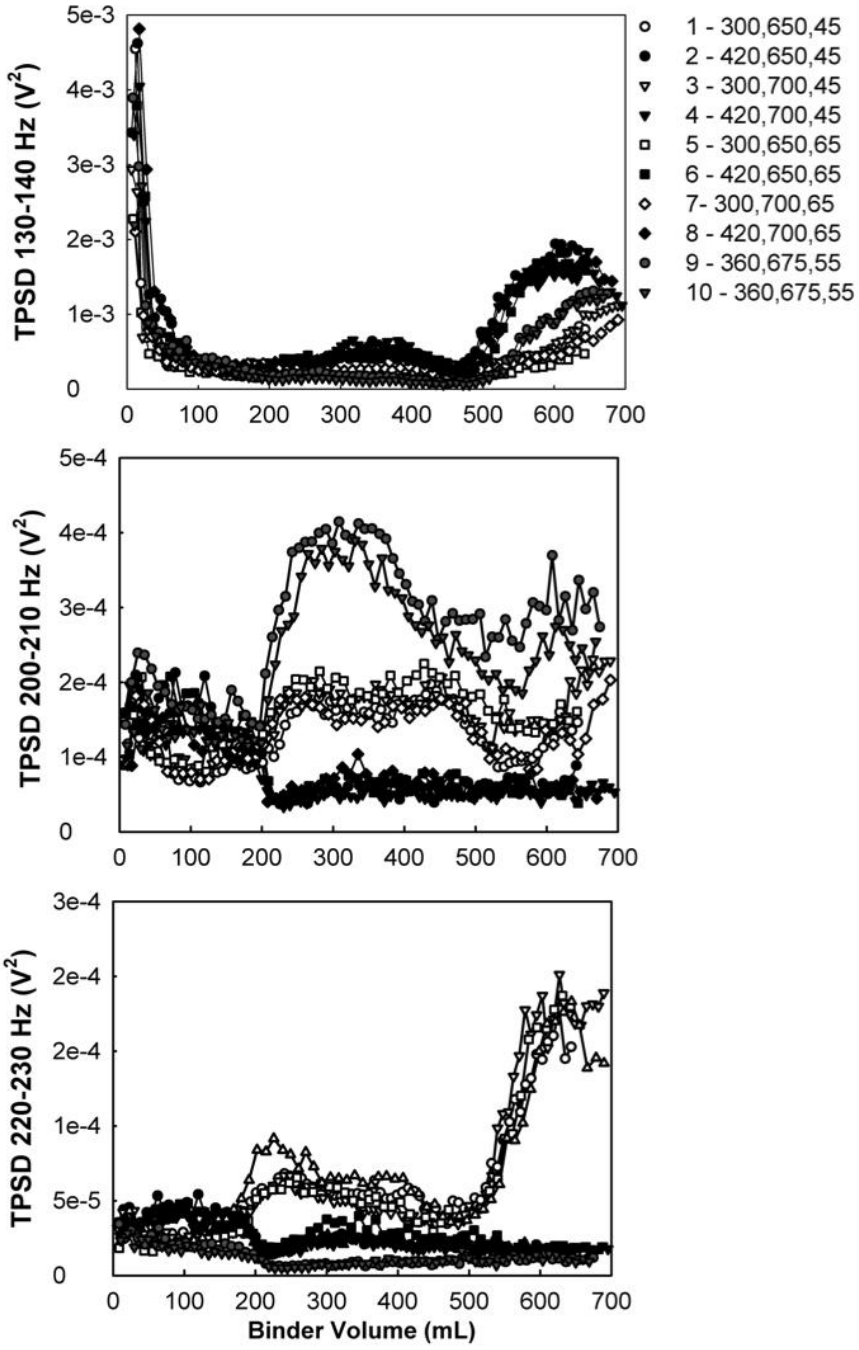
TPSD 130-140 Hz (V²)
5e-3
4e-3
3e-3
2e-3
1e-3
0
0 100 200 300 400 500 600 700
1 - 300,650,45
2 - 420,650,45
3 - 300,700,45
4 - 420,700,45
5 - 300,650,65
6 - 420,650,65
7- 300,700,65
8 - 420,700,65
9 - 360,675,55
10 - 360,675,55
TPSD 200-210 Hz (V²)
5e-4
4e-4
3e-4
2e-4
1e-4
0
0 100 200 300 400 500 600 700
TPSD 220-230 Hz (V²)
3e-4
2e-4
2e-4
1e-4
5e-5
0
0 100 200 300 400 500 600 700
Binder Volume (mL)

Curriculum Vitae

Erin M. Hansuld

EDUCATION

PhD, Chemical Engineering **2011**
The University of Western Ontario & GlaxoSmithKline Inc.

Bachelor of Engineering Science, Honors Chemical Engineering **2007**
The University of Western Ontario

Bachelor of Arts, Honors Business Administration **2007**
The Richard Ivey School of Business

SCHOLARSHIPS AND AWARDS

NSERC CGS-D **2009-2011**
Policy Conference Award, *WISE/OCEPP* **2010**
Claudette MacKay-Lassonde Ph.D. Scholarship, *CEMF* **2009-2010**
NSERC PGS-D **2008-2009**
NSERC CGS-M **2007-2008**
NSERC USRA **summer 2006**
Doreen M. Dinsdale Award, *The University of Western Ontario* **2007-2008**
Ontario Professional Engineers' Scholarship, *The University of Western Ontario* **2006-2007**

RELATED WORK EXPERIENCE

GlaxoSmithKline Inc., Pharmaceutical Development, *Internship Student* **2007 – 2011**
The University of Western Ontario, Chemical Engineering, *Teaching Assistant* **2007 – 2011**
The University of Western Ontario, Chemical Engineering, *Research Assistant* **Summer 2006**

PUBLICATIONS

Hansuld, E. M., Briens, L., McCann, J. & Sayani, A. (2009). *Int. J. Pharm*. 378, p. 37-44.

Hansuld, E., Briens, C. & Briens, L. (2008). *Chem. Eng. Process.* 47 (5), p. 871-878.

CONFERENCES

Hansuld, E., Briens, L., McCann, J. & Sayani, A. (2009). *CSPS Symposium*. Toronto, ON.

Hansuld, E., McCann, J., Arp, Z., Briens, L. & Sayani, A. (2008). *AAPS Annual Meeting*. Atlanta, GA.

Hansuld, E., McCann, J., Briens, L., Arp, Z. & Sayani, A. (2008). *ECI: Particulate Processes in the Pharmaceutical Industry II.* Rio Grande, Puerto Rico.

Hansuld, E., Downey, J., Briens, C. & Briens, L. (2006). A*IChE Annual Conference*. San Francisco, CA.